Probing new physics through semileptonic flavor changing neutral current transition

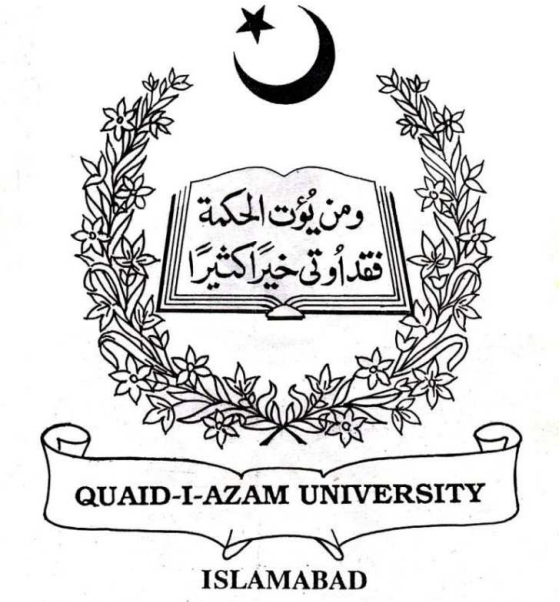

Ishtiaq Ahmed

Department of Physics

&

National Centre for Physics

Quaid-i-Azam University

Islamabad, Pakistan

December , 2012.

This work is submitted as a dissertation in partial fulfillment of the requirement for the degree of

DOCTOR OF PHILOSOPHY

IN PHYSICS

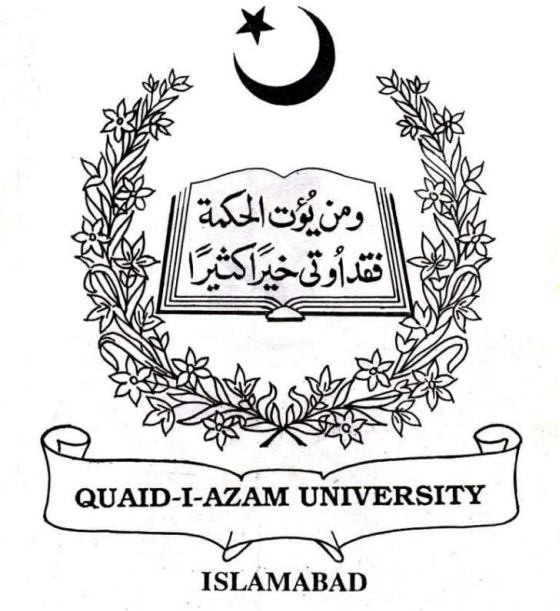

Department of Physics

&

National Centre for Physics

Quaid-i-Azam University

Islamabad, Pakistan

December, 2012.

Certificate

Certified that the work contained in this dissertation was carried out by Mr. Ishtiaq Ahmed for his PhD degree under my supervision.

Prof. Riazuddin

Supervisor,

National Centre for Physics,

&

Department of Physics,

Quaid-i-Azam University, Islamabad.

Submitted through

Prof. S. K. Hasanain

Chairman,

Department of Physics,

Quaid-i-Azam University, Islamabad.

To my loving Ammi and Abbu

Acknowledgements

First and foremost, I want to express my deepest gratitude to my venerable teachers and supervisiors, Prof. **Riazuddin** and Prof. **Fayyazuddin**, for their worthy kindness and invaluable favors. They guided my work with great patience, enthusiasm and a great amount of tolerance. With all my ventures, I could always rely on their remarkable ability to quickly distill any problem to its essence. Their reverential personalities and exclusive vision, as a tower of light, guide new researchers not only in Physics but also in other aspects of life. I am inspired from their working style, fatherly attitude. I feel comfortable to talk to them.

My heartiest thanks to all members of High Energy Theory Group at National Centre for Physics, for many fruitful discussions. I highly value advices from my collaborators, Ali Paracha and M.Jamil Aslam. They always encouraged me when the load was heavy. Special thanks to Ali Paracha for being such a terrific fellow throughout this work. He never failed to show concern when things got stressful. Away from work, I wish to thank all my friends, seniors and juniors, for their love, humor and tolerance.

I can never thank enough my parents for everything they have done for me. Even then, I wish to record my deepest obligations to my father who always loves me and my mother for her endless contribution to make me stay on track. No one tolerates me more than they do.

Ishtiaq Ahmed

Contents

Abstract

In this thesis, the exclusive semileptonic rare B-mesons decays which are induced by the flavor changing neutral current transition (FCNC) have been studied within and beyond the Standard Model (SM). To probe physics beyond the SM, $B \to K^*\ell^+\ell^-$, $B \to K_1\ell^+\ell^-$, $B \to K_2^*\ell^+\ell^-$ and $B_c \to D_s^*\ell^+\ell^-$ decays are considered. At quark level, these FCNC transitions arises as $b \to s\ell^+\ell^-$ and, in the SM, are forbidden at tree level but are allowed at loop level through Glashow-Iliopoulos-Maiani (GIM) mechanism. Moreover, FCNC transitions are further suppressed due to the fact that they are directly proportional to the off diagonal elements of the Cabibo Kobayashi Maskawa (CKM) matrix. Because of these two conditions FCNC transitions are relatively rare and become important to investigate the physics beyond the SM, usually known as new physics (NP). The important points of the thesis are in order:

- We study the exclusive channel of flavor changing neutral current transition (FCNC) i.e. $B \to K^*\ell^+\ell^-$ in the frame work of a family of non-universal Z' model. In this model, the Z' boson couplings to the fermions could lead to FCNC transition at tree level. In addition, the off-diagonal elements of these effective chiral Z' couplings can contain new weak phases that provide a new source of CP violation and, therefore, could explain the CP asymmetries in the current high energy colliders. In this context, we have studied the polarized and unpolarized CP violation asymmetries for the said decay. These asymmetries are highly suppressed in the standard model but significantly enhanced in the Z' model. In addition to the CP violation asymmetries, the single lepton polarization asymmetries are also studied and found them sensitive to the couplings of the Z' boson. Finally, it is analyzed that all these asymmetries which will hopefully be tested at LHC can serve to probe the non-universal Z' model, particularly, the accurate measurements of these asymmetries may play a crucial role to extract the precise values of the coupling parameters of Z' boson.

- The sensitivity of the zero position of the forward backward asymmetry $\mathcal{A}_{FB}$ for the exclusive $B \to K_1(1270)\mu^+\mu^-$ decay is examined by using most general non-standard 4-fermion interactions. Our analysis shows that the zero position of the forward backward asymmetry is very sensitive to the sign and size of the Wilson coefficients corresponding to the new vector type interactions, which are the counter partners of the usual Standard Model operators but have opposite chirality. In addition to these, the other significant effect comes from the interference of Scalar-Psudoscalar and Tensor type operators. These results will not only enhance our theoretical understanding about the axial vector mesons but will also serve as a good tool to look for physics beyond the SM.

- A detailed study of the impact of New Physics (NP) operators with different Lorentz structures, which are absent in the Standard Model Hamiltonian, on the $B \to K_2^*(1430)\mu^+\mu^-$ decay is performed. In this context, the various observables such as branching ratio, forward-backward asymmetry of leptons, lepton polarization asymmetries and the helicity fractions of the final state $K_2^*(1430)$ meson have been studied. We have examined the effects of new vector-axial vector, scalar-pseudoscalar and tensor type interactions for this decay $B \to K_2^*(1430)\mu^+\mu^-$ by using the constraints on different NP couplings which come from the $B_s \to \mu^+\mu^-$, $B \to X_s\mu^+\mu^-$ and $\bar{B} \to \bar{K}^*\mu^+\mu^-$ decays. It is found that the effects of VA, SP and T operators are significant on the zero position of $A_{FB}(q^2)$ as well as on its magnitude. In addition to this these NP operators also give significant effects on the differential decay rate, lepton polarization asymmetries and helicities fractions of final state $K_2^*(1430)$ meson.

- The semileptonic $B_c \to D_s^*\ell^+\ell^-$ ($\ell = \mu, \tau$) decays have been studied in the Standard Model (SM) and in the Universal Extra Dimension (UED) model. In addition to the contribution from the Flavor Changing Neutral Current (FCNC) transitions the weak annihilation (WA) contribution is also important for this decay because of enhanced CKM matrix elements $V_{cb}^*V_{cs}$. It is found that the WA gives 6.7 times larger branching ratio than the penguin contribution for the decay $B_c \to D_s^*\mu^+\mu^-$. The contribution from the WA and FCNC transitions are parameterized in terms of the form factors. In this work we first relate the form factors through Ward identities and then express them in terms of $g_+(0)$ which is extracted from the decay $B_c \to D_s^*\gamma$ through QCD sum rules approach. These form factors are then used to analyze the physical observables like branching ratio and helicity fractions of the final state D_s^* meson in the SM. This analysis is then extended to the UED model where the dependency of above mentioned physical observables depend on the compactification radius R. It is shown that the helicity fractions of D_s^* are sensitive to the UED model especially when we have muons as the final state lepton. This sensitivity is marked up at low q^2 region, irrespective of the choice of the form factors. It is hoped that in the next couple of years LHC will provide enough data on the $B_c \to D_s^*\ell^+\ell^-$ channel, and then , these helicity fractions would serve as a useful tool to establish new physics predicted by the UED model.

Chapter 1

Introduction

The understanding of flavor physics is one of the important goals of elementary particle physics. This is because this understanding gives us more insight into the short distance physics which helps us to explain the physical processes at short distance scales. Within the Standard Model (SM), flavor changing (FC) interactions are controlled by the Cabibbo-Kobayashi-Maskawa (CKM) mixing matrix and this is the only source of FC interactions. To date, SM explains the flavor dynamics with amazing accuracy but it is still required to be tested at high energy scales (TeV) where New Physics (NP) is widely expected. Moreover, despite many hallmarks of the SM one cannot consider it as a fundamental theory due to some basic deficiencies which are given below:

(i) 22 free parameters which appear in the Yukawa sector of the SM including the masses and mixing angles of particles.

(ii) Why is the intergeneration mixing small?

(iii) Why do we have three families?

(iv) Why are 3 generations identical in representation content but vastly different in mass

(v) Higgs mass (m_H) is not protected by any internal symmetry.

(vi) Why is there no CP violation in Flavour-diagonal processes

(vii) How to include gravity at very small distances?

(viii) Are there extra space-time dimensions?, etc.

These short comings impede SM to become a complete theory. The various extensions of the SM try to overcome some of these questions. In addition, during the last few years some mismatches between the SM predictions and experimental measurements are also found [1, 2, 3, 4, 5] which could be taken as an indication of new physics.

On the other hand, from theoretical point of view, B meson physics provides an important ingredient to understand the nature of flavor dynamics because of two weighty reasons: (i) B decays show an extremely rich

phenomenology and (ii) theoretical techniques using an expansion in the heavy mass allow for some model-independent predictions. In particular, the study of rare B decays which are induced by the flavor changing neutral currents (FCNC) is an interesting research area in flavor physics. These decays not only provide us a ground to check the SM but also a probe for NP searches i.e. where one can look for deviations from the SM expectations. The very low SM rate of these decays often make them unaccessible with the present experimental data sets, unless NP effects enhance the rate up to the current experimental sensitivity. Thus, if a suppressed decay is observed, a clear sign of NP is obtained.

Within the SM, FCNC processes are governed by

• the unitary CKM matrix that parameterizes the weak charged current interactions of quarks,

• While the FCNC processes are forbidden at tree level, the Glashow-Iliopoulos-Maiani (GIM) mechanism provides the size of its violation at the one loop level depending sensitively on the CKM parameters and the masses of exchanged particles,

Further, the asymptotic freedom of QCD allows us to calculate the effect of strong interaction on weak decays at sufficiently short distance scales within the framework of renormalization group improved perturbation theory. Thus for the exclusive decays of B meson, the b quark mass being large compared to the typical QCD scale Λ_{QCD}, one can use the factorization ansatz to separate out the relevant hadronic matrix elements of local operators in the weak Hamiltonian, which encode the long distance contributions to the process, from a perturbatively calculable short distance part. The latter depends only on the large scale m_b, in the operator product expansion (OPE) of the effective Hamiltonian. This involves local operators which have a specific Dirac structure and their matrix elements are calculated by means of non-perturbative methods or in certain cases extracted from experimental data on tree level decays with the help of flavor symmetries.

The theoretical understanding of FCNC transitions of hadrons and the measurements of the corresponding CKM matrix elements are consistently hampered by the presence of long distance QCD effects that are responsible for the binding of quarks into hadrons. These effects are hard to evaluate in a model independent way, and as such tend to bring large uncertainties to the theoretical predictions for the weak decay amplitudes. They appear in the calculation of the matrix elements of the hadronic operators, between the initial and final hadronic states. The dynamical content of hadronic current matrix elements is described by Lorentz invariant form factors. The calculation of these form factors requires a non-perturbative treatment and are source of large theoretical uncertainties. Knowledge of these form factors is essential for the description of semileptonic and non-leptonic weak decay processes and in particular for the experimental determination of CKM matrix elements [6].

The experimental observation of inclusive [7] and exclusive [8] decays, $B \to X_s\gamma$ and $B \to K^*\gamma$, has prompted a lot of theoretical interest on rare B meson decays. Though the inclusive decays are theoretically better understood but are extremely difficult to be measured in a hadron machine, such as the LHC, which is the only collider, except for a Super-B factory, that could provide enough luminosity for the precise study of the decay distribution of such rare processes. In contrast, the exclusive decays are easy to detect experimentally but are challenging to calculate

theoretically and the difficulty lies in describing the hadronic structure. This provides the main uncertainty in the predictions of exclusive rare decays. In exclusive $B \to K, K^*$ decays the long-distance effects in the meson transition amplitude of the effective Hamiltonian are encoded in the meson transition form factors (as we mentioned above) which are the scalar functions of the square of momentum transfer and are model dependent quantities. Many exclusive B meson processes based on $b \to s\,(d)\,\ell^+\ell^-$ such as $B \to K\,(K^*)\,\ell^+\ell^-$[9, 10, 11, 12, 13, 14, 15, 16], $B \to \phi\ell^+\ell^-$[17], $B \to \gamma\ell^+\ell^-$[18, 19, 20] and $B \to \ell^+\ell^-$[21] have been studied in literature. In these studies various fameworks have been applied to the description of meson transition form factors of initial and final state meson like constituent quark models, QCD sum rules, lattice QCD, etc.

Regarding exploring the new physics (NP), many inclusive $B-$meson decays such as $B \to X_{d,s}\ell^+\ell^-$ and their corresponding exclusive processes, $B \to M\ell^+\ell^-$ with $M = K, K^*, K_1, \rho$ etc have been investigated in literature [22, 23]. These studies indicated that the said inclusive and exclusive processes of $B-$meson are very sensitive to the flavor structure of the Standard Model and could play a very crucial role to dig out the status of NP. In this context, in general, there are two different techniques to search NP which are considered to overcome the deficiencies of SM as well as to resolve the anomalies in the experimental measurements. One is the direct search which can be achieved by increasing the energies of colliders and find the predicted new particles but these particles are quite massive and therefore hard to produce. The other one is indirect search where the new heavy particles could manifest themselves virtually through loops, consequently, Wilson coefficients get modified. In addition, some of these new particles due to nature of their couplings with fermions could allow some of the processes, which otherwise occur at loop level, at the tree level. This necessitates introduction of new operators that are absent in the SM.

The indirect searches are comparatively easier than the direct searches due to the fact that one can see the effects of heavy particles at low energy on the values of different observables due to the involvement of these new particles. The decays based on the $b \to s\ell^+\ell^-$ transitions involve the Wilson coefficients C_7^{eff}, C_9^{eff} and C_{10}^{eff}, henceforth, are considered as a handy tool to determine the precise values of Wilson coefficients C_7^{eff}, C_9^{eff} and C_{10}^{eff}. Finally, one can say that, the precise measurements of different observables for $b \to s\ell^+\ell^-$ transitions such as branching ratio, forward-backward asymmetry, various polarization asymmetries of the final state leptons, etc, particularly at LHC, could play a vital role in near future to reveal the NP and its shape.

This thesis is organized in the following way. In Chapter 2, we briefly review the theoretical formulation required to analyze $b \to s\ell^+\ell^-$ transition within and beyond the SM. Section 2.1 contains the expression of effective Hamiltonian, the explicit forms of six dimensional operators at quark level and the amplitude for the above mentioned transition. Sections 2.2, 2.3 and 2.4 provide a brief introduction to the model independent approach, the non-Universal family of Z' model and the single Universal extra dimensional model, the latter on suggested by Appelquist, Cheng and Dobrescu.

In chapter 3 we study the Exclusive $B \to K^*\ell^+\ell^-$ decay in the family of non- universal Z' boson model. In section 3.2, with little modification, we rewrite the additional part of the effective Hamiltonian due to the Z' boson

contribution. Section 3.3 consists of the definition and the explicit expressions of physical observables such as single lepton polarization and CP asymmetries. In section 3.4 we discuss the phenomenological analysis of said observables under the influence of Z' boson. In the last section, 3.5, we summarize and conclude our findings.

In chapter 4 we analyze the $B \to K_1 \ell^+ \ell^-$ decay through model independent approach. In section 4.2 we present the matrix elements for the said decay, Ward identities are used to find the relations between the form factors which results in reducing the number of unknown quantities. In section 4.3, we write the general amplitude for $B \to K_1 \ell^+ \ell^-$ as well as the formula and the explicit expression of the forward backward asymmetry. In section 4.4, we discuss the numerical analysis where we extract the new physics effects through the shifting in the zero position of the forward-backward asymmetry which comes through the different type of new operators such as scalar, vector and tensor operators. In section 4.5, we conclude our work.

In chapter 5 we apply the model independent approach to $B \to K_2 \ell^+ \ell^-$ channel. In section 5.2 we define the matrix elements and parameterize these matrix elements in terms of the form factors. In section 5.3 we discuss some phenomenological constraints on the numerical values of the new physics parameters. In section 5.4 we calculate the general expressions of the different observables such as forward-backward and lepton polarization asymmetries and the helicity fractions of the final state meson. In section 5.5 we describe the numerical analysis that how much the values of said observables are influenced due to the implication of the different types of new operators which are absent in the SM. In section 5.6 we present the important points and give conclusive remarks of our work.

In Chapter 6 we present the semileptonic charm B-meson decays in universal extra dimension model. In section 6.1 we give the introduction of charm B-meson decays and its importance in phenomenology. In section 6.2 we present the matrix element and form factors for the decay $B_c \to D_s^* \ell^+ \ell^-$ and we also discuss the weak annihilation form factors for the said decay. In section 6.3 the pole contribution for the said decay is discussed. In section 6.4 we give the formulas for the physical observables such as branching ratio and helicity fractions of D_s^*-meson for the decay $B_c \to D_s^* \ell^+ \ell^-$. In section 6.5 we present the numerical analysis of the above physical observables and also compare our form factors with QCD sum rules for the same observables. Finally, we summarize the main points of our study in section 6.6.

This thesis is based upon the following published research work.

1. Polarized, Unpolarized Direct CP violation and Single Lepton Polarization Asymmetries of $B \to K^* \ell^+ \ell^-$ decay in Z' model. **Ishtiaq Ahmed**, Phys. Rev. D 86, 095022 (2012).

2. Model Independent Analysis of the Forward-Backward Asymmetry for the $B \to K_1 \mu^+ \mu^-$ Decay, **Ishtiaq Ahmed**, M. Ali Paracha and M. J. Aslam, Eur. Phys. J. C **71** (2011) 1521

3. Model independent analysis of $B \to K_2^*(1430) \mu^+ \mu^-$ decay, **Ishtiaq Ahmed**, M. J. Aslam, M. Junaid and S. Shafaq, JHEP **1202** (2012) 045.

4. Semileptonic charmed B meson decays in Universal Extra Dimension Model, M.Ali Paracha, **Ishtiaq**

Ahmed and M.Jamil Aslam, Phys.Rev.D 84: 035003, 2011.

Chapter 2

The Basic Formulism

In this chapter we present the theoretical framework needed to study the processes based upon $b \to s\ell^+\ell^-$ both in the Standard Model and in NP models. In this context, we only present the main points of the NP scenarios which are analyzed in this thesis such as model independent approach, a family of non-Universal Z' Model and universal extra dimension model (UED). The phenomenological implications of these new physics scenarios will be discussed in next chapters.

2.1 Effective Hamiltonian

The basic starting point to do phenomenology of weak decays of hadrons is the effective Hamiltonian which has the following generic structure

$$\mathcal{H}_{eff} = \frac{G_F}{\sqrt{2}} \sum_i V_{CKM} C_i(\mu) Q_i \tag{2.1}$$

Here G_F is the Fermi coupling constant, V_{CKM} are the CKM matrix elements, Q_i are the four-quark operators and $C_i(\mu)$ are the corresponding Wilson coefficients at the energy scale μ. The explicit expressions of Wilson Coefficients at NLO and NNLL are given in [24, 25, 26, 27, 28, 29, 30, 31, 32, 33]. The six classes of operators are given below [34]:

Current Current Operators

$$Q_1 = (\bar{c}_\alpha b_\beta)_{V-A} (\bar{s}_\beta c_\alpha)_{V-A} \qquad Q_2 = (\bar{c}b)_{V-A} (\bar{s}c)_{V-A} \tag{2.2}$$

QCD-Penguins

$$\begin{aligned} Q_3 &= (\bar{s}b)_{V-A} \sum_{q=u,d,s,c,b} (\bar{q}q)_{V-A} & Q_4 &= \left(\bar{s}_\alpha b_\beta\right)_{V-A} \sum_{q=u,d,s,c,b} \left(\bar{q}_\beta q_\alpha\right)_{V-A} \\ Q_5 &= (\bar{s}b)_{V-A} \sum_{q=u,d,s,c,b} (\bar{q}q)_{V+A} & Q_6 &= \left(\bar{s}_\alpha b_\beta\right)_{V-A} \sum_{q=u,d,s,c,b} \left(\bar{q}_\beta q_\alpha\right)_{V+A} \end{aligned} \tag{2.3}$$

Electroweak penguins

$$
\begin{aligned}
Q_7 &= \frac{3}{2}(\bar{s}b)_{V-A}\sum_{q=u,d,s,c,b} e_q\,(\bar{q}q)_{V+A} \qquad & Q_8 &= \frac{3}{2}\left(\bar{s}_\alpha b_\beta\right)_{V-A}\sum_{q=u,d,s,c,b}\left(\bar{q}_\beta q_\alpha\right)_{V+A} \\
Q_9 &= \frac{3}{2}(\bar{s}b)_{V-A}\sum_{q=u,d,s,c,b} e_q\,(\bar{q}q)_{V-A} \qquad & Q_{10} &= \frac{3}{2}\left(\bar{s}_\alpha b_\beta\right)_{V-A}\sum_{q=u,d,s,c,b}\left(\bar{q}_\beta q_\alpha\right)_{V-A}
\end{aligned} \tag{2.4}
$$

Magnetic Penguins

$$
Q_{7\gamma} = \frac{e}{8\pi^2} m_b \bar{s}_\alpha \sigma^{\mu\nu}(1+\gamma^5) b_\alpha F_{\mu\nu} \qquad Q_{8G} = \frac{g}{8\pi^2} m_b \bar{s}_\alpha \sigma^{\mu\nu}(1+\gamma^5) T^a_{\alpha\beta} b_\beta G^a_{\mu\nu} \tag{2.5}
$$

Semileptonic Operators

$$
\begin{aligned}
Q_9 &= (\bar{s}b)_{V-A}\left(\bar{\ell}\ell\right)_V \qquad & Q_{10} &= (\bar{s}b)_{V-A}\left(\bar{\ell}\ell\right)_A \\
Q_{\nu\bar{\nu}} &= (\bar{s}b)_{V-A}\,(\bar{\nu}\nu)_{V-A} \qquad & Q_{\ell\bar{\ell}} &= (\bar{s}b)_{V-A}\left(\bar{\ell}\ell\right)_{V-A}
\end{aligned} \tag{2.6}
$$

The above set of operators is characteristic for any consideration of the interplay of QCD and electroweak effects. The decay channels in which we are interested ($B \to (K^*, K_1, K_2, D_s^*) l^+ l^-, \quad l = \mu, \tau$) are the FCNC transition and originates from the quark level transition $b \to s l^+ l^-$ and are based on the following operators

$$
\begin{aligned}
Q_7 &= \frac{e^2}{16\pi^2} m_b \left(\bar{s}\sigma_{\mu\nu} P_R b\right) F^{\mu\nu}, \\
Q_9 &= \frac{e^2}{16\pi^2} (\bar{s}\gamma_\mu P_L b)(\bar{l}\gamma^\mu l), \\
Q_{10} &= \frac{e^2}{16\pi^2} (\bar{s}\gamma_\mu P_L b)(\bar{l}\gamma^\mu \gamma_5 l),
\end{aligned} \tag{2.7}
$$

with $P_{L,R} = (1 \pm \gamma_5)/2$.

In term of these operators and neglecting the mass of the s-quark, the effective Hamiltonian takes the form

$$
\begin{aligned}
\mathcal{H}_{eff}^{SM} = -\frac{G_F \alpha}{\sqrt{2}\pi} V_{tb} V_{ts}^* \Big\{ & C_9^{SM} (\bar{s}\gamma_\mu P_L b)(\bar{l}\gamma^\mu l) + C_{10}^{SM} (\bar{s}\gamma_\mu P_L b)(\bar{l}\gamma^\mu \gamma_5 l) \\
& -2 m_b C_7^{SM} (\bar{s} i\sigma_{\mu\nu} \frac{q^\nu}{q^2} P_R b)(\bar{l}\gamma^\mu l) \Big\}.
\end{aligned} \tag{2.8}
$$

The above effective Hamiltonian gives the following amplitude

$$
\begin{aligned}
\mathcal{M}_{SM}(B \to M l^+ l^-) = \frac{\alpha_{em} G_F}{2\sqrt{2}\pi} V_{tb}^* V_{ts} \Big[& \langle M(k,\epsilon)|\bar{s}\gamma^\mu(1-\gamma^5) b|B(p)\rangle \times \left\{ C_9^{eff} (\bar{l}\gamma^\mu l) + C_{10} (\bar{l}\gamma^\mu \gamma^5 l) \right\} \\
& -2 C_7^{eff} m_b \langle M(k,\epsilon)|\bar{s} i\sigma_{\mu\nu} \frac{q^\nu}{s}(1+\gamma^5) b|B(p)\rangle (\bar{l}\gamma^\mu l) \Big]
\end{aligned} \tag{2.9}
$$

where M is the final state meson and q is the momentum transfer to the final lepton pair i.e. $q = p_1 + p_2$ where p_1 and p_2 are the momenta of l^- and l^+ respectively and s is the squared of the momenta transfer. $V_{tb}^* V_{ts}$ are the Cabibo-Kobayashi-Maskawa (CKM) matrix elements.

The Wilson coefficient C_9^{eff} in Eq. (3) contains a perturbative part C_9^{per} which includes the indirect contributions of operators Q_i where $i = 1$ to 6 to $b \to s$ and a non-perturbative part C_9^{res} which contain the long-distance resonance effects due to conversion of the real $c\bar{c}$ into the lepton pair l^+l^-. Therefore, C_9^{eff} can be written as

$$C_9^{eff} = C_9^{per} + C_9^{res} \tag{2.10}$$

where the C_9^{per} is read as [35]

$$\begin{aligned} C_9^{per} &= C_9(m_b) + g(m_c, s)\left(\frac{4}{3}C_1 + C_2 + 6C_3 + 60C_5\right) \\ &\quad -\frac{2}{2}g(m_b, s)\left(7C_3 + \frac{4}{3}C_4 + 76C_5 + \frac{64}{3}C_6\right) \\ &\quad -\frac{1}{2}g(0, s)\left(C_3 + \frac{4}{3}C_4 + 16C_5 + \frac{64}{3}\right) + \frac{4}{3}C_3 \\ &\quad +\frac{64}{9}C_5 + \frac{64}{27}C_6. \end{aligned} \tag{2.11}$$

Here the functions $g(m_i, s)$ includes the one loop correction to the four-quark operators $Q_1, ...Q_6$ and have the form [25, 36]

$$\begin{aligned} g(m_i, s) &= \frac{8}{27} - \frac{8}{9}\ln(m_i) + \frac{4}{9}y_i \\ &\quad -\frac{2}{9}(2 + y_i)\sqrt{|1 - y_i|} \times \begin{cases} (\ln|\frac{\sqrt{1-y_i}+1}{\sqrt{1-y_i}-1}| - i\pi), & \text{for } y_i \le 1 \\ 2\arctan\frac{1}{\sqrt{y_i-1}}, & \text{for } y_i > 1 \end{cases} \end{aligned}$$

where $y \equiv 4m_i^2/s$. As mentioned above that the non-perturbative part C_9^{res} arise from the intermediate states of the real $c\bar{c}$ states and can be parameterized by using the Breit-Wigner formula in the following way

$$\begin{aligned} C_9^{res} &= -\frac{3\pi}{\alpha^2}\kappa[3C_1 + C_2 + 3C_3 + C_4 + 3C_5 + C_6] \\ &\quad \times \sum_{V=\psi} \frac{m_V B_r(V \to l^+l^-)\Gamma^V_{total}}{s - m_V^2 + im_V\Gamma_{total^V}} \end{aligned} \tag{2.12}$$

Now in the following sections we will briefly discuss some new physics models which we have analyzed in this thesis.

2.2 Model Independent Approach

As we have mentioned in the introduction that the NP effects in semileptonic B meson decays can be established in two ways: in one case we can change the Wilson Coefficients but leave the operator basis same as that of the SM and in other case we can add new operators too. In the model independent approach, we do not restrict ourself to any model and discuss all possible operators that corresponds to $b \to sl^+l^-$ decays. The most general form of the effective Hamiltonian contains 10 local four fermion interactions which can contribute to the $b \to sl^+l^-$ decay and can be written as:

Vector Operators

$$\begin{aligned} Q_1^{VA} &= C_{LL}\bar{s}_L\gamma^\mu b_L\bar{l}_L\gamma^\mu l_L \qquad & Q_2^{VA} &= C_{LR}\bar{s}_L\gamma^\mu b_L\bar{l}_R\gamma^\mu l_R \\ Q_3^{VA} &= C_{RL}\bar{s}_R\gamma^\mu b_R\bar{l}_L\gamma^\mu l_L \qquad & Q_4^{VA} &= C_{RR}\bar{s}_R\gamma^\mu b_R\bar{l}_R\gamma^\mu l_R \end{aligned} \tag{2.13}$$

Scalar Operators

$$\begin{aligned} Q_1^{SP} &= C_{LRLR}\bar{s}_L b_R\bar{l}_L l_R \qquad & Q_2^{SP} &= C_{RLLR}\bar{s}_R b_L\bar{l}_L l_R \\ Q_3^{SP} &= C_{LRRL}\bar{s}_L b_R\bar{l}_R l_L \qquad & Q_4^{SP} &= C_{RLRL}\bar{s}_R b_L\bar{l}_R l_L \end{aligned} \tag{2.14}$$

Tensor Operators

$$Q_1^T = C_T\bar{s}\sigma_{\mu\nu}b\bar{l}\sigma^{\mu\nu}l \qquad Q_2^T = iC_{TE}\epsilon_{\mu\nu\alpha\beta}\bar{l}\sigma^{\mu\nu}l\bar{s}\sigma^{\alpha\beta}b \tag{2.15}$$

By using these operators, the new contributions to the effective Hamiltonian are

$$\begin{aligned} \mathcal{H}_{\text{new}}(b \to sl^+l^-) &= \mathcal{H}^{V-A} + \mathcal{H}^{S-P} + \mathcal{H}^T \\ \mathcal{H}^{V-A} &= \frac{G_F\alpha}{\sqrt{2}\pi}V_{ts}^*V_{tb}\left\{C_{LL}\bar{s}_L\gamma^\mu b_L\bar{l}_L\gamma^\mu l_L + C_{LR}\bar{s}_L\gamma^\mu b_L\bar{l}_R\gamma^\mu l_R + C_{RL}\bar{s}_R\gamma^\mu b_R\bar{l}_L\gamma^\mu l_L + C_{RR}\bar{s}_R\gamma^\mu b_R\bar{l}_R\gamma^\mu l_R\right\} \\ \mathcal{H}^{S-P} &= \frac{G_F\alpha}{\sqrt{2}\pi}V_{ts}^*V_{tb}\left\{C_{LRLR}\bar{s}_L b_R\bar{l}_L l_R + C_{RLLR}\bar{s}_R b_L\bar{l}_L l_R + C_{LRRL}\bar{s}_L b_R\bar{l}_R l_L + C_{RLRL}\bar{s}_R b_L\bar{l}_R l_L\right\} \\ \mathcal{H}^T &= \frac{G_F\alpha}{\sqrt{2}\pi}V_{ts}^*V_{tb}\left\{C_T\bar{s}\sigma_{\mu\nu}b\bar{l}\sigma^{\mu\nu}l + iC_{TE}\epsilon_{\mu\nu\alpha\beta}\bar{l}\sigma^{\mu\nu}l\bar{s}\sigma^{\alpha\beta}b\right\} \end{aligned} \tag{2.16}$$

or if we define

$$\begin{aligned} R_V &= C_{LL} + C_{LR} \qquad & R_V' &= C_{RR} + C_{RL} \qquad & R_A &= C_{LL} - C_{LR} \qquad & R_A' &= C_{RR} - C_{RL} \\ R_S &= C_{LRLR} + C_{LRRL} \qquad & R_S' &= C_{RLLR} + C_{RLRL} \qquad & R_P &= C_{LRLR} - C_{LRRL} \qquad & R_P' &= C_{RLLR} - C_{RLRL} \end{aligned} \tag{2.17}$$

our total Hamiltonian becomes

$$\mathcal{H}_{eff} = \mathcal{H}_{eff}^{SM} + \mathcal{H}_{eff}^{VA} + \mathcal{H}_{eff}^{SP} + \mathcal{H}_{eff}^{T}, \tag{2.18}$$

where $\mathcal{H}_{eff}^{SM}$ is given in Eq. (2.8), while the others are [37]

$$\begin{aligned}
\mathcal{H}_{eff}^{VA} &= -\frac{4G_F}{\sqrt{2}}\frac{\alpha}{\pi}V_{ts}^*V_{tb}\Big\{R_V\left(\bar{s}\gamma^\mu P_L b\right)\bar{\mu}\gamma_\mu\mu + R_A\left(\bar{s}\gamma^\mu P_L b\right)\bar{\mu}\gamma_\mu\gamma_5\mu \\
&\quad + R'_V\left(\bar{s}\gamma^\mu P_R b\right)\bar{\mu}\gamma_\mu\mu + R'_A\left(\bar{s}\gamma^\mu P_R b\right)\bar{\mu}\gamma_\mu\gamma_5\mu\Big\}, \qquad (2.19)\\
\mathcal{H}_{eff}^{SP} &= -\frac{4G_F}{\sqrt{2}}\frac{\alpha}{\pi}V_{ts}^*V_{tb}\{R_S\left(\bar{s}P_R b\right)\bar{\mu}\mu + R_P\left(\bar{s}P_R b\right)\bar{\mu}\gamma_5\mu \\
&\quad + R'_S\left(\bar{s}P_L b\right)\bar{\mu}\mu + R'_P\left(\bar{s}P_L b\right)\bar{\mu}\gamma_5\mu\}, \qquad (2.20)\\
\mathcal{H}_{eff}^{T} &= -\frac{4G_F}{\sqrt{2}}\frac{\alpha}{\pi}V_{ts}^*V_{tb}\left\{C_T\left(\bar{s}\sigma_{\mu\nu}b\right)\bar{\mu}\sigma_{\mu\nu}\mu + iC_{TE}\left(\bar{s}\sigma_{\mu\nu}b\right)\bar{\mu}\sigma_{\alpha\beta}\mu\epsilon^{\mu\nu\alpha\beta}\right\} \qquad (2.21)
\end{aligned}$$

Here, $R_V, R_A, R_V, R'_A, R_S, R_P, R'_S, R'_P, C_T$ and C_{TE} are the NP effective couplings. The constraints on the numerical values of these NP coupling from different B meson decays will be given later in chapter 5.

Thus the explicit form of the free quark amplitude $\mathcal{M}$ for the $b \to sl^+l^-$ transition can be written as sum of the SM amplitude Eq. (2.9) and of the new physics contributions, i.e.

$$\mathcal{M} = \mathcal{M}_{SM} + \mathcal{M}_{new} \tag{2.22}$$

where $\mathcal{M}_{\text{new}}$ is

$$\begin{aligned}
\mathcal{M}_{\text{new}}(B &\to Ml^+l^-) = \mathcal{M}^{VA} + \mathcal{M}^{SP} + \mathcal{M}^{T} \\
\mathcal{M}^{VA} &= \frac{G_F\alpha}{\sqrt{2}\pi}V_{ts}^*V_{tb}\left\{\langle M|\bar{s}_L\gamma^\mu b_L|B\rangle(R_V\bar{l}\gamma^\mu l + R_A\bar{l}\gamma^\mu\gamma^5 l) + \langle M|\bar{s}_R\gamma^\mu b_R|B\rangle(R'_V\bar{l}\gamma^\mu l + R'_A\bar{l}\gamma^\mu\gamma^5 l)\right\} \\
\mathcal{M}^{SP} &= \frac{G_F\alpha}{\sqrt{2}\pi}V_{ts}^*V_{tb}\left\{\langle M|\bar{s}_L b_R|B\rangle(R_S\bar{l}l + R_P\bar{l}\gamma^5 l) + \langle M|\bar{s}_R b_L|B\rangle(R'_S\bar{l}l + R'_P\bar{l}\gamma^5 l)\right\} \\
\mathcal{M}^{T} &= \frac{G_F\alpha}{\sqrt{2}\pi}V_{ts}^*V_{tb}\langle M|\bar{s}\sigma_{\mu\nu}b|B\rangle\left\{C_T\bar{l}\sigma^{\mu\nu}l + iC_{TE}\epsilon^{\mu\nu\alpha\beta}\bar{l}\sigma_{\alpha\beta}l\right\} \qquad (2.23)
\end{aligned}$$

We use the model independent approach for $B \to K_1\ell^+\ell^-$ and $B \to K_2^*\ell^+\ell^-$ decays which will be discussed in chapter 4 and 5 respectively.

2.3 Family Non-universal Z' Model

A family non-universal Z' model could naturally be derived in many extensions of the SM. The most economical way to get it by including an additional $U'(1)$ gauge symmetry. The model is formulated in detail by Langacker and Plümacher [38]. The current in this model can be given as follows in a proper gauge basis

$$J^\mu_{Z'} = \sum_i \bar{\psi}_i\gamma^\mu\left[\epsilon_i^{\psi_i}P_L + \epsilon_i^{\psi_R}P_R\right]\psi_i \tag{2.24}$$

where i represents the family index and ψ represents the families of up or down type quarks or charged or neutral leptons. According to some GUT or string construction models such as E_6, there is a possibility to have a family of non-universal Z' couplings such as $\epsilon_i^{L,R}$ which are diagonal and as a result the gauge couplings are family non universal. In a family non-universal Z'-model, FCNCs generally appear at tree level in both left and right handed sectors, after rotating the physical basis of non-universal Z'-couplings $\epsilon_i^{L,R}$ and one can write explicitly,

$$B^{\psi_L} = V_{\psi_L}\epsilon^{\psi_L}V_{\psi_L}^{\dagger}, B^{\psi_R} = V_{\psi_R}\epsilon^{\psi_R}V_{\psi_R}^{\dagger} \tag{2.25}$$

Further these couplings might contains CP-violating phase, which is beyond that of SM. Making use of assumption that the couplings of right handed quarks flavors with Z' boson are diagonal, so the effective Hamiltonian in family non-universal Z' model for the decay $b \to s\ell^+\ell^-$ can be written as [39, 40, 41, 42]

$$\mathcal{H}_{eff}^{Z'}(b \to s\ell^+\ell^-) = -\frac{2G_F}{\sqrt{2}}V_{tb}V_{ts}^*[-\frac{B_{sb}^L B_{\ell\ell}^L}{V_{tb}V_{ts}^*}\bar{s}_L\gamma_\mu b_L\bar{\ell}_L\gamma^\mu\ell_L - \frac{B_{sb}^L B_{\ell\ell}^R}{V_{tb}V_{ts}^*}\bar{s}_L\gamma_\mu b_L\bar{\ell}_R\gamma^\mu\ell_R] \tag{2.26}$$

One can reformulate the effective Hamiltonian given above as

$$H_{eff}^{Z'}(b \to s\ell^+\ell^-) = -\frac{4G_F}{\sqrt{2}}V_{tb}V_{ts}^*\left[\Delta C_9(\bar{s}\gamma_\mu(1-\gamma^5)b)\bar{\ell}\gamma^\mu\ell + \Delta C_{10}(\bar{s}\gamma_\mu(1-\gamma^5)b)\bar{\ell}\gamma^\mu\gamma^5\ell\right] \tag{2.27}$$

where

$$\Delta C_9 = -\frac{B_{sb}^L}{V_{tb}V_{ts}^*}\left(B_{\ell\ell}^L + B_{\ell\ell}^R\right),\ \Delta C_{10} = \frac{B_{sb}^L}{V_{tb}V_{ts}^*}\left(B_{\ell}^L - B_{\ell}^R\right)$$

The quantities B_{sb}^L and $B_{\ell}^{L,R}$ denote the effective chiral Z' couplings to quarks and leptons. The off diagonal element B_{sb}^L contain a new weak phase and could be written as $|B_{sb}|e^{i\phi_s^L}$. The contribution of Z' can be represented as modification of Wilson coefficient of the semileptonic operators Q_9 and Q_{10} i.e.

$$C_9^{Z'} = C_9^{\rm SM} - \frac{4\pi}{\alpha}\frac{B_{sb}^L}{V_{tb}V_{ts}^*}\left(B_{ll}^L + B_{ll}^R\right) \tag{2.28}$$

$$C_{10}^{Z'} = C_{10}^{\rm SM} + \frac{4\pi}{\alpha}\frac{B_{sb}^L}{V_{tb}V_{ts}^*}\left(B_{ll}^L - B_{ll}^R\right) \tag{2.29}$$

We analyze this model in the next chapter through $B \to K^*\ell^+\ell^-$ decay.

2.4 Appelquist Cheng and Dobrescu Model

In our universe we have 3 spatial +1 temporal dimensions and if an extra dimension exists and is compactified, fields living in all dimensions would menifest themselves in the 3 + 1 space by the appearence of Kaluza-Klein excitations. The most pertinent question is whether ordinary fields propagate or not in all extra dimensions. One

obvious possibilty is that only gravity propagates in ordinary plus extra dimensional universe, the "bulk". Contrary to this there are the models with universal extra dimensions (UED) in which all the fields propagate in all available dimensions [43] and Appelquist, Cheng and Dobrescu (ACD) model belongs to one of UED scenarios [44].

This model is minimal extension of the SM in $4 + \delta$ dimensions, and in literature a simple case $\delta = 1$ is considered [44]. The topology for this extra dimension is orbifold S^1/Z_2, and the coordinate $X_5 = y$ runs from 0 to $2\pi R$, where R is the the compactification radius. The Kaluza-Klein (KK) mode expansion of the fields are determined from the boundary conditions at two fixed points $y = 0$ and $y = \pi R$ on the orbifold. Under parity transformation $P_5 : y \to -y$ the fields may be even or odd. Even fields have their correspondent in the 4 dimensional SM and their zero mode in the KK mode expansion can be interpreted as the ordionary SM field. The odd fields do not have their correspondent in the SM and therefore do not have zero mode in the KK expansion.

The significant features of the ACD model are:

i) the compactification radius R is the only free parameter with respect to SM

ii) no tree level contribution of KK modes in low energy processes (at scale $\mu \ll 1/R$) and no production of single KK excitation in ordinary particle interactions is a consequence of conservation of KK parity.

The detailed description of ACD model is provided in [45]; here we summarize main features of its construction from [44].

Gauge group

As ACD model is the minimal extension of SM therefore the gauge bosons associated with the gauge group $SU(2)_L \times U(1)_Y$ are W_i^a $(a = 1, 2, 3,\ i = 0, 1, 2, 3, 5)$ and B_i, and the gauge couplings are $\hat{g}_2 = g_2\sqrt{2\pi R}$ and $\hat{g}' = g'\sqrt{2\pi R}$ (the hat on the coupling constant refers to the extra dimension). The charged bosons are $W_i^{\pm} = \frac{1}{\sqrt{2}}\left(W_i^1 \mp W_i^2\right)$ and the mixing of W_i^3 and B_i give rise to the fields Z_i and A_i as they do in the SM. The relations for the mixing angles are:

$$c_W = \cos\theta_W = \frac{\hat{g}_2}{\sqrt{\hat{g}_2^2 + \hat{g}'^2}} \qquad c_W = \sin\theta_W = \frac{\hat{g}'}{\sqrt{\hat{g}_2^2 + \hat{g}'^2}} \tag{2.30}$$

The Wein berg angle remains the same as in the SM, due to the relationship between five and four dimensional constants. The gluons which are the gauge bosons associated to $SU(3)_C$ are $G_i^a(X, y)$ $(a = 1, \ldots, 8)$.

Higgs sector and mixing between Higgs fields and gauge bosons

The Higgs doublet can be written as:

$$\phi = \begin{pmatrix} i\chi^+ \\ \frac{1}{\sqrt{2}}\left(\psi - i\chi^3\right) \end{pmatrix} \tag{2.31}$$

with $\chi^{\pm} = \frac{1}{\sqrt{2}}\left(\chi^1 \mp \chi^2\right)$. Now only field ψ has a zero mode, and we assign vacuum expectation value $\hat{v}$ to such mode, so that $\psi \to \hat{v} + H$. H is the the SM Higgs field, and the relation between expectation values in five and four dimension is: $\hat{v} = v/\sqrt{2\pi R}$.

The Goldstone fields $G^0_{(n)}$, $G^{\pm}_{(n)}$ aries due to the mixing of charged $W^{\pm}_{5(n)}$ and $\chi^{\pm}_{(n)}$, as well as neutral fields $Z_{5(n)}$. These Goldstone modes are then used to give masses to the $W^{\pm\mu}_{(n)}$ and $Z^{\mu}_{(n)}$, and $a^0_{(n)}$, $a^{\pm}_{(n)}$, new physical scalars.

Yukawa terms

In SM, Yukawa coupling of the Higgs field to the fermion provides the fermion mass terms. The diagonalization of such terms leads to the introduction of the CKM matrix. In order to have chiral fermions in ACD model, the left and right-handed components of the given spinor cannot be simultaneously even under P_5. This makes the ACD model to be the minimal flavor violation model, since there are no new opeators beyond those present in the SM and no new phase beyond the CKM phase and the unitarity triangle remains the same as in SM [45]. In order to have 4-d mass eigenstates of higher KK levels, a further mixing is introduced among the left-handed doublet and right-handed singlet of each flavor f. The mixing angle is such that $\tan\left(2\alpha_{f(n)}\right) = \frac{m_f}{n/R}\,(n \geq 1)$ giving mass $m_{f(n)} = \sqrt{m_f^2 + \frac{n^2}{R^2}}$, so that it is negligible for all flavors except the top [44].

Integrating over the fifth-dimension y gives the four-dimensional Lagrangian:

$$\mathcal{L}_4\,(X) = \int_0^{2\pi R} \mathcal{L}_5\,(X, y) \tag{2.32}$$

which describes: (i) zero modes corresponding to the SM fields, (ii) their massive KK excitations, (iii) KK excitations without zero modes which do not correspond to any field in SM. Feynman rules used in the further calculation are given in Ref. [45].

In ACD model the new physics comes through the modification of Wilson coefficients. Buras et al. have computed the above coefficients at NLO in ACD model including the effects of KK modes [45, 46]; we use these results to study $B_c \to D_s^* \ell^+ \ell^-$ decay. As it has already been mentioned that ACD model is the minimal extension of SM with only one extra dimension and it has no extra operator other than the SM, therefore, the whole contribution from all the KK states is in the Wilson coefficients, i.e. now they depend on the additional ACD parameter, the inverse of compactification radius R. At large value of $1/R$ the SM phenomenology should be recovered, since the new states, being more and more massive, decoupled from the low-energy theory.

In ACD model, the Wilson coefficients are modified and they contain the contribution from new particles which are not present in the SM and comes as an intermediate state in penguin and box diagrams. Thus, these coefficients can be expressed in terms of the functions $F\,(X_t, 1/R)$, $X_t = \frac{m_t^2}{M_W^2}$, which generalize the corresponding SM function $F_0\,(X_t)$ according to:

$$F\,(X_t, 1/R) = F_0\,(X_t) + \sum_{n=1}^{\infty} F_n\,(X_t, X_n) \tag{2.33}$$

with $X_n = \frac{m_n^2}{M_W^2}$ and $m_n = \frac{n}{R}$ [44]. The relevant diagrams are Z^0 penguins, γ penguins, gluon penguins, γ magnetic penguins, Chormomagnetic penguins and the corresponding functions are $C\,(X_t, 1/R)$, $D\,(X_t, 1/R)$, $E\,(X_t, 1/R)$, $D'\,(X_t, 1/R)$ and $E'\,(X_t, 1/R)$ respectively. These functions can be found in [45, 46] but to make the thesis self

contained, we collect here the formulae needed for our analysis.

•C_7

In place of C_7, one defines an effective coefficient $C_7^{(0)eff}$ which is renormalization scheme independent [47]:

$$C_7^{(0)eff}(\mu_b) = \eta^{\frac{16}{23}} C_7^{(0)}(\mu_w) + \frac{8}{3}(\eta^{\frac{14}{23}} - \eta^{\frac{16}{23}}) C_8^{(0)}(\mu_w) + C_2^{(0)}(\mu_w) \sum_{i=1}^{8} h_i \eta^{\alpha_i} \tag{2.34}$$

where $\eta = \frac{\alpha s(\mu_w)}{\alpha_s(\mu_b)}$, and

$$C_2^{(0)}(\mu_w) = 1,\ C_7^{(0)}(\mu_w) = -\frac{1}{2} D'(X_t, \frac{1}{R}),\ C_8^{(0)}(\mu_w) = -\frac{1}{2} E'(X_t, \frac{1}{R}); \tag{2.35}$$

the superscript (0) stays for leading log approximation. Furthermore:

$$\begin{aligned}
\alpha_1 &= \frac{14}{23} \quad \alpha_2 = \frac{16}{23} \quad \alpha_3 = \frac{6}{23} \quad \alpha_4 = -\frac{12}{23} \\
\alpha_5 &= 0.4086 \quad \alpha_6 = -0.4230 \quad \alpha_7 = -0.8994 \quad \alpha_8 = -0.1456 \\
h_1 &= 2.996 \quad h_2 = -1.0880 \quad h_3 = -\frac{3}{7} \quad h_4 = -\frac{1}{14} \\
h_5 &= -0.649 \quad h_6 = -0.0380 \quad h_7 = -0.0185 \quad h_8 = -0.0057.
\end{aligned} \tag{2.36}$$

The functions D' and E' are given in eq. (2.36) with

$$D_0'(X_t) = -\frac{(8X_t^3 + 5X_t^2 - 7X_t)}{12(1-X_t)^3} + \frac{X_t^2(2-3X_t)}{2(1-X_t)^4} \ln X_t \tag{2.37}$$

$$E_0'(X_t) = -\frac{X_t(X_t^2 - 5X_t - 2)}{4(1-X_t)^3} + \frac{3X_t^2}{2(1-X_t)^4} \ln X_t \tag{2.38}$$

$$\begin{aligned}
D_n'(X_t, X_n) = &\frac{X_t(-37 + 44X_t + 17X_t^2 + 6X_n^2(10 - 9X_t + 3X_t^2) - 3X_n(21 - 54X_t + 17X_t^2))}{36(X_t-1)^3} \\
&+ \frac{X_n(2 - 7X_n + 3X_n^2)}{6} \ln \frac{X_n}{1+X_n} \\
&- \frac{(-2 + X_n + 3X_t)(X_t + 3X_t^2 + X_n^2(3+X_t) - X_n)(1 + (-10 + X_t)X_t))}{6(X_t-1)^4} \ln \frac{X_n + X_t}{1+X_n}
\end{aligned} \tag{2.39}$$

$$\begin{aligned}
E_n'(X_t, X_n) = &\frac{X_t(-17 - 8X_t + X_t^2 + 3X_n(21 - 6X_t + X_t^2) - 6X_n^2(10 - 9X_t + 3X_t^2))}{12(X_t-1)^3} \\
&+ -\frac{1}{2} X_n(1+X_n)(-1+3X_n) \ln \frac{X_n}{1+X_n} \\
&+ \frac{(1+X_n)(X_t + 3X_t^2 + X_n^2(3+X_t) - X_n(1 + (-10 + X_t)X_t))}{2(X_t-1)^4} \ln \frac{X_n + X_t}{1+X_n}
\end{aligned} \tag{2.40}$$

Following [46] one gets the expressions for the sum over n :

$$\begin{aligned}
\sum_{n=1}^{\infty} D_n'(X_t, X_n) &= -\frac{X_t(-37 + X_t(44 + 17X_t))}{72(X_t-1)^3} \\
&\quad + \frac{\pi M_w R}{2} [\int_0^1 dy \frac{2y^{\frac{1}{2}} + 7y^{\frac{3}{2}} + 3y^{\frac{5}{2}}}{6}] \coth(\pi M_w R \sqrt{y})
\end{aligned}$$

$$
\begin{aligned}
&+\frac{(-2+X_t)X_t(1+3X_t)}{6(X_t-1)^4}J(R,-\frac{1}{2})\\
&-\frac{1}{6(X_t-1)^4}[X_t(1+3X_t)-(-2+3X_t)(1+(-10+X_t)X_t)]J(R,\frac{1}{2})\\
&+\frac{1}{6(X_t-1)^4}[(-2+3X_t)(3+X_t)-(1+(-10+X_t)X_t)]J(R,\frac{3}{2})\\
&-\frac{(3+X_t)}{6(X_t-1)^4}J(R,\frac{5}{2})]
\end{aligned}
\tag{2.41}
$$

$$
\begin{aligned}
\sum_{n=1}^{\infty}E'_n(X_t,X_n) &= -\frac{X_t(-17+(-8+X_t)X_t)}{24(X_t-1)^3}\\
&+\frac{\pi M_w R}{2}[\int_0^1 dy(y^{\frac{1}{2}}+2y^{\frac{3}{2}}-3y^{\frac{5}{2}})\coth(\pi M_w R\sqrt{y})]\\
&-\frac{X_t(1+3X_t)}{(X_t-1)^4}J(R,-\frac{1}{2})\\
&+\frac{1}{(X_t-1)^4}[X_t(1+3X_t)-(1+(-10+X_t)X_t)]J(R,\frac{1}{2})\\
&-\frac{1}{(X_t-1)^4}[(3+X_t)-(1+(-10+X_t)X_t)]J(R,\frac{3}{2})\\
&+\frac{(3+X_t)}{(X_t-1)^4}J(R,\frac{5}{2})]
\end{aligned}
\tag{2.42}
$$

where

$$
J(R,\alpha)=\int_0^1 dy y^{\alpha}[\coth(\pi M_w R\sqrt{y})-X_t^{1+\alpha}\coth(\pi m_t R\sqrt{y})]. \tag{2.43}
$$

•C_9

In the ACD model and in the NDR scheme one has

$$
C_9(\mu)=P_0^{NDR}+\frac{Y(X_t,\frac{1}{R})}{\sin^2\theta_W}-4Z(X_t,\frac{1}{R})+P_E E(X_t,\frac{1}{R}) \tag{2.44}
$$

where $P_0^{NDR}=2.60\pm0.25$ [48] and the last term is numerically negligible. Besides

$$
\begin{aligned}
Y(X_t,\frac{1}{R}) &= Y_0(X_t)+\sum_{n=1}^{\infty}C_n(X_t,X_n)\\
Z(X_t,\frac{1}{R}) &= Z_0(X_t)+\sum_{n=1}^{\infty}C_n(X_t,X_n)
\end{aligned}
\tag{2.45}
$$

$$
\begin{aligned}
Y_0(X_t) &= \frac{X_t}{8}[\frac{X_t-4}{X_t-1}+\frac{3X_t}{(X_t-1)^2}\ln X_t]\\
Z_0(X_t) &= \frac{18X_t^4-163X_t^3+259X_t^2-108X_t}{144(X_t-1)^3}\\
&+[\frac{32X_t^4-38X_t^3+15X_t^2-18X_t}{72(X_t-1)^4}-\frac{1}{9}]\ln X_t
\end{aligned}
\tag{2.46}
$$

$$
C_n(X_t,X_n)=\frac{X_t}{8(X_t-1)^2}[X_t^2-8X_t+7+(3+3X_t+7X_n-X_tX_n)\ln\frac{X_t+X_n}{1+X_n}] \tag{2.47}
$$

and

$$\sum_{n=1}^{\infty} C_n(X_t, X_n) = \frac{X_t(7 - X_t)}{16(X_t - 1)} - \frac{\pi M_w R x_t}{16(X_t - 1)^2}[3(1 + X_t)J(R, -\frac{1}{2}) + (X_t - 7)J(R, \frac{1}{2})] \tag{2.48}$$

•C_{10}

C_{10} is μ independent and is given by

$$C_{10} = -\frac{Y(X_t, \frac{1}{R})}{\sin^2 \theta_w}. \tag{2.49}$$

The normalization scale is fixed to $\mu = \mu_b \simeq 5$ GeV.

We use these values of Wilson coefficients in the process $B_c \to D_s^* \ell^+ \ell^-$ and will be discussed in Chapter 5.

Chapter 3

Polarized, Unpolarized Direct CP violation and Single Lepton Polarization Asymmetries of $B \to K^* \ell^+ \ell^-$ decay in Z' model.

3.1 Introduction

As we have already mentioned in chapter 1 that the study of rare B-meson decays which are induced by the flavor changing neutral currents (FCNC) is highly interesting research area in flavor physics because these transitions provide a fertile ground to check the SM and to probe new physics (NP) i.e. the physics beyond the SM. Similarly, we have also indicated that to overcome the fundamental shortcomings in the SM and accommodate the experimental measurements with the theory many models are cooked [49, 50, 51, 52, 53, 38]. Among them the non universal Z' model (summarized in chapter 2) looks an attractive extension of the SM (for a detailed review see Ref. [38]). As the behavior of the off diagonal couplings of the non-universal Z' boson with the fermions, the FCNC transitions can occur at tree level as well as this model is help out to resolve some puzzles in the data of rare B-meson decays such as anomaly in the $B_s - \bar{B}_s$ mixing phase [54, 55] and $\pi - K$ puzzle [56], etc.

The investigation of the couplings of non universal family of Z' boson with the fermions through FCNC transitions have also been studied by considering different observables such as branching ratio and forward backward asymmetry [57, 39]. In this context, the behavior of the other observables in the presence of Z' boson may also play a crucial role to refine our knowledge about the family of non universal Z' model. With this motivation we have studied single lepton polarization asymmetries, polarized and unpolarized CP violation asymmetries in the Z'

model. In the context of CP asymmetry, it is important to emphasis here that the FCNC transitions are proportional to three CKM matrix elements, namely, $V_{tb}V_{ts}^*$, $V_{cb}V_{cs}^*$ and $V_{ub}V_{us}^*$ but due to the unitarity condition and neglecting $V_{ub}V_{us}^*$ in comparison of $V_{cb}V_{cs}^*$ and $V_{tb}V_{ts}^*$, the CP asymmetry is highly suppressed in the SM. Therefore, the measurement of CP violation asymmetries in FCNC processes could provide a key evidence for new physics.

The scheme of this chapter is as follows. The section 3.2 contains the theoretical formulation of the Hamiltonian with Z' contribution, the matrix elements and the final amplitude which is necessary to calculate the different physical observables for $B \to K^*\ell^+\ell^-$. In section 3.3, we give the formulas and explicit expressions of observables which are under consideration in this chapter. In section 3.4 we present the numerical analysis to show how the lepton polarization asymmetries and CP violation asymmetries are influenced due to the contribution of Z' boson. In the last section, we give our conclusions.

3.2 Effective Hamiltonian with Z' boson

As stated in Chapter 2, due to the presence of off-diagonal couplings in the Z' model, FCNC transitions can occur at tree level. In this regard, to reduce the number of parameters, the $Z - Z'$ mixing and the interaction of right handed quark with Z' are usually ignored [58]. Therefore, Z' boson contribution is only to modify the Wilson coefficients C_9 and C_{10}. With these assumptions, the additional part of the effective Hamiltonian due to the Z' contribution given in Eq. (2.27) can also be written as

$$\begin{aligned}\mathcal{H}_{eff}^{Z'} &= -\frac{2G_F}{\sqrt{2}}\bar{s}\gamma^\mu(1-\gamma^5)b \\ &\times \; B_{sb}\Big[\mathcal{S}_{\ell\ell}^L\bar{\ell}\gamma^\mu(1-\gamma^5)\ell - \mathcal{S}_{\ell\ell}^R\bar{\ell}\gamma^\mu(1+\gamma^5)\ell\Big] + h.c,\end{aligned} \tag{3.1}$$

where B_{sb} is the off diagonal left handed coupling of Z' boson with quarks and $\mathcal{S}_{\ell\ell}^L$ and $\mathcal{S}_{\ell\ell}^R$ represent the left and right handed couplings of Z' boson with leptons, respectively. It is to be noted that if a new weak phase ϕ_{sb} is introduced in the off-diagonal coupling B_{sb} then this coupling could be read as $B_{sb} = \mathcal{R}e(B_{sb})e^{-i\phi_{sb}}$. Therefore, one can also put the above equation in the following form

$$\mathcal{H}_{eff}^{Z'} = -\frac{4G_F}{\sqrt{2}}V_{tb}V_{ts}^*\Big[\Lambda_{sb}C_9^{Z'}Q_9 + \Lambda_{sb}C_{10}^{Z'}Q_{10}\Big] + h.c. \tag{3.2}$$

where

$$\begin{aligned}
\Lambda_{sb} &= \frac{4\pi e^{-i\phi_{sb}}}{\alpha V_{ts}^* V_{tb}} \\
C_9^{Z'} &= \mathcal{R}e(B_{sb}) S_{LL};\ C_{10}^{Z'} = \mathcal{R}e(B_{sb}) D_{LL} \\
S_{LL} &= \mathcal{S}_{\ell\ell}^L + \mathcal{S}_{\ell\ell}^R;\ D_{LL} = \mathcal{S}_{\ell\ell}^L - \mathcal{S}_{\ell\ell}^R
\end{aligned} \tag{3.3}$$

Thus, to include the Z' effects in the problem under consideration one has to make the following replacements in the Wilson coefficients C_9 and C_{10}, while, C_7 remains unchanged

$$\begin{aligned}
C_9^{tot} &= C_9^{eff} + \Lambda_{sb} C_9^{Z'}, \\
C_{10}^{tot} &= C_{10} + \Lambda_{sb} C_{10}^{Z'}.
\end{aligned} \tag{3.4}$$

The matrix elements in the $B \to K^* l^+ l^-$ decay amplitude in Eq. (2.9) can be parameterized in terms of the form factors as follows [59, 25, 32, 60, 61, 62]

$$\begin{aligned}
\langle K^*(k,\epsilon)|\bar{s}\gamma^\mu(1\pm\gamma^5)b|B(p)\rangle &= \mp i q_\mu \frac{2m_{K^*}}{s}\epsilon^*\cdot q\Big[A_3(s) - A_0(s)\Big] \\
&\pm i\epsilon_\mu^*(m_B + m_{K^*})A_1(s) \mp i(p+k)_\mu \epsilon^*\cdot q\frac{A_2(s)}{(m_B+m_{K^*})} \\
&- \epsilon_{\mu\nu\lambda\sigma}p^\lambda q^\sigma \frac{2V(s)}{(m_B+m_{K^*})}
\end{aligned} \tag{3.5}$$

Contracting above equation by q_μ and using the equation of motion, the form factors $A_3(s)$ can be expressed in terms of the $A_1(s)$ and $A_2(s)$ form factors as follows

$$A_3(s) = \frac{m_B + m_{K^*}}{2mK^*}A_1(s) - \frac{m_B - m_{K^*}}{2mK^*}A_2(s) \tag{3.6}$$

and

$$\begin{aligned}
\langle K^*(k,\epsilon)|\bar{s}i\sigma_{\mu\nu}q^\nu(1\pm\gamma^5)b|B(p)\rangle &= 2\epsilon_{\mu\nu\lambda\sigma}p^\lambda q^\sigma F_1(s) \\
&\pm i\left\{\epsilon_\mu^*(m_B^2 - m_{K^*}^2) - (p+k)_\mu\epsilon^*\cdot q\right\}F_2(s) \\
&\pm i\epsilon^*\cdot q\left\{q_\mu - \frac{(p+k)_\mu}{(m_B^2 - m_{K^*}^2)}\right\}F_3(s)
\end{aligned} \tag{3.7}$$

These seven independent form factors $V(s)$, $A_1(s)$, $A_2(s)$, $A_0(s)$, $F_1(s)$, $F_2(s)$ and $F_3(s)$ are the scalar function of the square of the momentum transfer $s = q^2 = (p-k)^2$ and are non-perturbative quantities. These form factors are the main source of hadronic uncertainties and are calculated by different non perturbative schemes such as lattice QCD, Quark model (QM) [63] , perturbative QCD (PQCD) and light cone-QCD sum rules (LCSR)

[64, 65], etc.

By using the matrix elements which are parameterized in terms of the form factors (Eqs. 3.5 and 3.7) with the expression (2.9), the decay amplitude for $B \to K^* l^+ l^-$ can be written as

$$\begin{aligned}
\mathcal{M} &= \frac{\alpha G_F}{4\sqrt{2}\pi} V_{tb}^* V_{ts} \Big[\bar{l}\gamma^\mu (1-\gamma^5) l \times (-2\mathcal{A}\epsilon_{\mu\nu\lambda\sigma}\epsilon^* k^\lambda q^\sigma \\
&\quad -i\mathcal{B}_1 \epsilon_\mu^* + i\mathcal{B}_2 \epsilon^* \cdot q (p+k)_\mu + i\mathcal{B}_0 \epsilon^* \cdot q q_\mu) \\
&\quad + \bar{l}\gamma^\mu (1+\gamma^5) l \times (-2\mathcal{C}\epsilon_{\mu\nu\lambda\sigma}\epsilon^* k^\lambda q^\sigma \\
&\quad -i\mathcal{D}_1 \epsilon_\mu^* + i\mathcal{D}_2 \epsilon^* \cdot q (p+k)_\mu + i\mathcal{D}_0 \epsilon^* \cdot q q_\mu) \Big]
\end{aligned} \tag{3.8}$$

Here the last term in the first line of the above equation will survive only for $\bar{l}\gamma^\mu\gamma^5 l$ due to the fact that $q_\mu(\bar{l}\gamma^\mu\gamma^5 l) = 2m_l(\bar{l}\gamma^5 l)$ and will vanish for $\bar{l}\gamma^\mu l$ because of $q_\mu(\bar{l}\gamma^\mu l) = 0$. However, the auxiliary functions $\mathcal{A}$, $\mathcal{C}$, $\mathcal{B}_1$, $\mathcal{D}_1$, $\mathcal{B}_2$ $\mathcal{D}_2$, $\mathcal{B}_0$ and $\mathcal{D}_0$ contain both long and short distance physics which are encapsulated in the form factors and in the Wilson coefficients, respectively, and can be written in the following form.

$$\begin{aligned}
\mathcal{A} &= 2C_{LL}\mathcal{H}_1 + 4m_b C_7^{eff} \frac{F_1(s)}{s}, \\
\mathcal{B}_1 &= 2C_{LL}\mathcal{H}_3 + \frac{4m_b}{s} C_7^{eff} \mathcal{H}_4 \\
\mathcal{B}_2 &= 2C_{LL}\mathcal{H}_6 + 4\frac{m_b C_7^{eff}}{s} \times \mathcal{H}_5 \\
\mathcal{B}_0 &= \frac{2m_{k^*}}{s}\mathcal{H}_7 - \frac{4m_b}{s} C_7^{eff} F_3(s) \\
\mathcal{C} &= \mathcal{A}(C_{LL} \to C_{LR}) \qquad \mathcal{D}_1 = \mathcal{B}_1(C_{LL} \to C_{LR}) \\
\mathcal{D}_2 &= \mathcal{B}_2(C_{LL} \to C_{LR}) \qquad \mathcal{D}_0 = \mathcal{B}_0(C_{LL} \to C_{LR})
\end{aligned} \tag{3.9}$$

where

$$\begin{aligned}
C_{LL} &= C_9^{tot} - C_{10}^{tot} \qquad C_{LR} = C_9^{tot} + C_{10}^{tot} \\
\mathcal{H}_1 &= \frac{V(s)}{(mB + m_{K^*})} \\
\mathcal{H}_3 &= (m_B + m_{K^*}) A_1(s) \\
\mathcal{H}_4 &= (m_B^2 - m_{K^*}^2) F_2(s) \\
\mathcal{H}_6 &= \frac{A_2(s)}{(mB + m_{K^*})} \\
\mathcal{H}_5 &= \left[F_2(s) + \frac{s}{(m_B^2 - m_{K^*}^2)} F_3(s) \right] \\
\mathcal{H}_7 &= (A_3 - A_0)
\end{aligned} \tag{3.10}$$

3.3 Physical Observables

Now, we have all the ingredients to calculate the physical observables. The double differential decay rate is given in [66]

$$\frac{d^2\Gamma(B \to K^* l^+ l^-)}{d\cos\theta ds} = \frac{1}{2m_B^3}\frac{2\beta\sqrt{\lambda}}{(8\pi)^3}|\mathcal{M}|^2 \tag{3.11}$$

where $\beta \equiv \sqrt{1-\frac{4m_l^2}{s}}$ and $\lambda \equiv m_B^4 + m_{k^*}^4 + s - 2m_B^2 m_{k^*}^2 - 2m_B^2 s - 2m_{k^*}^2 s$. By using the expression of the decay amplitude given in Eq. (3.8) one can get the expression of the dilepton invariant mass spectrum as

$$\frac{d\Gamma(B \to K^* l^+ l^-)}{ds} = \frac{G_F^2\alpha^2\beta\sqrt{\lambda}m_B}{2^{14}\pi^5}|V_{tb}V_{ts}^*|^2\Delta \tag{3.12}$$

where

$$\begin{aligned}
\Delta &= 4(2m_l^2+s)\{\frac{8\lambda}{3}\mathcal{R}e|\mathcal{A}|^2 + \frac{12m_{K^*}^2 s+\lambda}{3m_{K^*}^2 s}\mathcal{R}e|\mathcal{B}_1|^2 \\
&\quad -\frac{(m_B^2-m_{K^*}^2-s)}{3m_{K^*}^2 s}\mathcal{R}e(\mathcal{B}_1\mathcal{B}_2^*) + \frac{\lambda}{3m_{K^*}^2 s}\mathcal{R}e|\mathcal{B}_2|^2\} \\
&\quad +\frac{32\lambda}{3}(s-4m_l^2)\mathcal{R}e|\mathcal{C}|^2 + [\frac{4\lambda(2m^2+s)}{3m_{K^*}^2 s} + 16(s-4m_l^2)] \\
&\quad \times\mathcal{R}e|\mathcal{D}_1|^2 - \frac{4\lambda}{3m_{K^*}^2 s}\{[(2m_l^2+s)(m_B^2-m_{K^*}^2) \\
&\quad +s(s-4m_l^2)]\mathcal{R}e(\mathcal{D}_1\mathcal{D}_2^*) + [6m_l^2 s(2m_B^2+2m_{K^*}^2-s) \\
&\quad +\lambda(2m_l^2+s)]\mathcal{R}e|\mathcal{D}_2|^2 + \frac{8m_l^2\lambda}{m_{K^*}^2}(m_B^2-m_{K^*}^2)\mathcal{R}e(\mathcal{D}_2\mathcal{D}_0^*) \\
&\quad -\frac{8m_l^2\lambda}{m_{K^*}^2}\mathcal{R}e|\mathcal{D}_0|^2
\end{aligned} \tag{3.13}$$

3.3.1 Single Lepton Polarization Asymmetries

In this section we will compute the single lepton polarization asymmetries in the $B \to K^* l^+ l^-$ i.e. the asymmetries where only one of the final state lepton is polarized. For this purpose we first define the six orthogonal vectors belonging to the polarization of l^- and l^+ which we denote here by S_i and W_i respectively where i =L, N and T corresponding to the longitudinally, normally and transversally polarized lepton $l^\pm$ respectively. [27, 67]

$$\begin{aligned}
S_L^\mu &\equiv (0, \mathbf{e}_L^-) = \left(0, \frac{\mathbf{p}_-}{|\mathbf{p}_-|}\right) \\
S_N^\mu &\equiv (0, \mathbf{e}_N^-) = \left(0, \frac{\mathbf{k}\times\mathbf{p}_-}{|\mathbf{k}\times\mathbf{p}_-|}\right) \\
S_T^\mu &\equiv (0, \mathbf{e}_T^-) = (0, \mathbf{e}_N \times \mathbf{e}_L)
\end{aligned} \tag{3.14}$$

$$
\begin{aligned}
W_L^\mu &\equiv (0, \mathbf{e}_L^+) = \left(0, \frac{\mathbf{p}_+}{|\mathbf{p}_+|}\right) \\
W_N^\mu &\equiv (0, \mathbf{e}_N^+) = \left(0, \frac{\mathbf{k}\times\mathbf{p}_+}{|\mathbf{k}\times\mathbf{p}_+|}\right) \\
W_T^\mu &\equiv (0, \mathbf{e}_T^+) = (0, \mathbf{w}_N \times \mathbf{w}_L)
\end{aligned} \tag{3.15}
$$

where p_+, p_- and k denote the three momenta vectors of the final particles l^+, l^- and k respectively. These polarization vectors $S_i^\mu(W_i^\mu)$ in Eqs. (3.14) and (3.15) are defined in the rest frame of $l^-(l^+)$. When we apply lorentz boost to bring these polarization vectors from rest frame of $l^-(l^+)$ to the center of mass frame of final leptons, only the longitudinal polarization four vector is changed while the other two polarization vectors remain unchanged. After this operation the longitudinal four vectors read as

$$
\begin{aligned}
S_L^\mu &= \left(\frac{|p_-|}{m_l}, \frac{E_l\mathbf{p}_-}{m_l|\mathbf{p}_-|}\right) \\
W_L^\mu &= \left(\frac{|p_+|}{m_l}, -\frac{E_l\mathbf{p}_+}{m_l|\mathbf{p}_+|}\right)
\end{aligned} \tag{3.16}
$$

To achieve the polarization asymmetries one can use the spin projectors $\frac{1}{2}(1+\gamma_5 \not{S})$ and $\frac{1}{2}(1+\gamma_5 \not{W})$ for ℓ^- and ℓ^+, respectively. The single lepton polarization asymmetries formula which is given in [67, 68]

$$
P_i^\pm = \frac{\frac{d\Gamma(\mathbf{S}^\pm=\mathbf{e}_i^\pm)}{ds} - \frac{d\Gamma(\mathbf{S}^\pm=-\mathbf{e}_i^\pm)}{ds}}{\frac{d\Gamma(\mathbf{S}^\pm=\mathbf{e}_i^\pm)}{ds} + \frac{d\Gamma(\mathbf{S}^\pm=-\mathbf{e}_i^\pm)}{ds}} \tag{3.17}
$$

where i denotes the L, N and T and $\mathbf{S}^\pm$ is the spin direction of $l^\pm$. The relation between the polarized and unpolarized invariant dilepton mass spectrum for the $B \to K^* l^+ l^-$ read as

$$
\frac{d\Gamma(\mathbf{S}^\pm)}{ds} = \frac{1}{2}\left(\frac{d\Gamma}{ds}\right)\left[1 + (P_L\mathbf{e}_L^\pm + P_N\mathbf{e}_N^\pm + P_T\mathbf{e}_T^\pm)\cdot\mathbf{S}^\pm\right] \tag{3.18}
$$

By using the decay rate which is given in Eq. (3.12) with the polarization vectors defined in Eqs. (3.14-3.16), we get the following expressions for the single lepton polarization asymmetries

$$
\begin{aligned}
P_L(s) &= \frac{16\lambda}{3}\sqrt{s(s-4m_l^2)}\mathcal{R}e(\mathcal{A}\mathcal{C}^*) + \frac{4\sqrt{s-4m_l^2}}{3m_{K^*}^2\sqrt{s}}\{(12m_{K^*}^2 s + \lambda) \\
&\times\mathcal{R}e(\mathcal{B}_1\mathcal{D}_1^*) - \lambda(m_B^2 - m_{K^*}^2 - s)[\mathcal{R}e(\mathcal{B}_1\mathcal{D}_2^*) + \mathcal{R}e(\mathcal{B}_2\mathcal{D}_1^*)] \\
&+\lambda^2\mathcal{R}e(\mathcal{B}_2\mathcal{D}_2^*)\mathcal{R}e|\mathcal{B}_1|^2\}
\end{aligned} \tag{3.19}
$$

$$
\begin{aligned}
P_N(s) &= \frac{4\pi m_l\sqrt{\lambda}}{\sqrt{s}}\{s\mathcal{R}e(\mathcal{A}\mathcal{B}_1^*)+\frac{(m_B^2-m_{K^*}^2-s)}{4m_{K^*}^2}[\mathcal{R}e(\mathcal{B}_1\mathcal{D}_1^*)\\
&\quad -(m_B^2-m_{K^*}^2)\mathcal{R}e(\mathcal{B}_1\mathcal{D}_2^*)+s\mathcal{R}e(\mathcal{B}_1\mathcal{D}_0^*)]\}\\
&\quad -\frac{\lambda}{m_{K^*}^2}\{\mathcal{R}e(\mathcal{B}_2\mathcal{D}_1^*)+(m_B^2-m_{K^*}^2)\mathcal{R}e(\mathcal{B}_2\mathcal{D}_2^*)\\
&\quad +s\mathcal{R}e(\mathcal{B}_2\mathcal{D}_0^*)\}
\end{aligned}
\tag{3.20}
$$

$$
\begin{aligned}
P_T(s) &= 4\pi m_l\sqrt{\lambda(s-4m_l^2)}\{\mathcal{I}m(\mathcal{A}\mathcal{D}_1^*)+\mathcal{I}m(\mathcal{B}_1C^*)\\
&+ \frac{(m_B^2+3m_{K^*}^2-s)}{4m_{K^*}^2}\mathcal{I}m(\mathcal{D}_1\mathcal{D}_2^*)+\frac{(m_B^2-m_{K^*}^2-s)}{4m_{K^*}^2}\\
&\times \mathcal{I}m(\mathcal{D}_1\mathcal{D}_0^*)-\frac{\lambda}{m_{K^*}^2}\mathcal{I}m(\mathcal{D}_2\mathcal{D}_0^*)\}
\end{aligned}
\tag{3.21}
$$

3.3.2 Polarized and Unpolarized CP Asymmetries

The normalized CP violation asymmetries can be defined through the difference of the differential decay rates of particle and antiparticle decay modes as follows [69, 70]

$$
\mathcal{A}_{CP}(\mathbf{S}^{\pm}=\mathbf{e}_i^{\pm})=\frac{\frac{d\Gamma(\mathbf{S}^-)}{ds}-\frac{d\bar{\Gamma}(\mathbf{S}^+)}{ds}}{\frac{d\Gamma}{ds}-\frac{\bar{\Gamma}}{ds}}
\tag{3.22}
$$

where

$$
\begin{aligned}
\frac{d\Gamma}{ds} &= \frac{d\Gamma(B\to K^*\ell^+\ell^-(\mathbf{S}^-))}{ds}\\
\frac{d\bar{\Gamma}}{ds} &= \frac{d\bar{\Gamma}(B\to K^*\ell^+(\mathbf{S}^+))\ell^-}{ds}
\end{aligned}
$$

The differential decay rate of $b\to s\ell^+\ell^-$ is given in Eq. (3.18), analogously the CP conjugated differential decay width can be written as

$$
\frac{d\bar{\Gamma}(\mathbf{S}^{\pm})}{ds}=\frac{1}{2}\left(\frac{d\bar{\Gamma}}{ds}\right)\Big[1+(P_L\mathbf{e}_L^{\pm}+P_N\mathbf{e}_N^{\pm}+P_T\mathbf{e}_T^{\pm})\cdot\mathbf{S}^{\pm}\Big]
\tag{3.23}
$$

It is noted here, that $\frac{d\bar{\Gamma}}{ds}$ belongs to the transition $\bar{b}\to\bar{s}\ell^+\ell^-$ which can be obtained by replacing Λ_{sb} to Λ_{sb}^* in Eq. (3.2). Furthermore, by using the fact that $\mathbf{S}^+=-\mathbf{S}^-$ for L,N and $\mathbf{S}^+=\mathbf{S}^-$ for T we get

$$
\mathcal{A}_{CP}(\mathbf{S}^{\pm}=\mathbf{e}_i^{\pm}) = \frac{1}{2}\Big[\frac{\left(\frac{d\Gamma}{ds}\right)-\left(\frac{d\bar{\Gamma}}{ds}\right)}{\left(\frac{d\Gamma}{ds}\right)+\left(\frac{d\bar{\Gamma}}{ds}\right)}\pm\frac{\left(\frac{d\Gamma}{ds}\right)P_i-\{\left(\frac{d\Gamma}{ds}\right)P_i\}_{\Lambda_{sb}\to\Lambda_{sb}^*}}{\left(\frac{d\Gamma}{ds}\right)+\left(\frac{d\bar{\Gamma}}{ds}\right)}\Big]
$$

(3.24)

where i denotes the L, N or T polarizations of the final state leptons. By using Eq. (3.12) in the above equation, CP violation expression becomes

$$\mathcal{A}_{CP}(\mathbf{S}^{\pm} = \mathbf{e}_i^{\pm}) = \frac{1}{2}\Big[\frac{\Delta - \bar{\Delta}}{\Delta + \bar{\Delta}} \pm \frac{\Delta_i - \bar{\Delta}_i}{\Delta_i + \bar{\Delta}_i}\Big] \tag{3.25}$$

where $\bar{\Delta} = (\Delta)_{\Lambda_{sb}\to\Lambda^*_{sb}}$, $\bar{\Delta}_i = (\Delta_i)_{\Lambda_{sb}\to\Lambda^*_{sb}}$ and

$$\mathcal{A}_{CP}(s) = \frac{\Delta - \bar{\Delta}}{\Delta + \bar{\Delta}}, \quad \mathcal{A}^i_{CP}(s) = \frac{\Delta_i - \bar{\Delta}_i}{\Delta_i + \bar{\Delta}_i} \tag{3.26}$$

so by using these definitions normalized CP violation asymmetry can be written as follows

$$\mathcal{A}_{CP}(\mathbf{S}^{\pm} = \mathbf{e}_i^{\pm}) = \frac{1}{2}\Big[\mathcal{A}_{CP}(s) \pm \mathcal{A}^i_{CP}(s)\Big], \tag{3.27}$$

where the plus sign in the second term of the above expression corresponds to L and N polarizations, whereas the negative sign is for the T polarization.

The first term in $\mathcal{A}_{CP}(s)$ in Eq. (3.27) is the unpolarized CP violation asymmetry, while the second term $\mathcal{A}^i_{CP}(s)$ is called the polarized CP violation asymmetry which provide the modifications to the unpolarized CP violation. After some calculation we have found the following results for $\mathcal{A}_{CP}(s)$ and $\mathcal{A}^i_{CP}(s)$

$$\begin{aligned}
\mathcal{A}_{CP}(s) &= \frac{-4\mathcal{I}m(\Lambda_{sb})\Omega(s)}{2\Delta + 4\mathcal{I}m(\Lambda_{sb})\Omega(s)} \\
\mathcal{A}^i_{CP}(s) &= \frac{-4\mathcal{I}m(\Lambda_{sb})\Omega(s)}{2\Delta + 4\mathcal{I}m(\Lambda_{sb})\Omega^i(s)}
\end{aligned} \tag{3.28}$$

where $i = L, N$ or T, and the explicit expressions of $\Omega(s)$, the $\Omega^i(s)$ are given below

$$\begin{aligned}
\Omega(s) &= \mathfrak{A}_1\mathcal{I}m(C_7 C^*_{9Z'}) + \mathfrak{A}_2\mathcal{I}m(C^*_9 C_{9Z'}) \\
\Omega^L(s) &= \mathfrak{A}_3\{\mathcal{I}m(C_{10Z'}C^*_9) + \mathcal{I}m(C^*_{9Z'}C_{10})\} \\
\Omega^N(s) &= \mathfrak{A}_4\mathcal{I}m(C_7 C^*_{9Z'}) + \mathfrak{A}_5\{\mathcal{I}m(C_{10}C^*_{9Z'})\} \\
&\quad + \mathfrak{A}_6\mathcal{I}m(C^*_9 C_{9Z'}) \\
\Omega^T(s) &= \frac{\beta}{2}\mathfrak{A}_6\{\mathcal{I}m(C_{10}C^*_{9Z'}) + \mathcal{I}m(C_{10Z'}C^*_9)\}
\end{aligned}$$

with

$$
\begin{aligned}
\mathfrak{A}_1 &= \frac{64}{3m_{K^*}^2 s^2} m_b \Big[(\mathcal{H}_3\mathcal{H}_5 + \mathcal{H}_6\mathcal{H}_4)\lambda(m_{K^*}^2 - mB^2 + s) \\
&\quad + (\mathcal{H}_3\mathcal{H}_4 + \mathcal{H}_5\mathcal{H}_6)\lambda + (3\mathcal{H}_3\mathcal{H}_4 + 2\mathcal{H}_1 F_1(s)\lambda) \Big] \\
\mathfrak{A}_2 &= \frac{32(2m_\ell + s)}{3m_{K^*}^2 s} \Big[2\mathcal{H}_3\mathcal{H}_6\lambda(m_{K^*}^2 - mB^2 + s) \\
&\quad + 8\mathcal{H}_1^2 m_{K^*}^2 s\lambda + \mathcal{H}_3^2(12m_{K^*}^2 s + \lambda) + \mathcal{H}_6^2\lambda^2 \Big] \\
\mathfrak{A}_3 &= \frac{32\beta}{3m_{K^*}^2} \Big[2\lambda(mB^2 - m_{K^*}^2 - s)\mathcal{H}_3\mathcal{H}_6 \\
&\quad - \mathcal{H}_3^2(12m_{K^*}^2 s + \lambda) - \lambda(8m_{K^*}^2 s\mathcal{H}_1^2 + \lambda\mathcal{H}_6^2) \Big] \\
\mathfrak{A}_4 &= \frac{128\pi}{\sqrt{s}} m_\ell m_b \sqrt{\lambda} \Big[F_1(s)\mathcal{H}_3 + \mathcal{H}_1\mathcal{H}_4 \Big] \\
\mathfrak{A}_5 &= \frac{8\pi m_\ell \sqrt{\lambda}}{m_{K^*}^2 \sqrt{s}} \Big(\mathcal{H}_6(m_{K^*}^2 - m_B^2) + \mathcal{H}_3 - 2\mathcal{H}_7 \Big) \\
&\quad \times \Big(\mathcal{H}_3(m_{K^*}^2 - mB^2 + s) + \mathcal{H}_6\lambda \Big) \\
\mathfrak{A}_6 &= 128 m_l \pi \sqrt{\lambda s}\mathcal{H}_1\mathcal{H}_3
\end{aligned}
$$

3.4 Phenomenological Analysis

In this section we describe the numerical analysis for the aforementioned observables i.e. the polarized, unpolarized direct CP violation asymmetries and single lepton polarization asymmetries. The input parameters which we have used in the numerical calculations such as masses of particles, life times ,CKM matrix elements etc, are given in Table-3.1, while the Wilson coefficients are displayed in Table-3.2. For the form factors, we rely on the updated results of Light Cone QCD sum rule approach [73]. The values of these form factors and all relevant fitting parameters and their related fit formulas for the decay under consideration $B \to K^* \ell^+ \ell^-$ are recollected in ref [42].

As for as the numerical values of the Z' couplings are concerned, there are several severe constraints from different inclusive and exclusive B decays [55, 42]. These numerical values of coupling parameters of Z' model are recollected in Table-3.3 where $S1$ and $S2$ correspond to two different fittings values for $B_s - \bar{B}_s$ mixing data by the UTfit collaboration [71].

Table 3.1: Default values of input parameters used in the calculations [72]

$m_B = 5.28$ GeV, $m_b = 4.28$ GeV, $m_\mu = 0.105$ GeV,
$m_\tau = 1.77$ GeV, $f_B = 0.25$ GeV, $\lvert V_{tb}V_{ts}^*\rvert = 45 \times 10^{-3}$,
$\alpha^{-1} = 137$, $G_F = 1.17 \times 10^{-5}$ GeV^{-2},
$\tau_B = 1.54 \times 10^{-12}$ sec, $m_{K^*} = 0.892$ GeV, $m_{K_2^*} = 1.43$ GeV.

Before start the numerical analysis, it is better to mention again that S_{LL} and D_{LL} represent the combination of left and right handed couplings of Z' with the leptons and B_{sb} denotes the right handed coupling of Z' with

Table 3.2: The Wilson coefficients C_i^{μ} at the scale $\mu \sim m_b$ in the SM [64].

C_1	C_2	C_3	C_4	C_5	C_6	C_7	C_9	C_{10}
1.107	-0.248	-0.011	-0.026	-0.007	-0.031	-0.313	4.344	-4.669

Table 3.3: The numerical values of the Z' parameters [55, 71].

	$\mathcal{R}e(B_{sb}) \times 10^{-3}$	$\phi_{sb}(inDegree)$	$S_{LL} \times 10^{-2}$	$D_{LL} \times 10^{-2}$
$S1$	1.09 ± 0.22	-72 ± 7	-2.8 ± 3.9	-6.7 ± 2.6
$S2$	2.20 ± 0.15	-82 ± 4	-1.2 ± 1.4	-2.5 ± 0.9

the quarks [see Eq. (3.3)] and in our numerical analysis $S_{LL} = 0$ and $D_{LL} \neq 0$ depict the situation when the new physics comes only from the modification in the Wilson coefficient C_{10}, while, the opposite case, $S_{LL} \neq 0$ and $D_{LL} = 0$, indicates that the new physics is present in the process under consideration due to the change in the Wilson coefficient C_9 [see Eq. (3.4)]. In figs 3.1-3.5 we have displayed the results of single lepton polarization asymmetries as a function of square of the momentum s within the SM and in Z' model. It in important to note here that in all the graphs the solid line correspond to the SM values of observables, while, the other curves correspond to the values of observables when we include the Z' boson effects. With the help of these graphs our findings are in order.

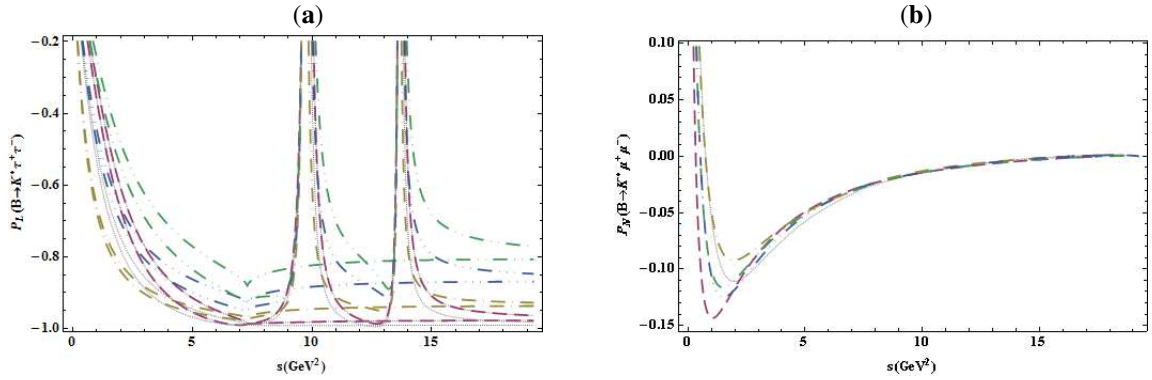

Figure 3.1: (a) Longitudinal and (b) Normal Polarization Asymmetries vs s with different values of Z' couplings in $S1$ and $S2$. Dashed line corresponds to $B_{sb} = 1.31$, $\phi_{sb} = -79°$, $S_{LL} = -6.7$, $D_{LL} = -9.3$. Dashed dotted line corresponds to $B_{sb} = 0.87$, $\phi_{sb} = -65°$, $S_{LL} = 1.1$, $D_{LL} = -4.1$. Dashed double dotted line corresponds to $B_{sb} = 1.09$, $\phi_{sb} = -72°$, $S_{LL} = -2.8$, $D_{LL} = -6.7$. Dashed triple dotted line corresponds to $B_{sb} = 2.05$, $\phi_{sb} = -78°$, $S_{LL} = -2.6$, $D_{LL} = -2.34$

- In figs. 3.1a and 3.1b, the longitudinal P_L and the normal polarization P_N asymmetries, respectively, as a function of s are displayed in the SM and in the Z' model for the case of muons as final sate leptons. To see the influence of Z' boson we have drawn these asymmetries with different values of chiral couplings of Z' for $S1$ and $S2$ which are listed in Table(3.2). These figures show that both the longitudinal and normal polarization asymmetries values are sensitive to the choice of the values of Z' couplings. It can also be noticed from these figures that the values of the longitudinal polarization asymmetries are sensitive throughout the s region while for the normal polarization asymmetry the Z' effects are only prominent in the low s region and vanish for high s region. It is noted here that the transverse polarization asymmetry P_T

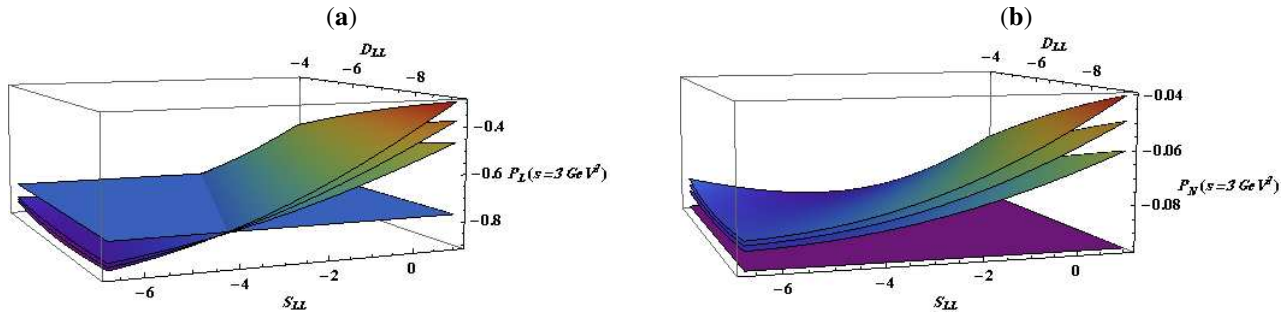

Figure 3.2: Longitudinal and Normal Polarization Asymmetries in $S1$ at $s = 3$ GeV^2, here the flat curves correspond to the SM values of P_L and P_N.

is too tiny both in the SM and the Z' new physics.

It is important to mention here that in order to show the uncertain non-perturbative kinematical region (7 GeV$^2 \leq s \leq 12$ GeV^2), we have also plotted P_L with charmed resonances (J/ψ) in fig. 3.1a. It is clear from fig 3.1a that in the resonance region we cannot rely on the predictions obtained by just taking into account perturbative contributions, however, one can also see from fig 3.1a that the effects are also well prominent and distinguished from the SM in the regions which are below (1 GeV$^2 \leq s \leq 6$ GeV^2) and above ($s \geq 14.4$ GeV^2) the resonance region.

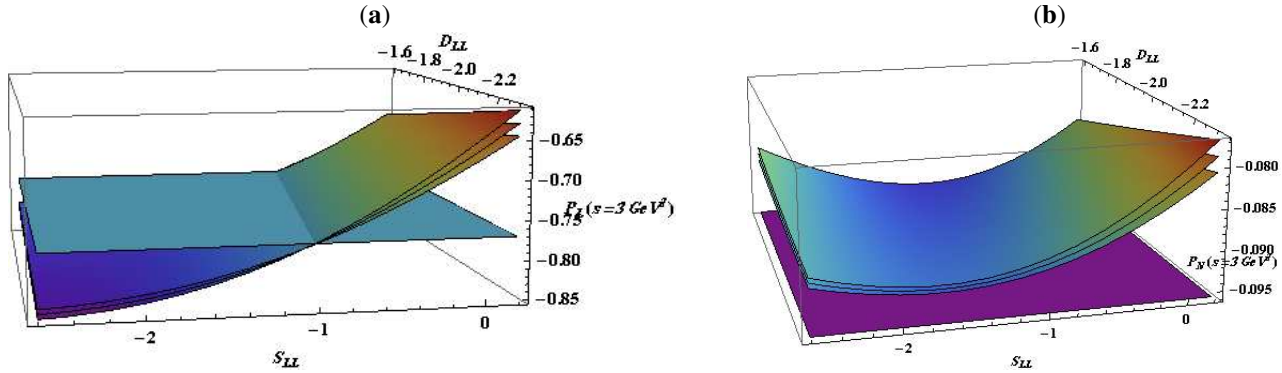

Figure 3.3: Legends are same as in fig. 3.2 but for $S2$.

- We have also plotted 3-dimensional graphs of P_L and P_N at $s = 3$GeV^2 (which is well below the resonance region) against the D_{LL} and S_{LL} in figs. 3.2 and 3.3 for S1 and S2, respectively for $B \to K^*\mu^+\mu^-$. From these graphs, one can clearly see the variation in the values of P_L upon varying the values of Z' couplings. For instance, from fig 3.2a one can extract that the SM value of P_L at $s = 3$GeV^2 is 0.76 which can be reduced up to 60% when we set $B_{sb} = 1.31 \times 10^{-3}$, $D_{LL} = -9.3$ and $S_{LL} = 1.1$. It is important to mention here that the values of P_L and P_N are insensitive to the value of new weak phase ϕ_{sb}.

- In fig. 3.4 the longitudinal polarization of $B \to K^*\tau^+\tau^-$ is portrayed against s. Similar to the case of muons the effects of Z' are also prominent, particularly, at high value of s which is far above the resonance region. From this graph it can be seen that the maximum value of P_L which lies at s_{max} can be increased

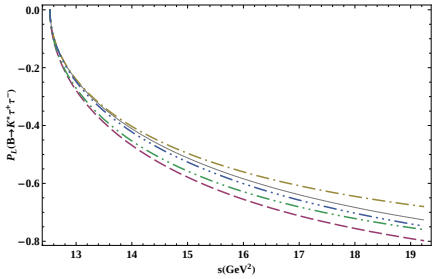

Figure 3.4: Legends are same as in fig. 3.1 but for the case of $\tau^+\tau^-$.

or decreased when we change the values of coupling parameters of Z' boson. As for the previous case of muons, the value of these asymmetry is also not sensitive to the value of new weak phase ϕ_{sb}.

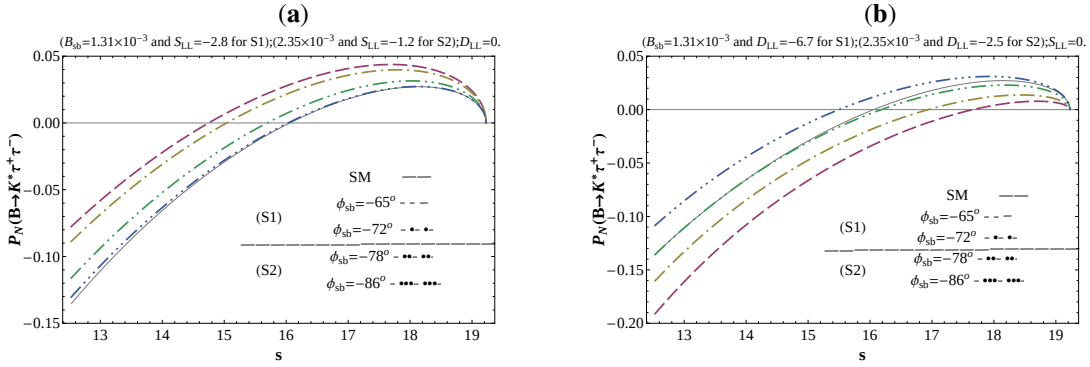

Figure 3.5: Normal Polarization Asymmetry as a function of s (a) for $S1$ and (b) for $S2$ with different values of Z' parameters.

- The normal polarization asymmetry P_N as a function of s for the case of tauons are shown in figs. 3.5a and 3.5b for $S_{LL} = 0$ and $D_{LL} = 0$, respectively, with different values of B_{sb} and new weak phase ϕ_{sb}. We have found that P_N is an interesting observable because the Z' effects are comparatively well prominent from the muon case (see fig. 3.1b) throughout the available kinematical space as well as its value is dependent on the new weak phase ϕ_{sb}. Fig. 3.5a depicts that due to the Z' effects the zero crossing of the asymmetry which lies approximately at 16GeV^2 is shifted towards lower values of s for both $S1$ and $S2$ when we decrease the value of new weak phase ϕ_{sb}. Furthermore, the maximum value of $P_N = 0.14$ lies at s_{min} reduced up to 43% when we set the value of $\phi_{sb} = -65°$. Similarly, due to the change in the value of ϕ_{sb} on setting $S_{LL} = 0$ the zero crossing of P_N is shifted towards left (right) for $S1$ ($S2$) as depicted in fig. 3.5b, while for the maximum value -0.14 is increased (decreased) for $S1$ ($S2$).

The average values of asymmetries are also very important tool to probe new physics and can be obtained by the following formula

$$\langle P_i \rangle = \frac{\int_{4m_l^2}^{(m_B^2 - m_{k^*}^2)} P_i \frac{d\Gamma}{ds} ds}{\int_{4m_l^2}^{(m_B^2 - m_{k^*}^2)} \frac{d\Gamma}{ds} ds} \tag{3.29}$$

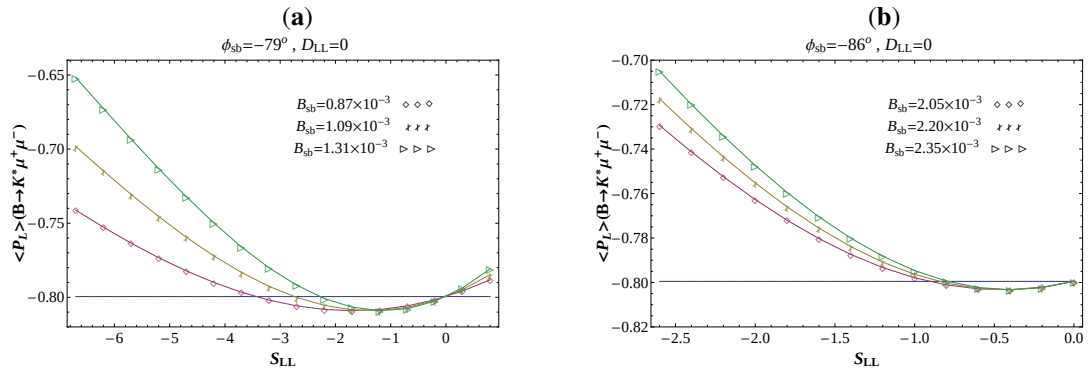

Figure 3.6: Average value of the Longitudinal Polarization Asymmetries $\langle P_L \rangle$ as a function of S_{LL} (a) in $S1$ and (b) in $S2$.

Table 3.4: Numerical values of $\langle P_L \rangle$ in Z' model for scenario-I

		$\langle P_L \rangle$ at $D_{LL} = 0$				$\langle P_L \rangle$ at $S_{LL} = 0$			
ϕ_{sb} in Degree	Decay Channel	S_{LL} −6.7		S_{LL} 1.1		D_{LL} −9.3		D_{LL} −4.1	
		B_{sb} = 0.87	1.31	0.87	1.31	0.87	1.31	0.87	1.31
−65°	$B \to K^*\mu^+\mu^-$	-0.785	-0.715	-0.774	-0.757	-0.597	-0.485	-0.731	-0.679
	$B \to K^*\tau^+\tau^-$	-0.423	-0.347	-0.526	-0.519	-0.515	-0.476	-0.538	-0.532
−79°	$B \to K^*\mu^+\mu^-$	-0.741	-0.651	-0.782	-0.772	-0.573	-0.442	-0.728	-0.669
	$B \to K^*\tau^+\tau^-$	-0.443	-0.354	-0.517	-0.506	-0.454	-0.394	-0.509	-0.490

Now we discuss the variation in the average values of single lepton polarization asymmetries $\langle P_i \rangle$, where $i = L, N$ or T, due to the influence of Z' boson effect. To achieve this purpose, we have displayed $\langle P_L \rangle$, $\langle P_N \rangle$ and $\langle P_T \rangle$ in figures 3.6-3.11 against the different coupling parameters of Z' models. From these graphs we have found the following results

- In figs. 3.6 and 3.7 we have plotted $\langle P_L \rangle$ for the case of muons and tauons as final state leptons, respectively, as a function of S_{LL} with the different values of Z' parameters where fig. a (b) correspond to $S1$ ($S2$). It is important to note here that the average value of P_L is not much affected due to the variation in the D_{LL} values. For this reason, we have not plotted $\langle P_L \rangle$ against D_{LL}. However, one can easily see from figures 3.6 and 3.7 that for the small values of S_{LL} the variation in the $\langle P_L \rangle$ is not much significant but when we increase the value of S_{LL}, the value of $\langle P_L \rangle$ is decreased accordingly for both muon and tauons in both the scenarios $S1$ and $S2$.

  On the other hand to see the dependence of $\langle P_L \rangle$ on new weak phase ϕ_{sb} we have listed its values with the different Z' parameters in Tables-3.4 (3.5) for $S1$ ($S2$). From these tables one can extract the variation in the values of $\langle P_L \rangle$ due to the change in the values of ϕ_{sb} by keeping the other parameters of Z' to be fixed.

- For $\langle P_N \rangle$, it should be noted here that the SM value of $\langle P_N \rangle$ is +0.01 and due to the influence of Z' boson it will become too suppressed to be measured. On the other hand for the case of tauons $\langle P_N \rangle$ is displayed vs S_{LL} in figs. 3.8a (3.8b) for $S1$ (S2), respectively. It is also worthwhile to mention here that similar to the case of $\langle P_L \rangle$, we have found that the value of $\langle P_N \rangle$ is mildly dependent on the value of D_{LL}. However,

Table 3.5: Numerical values of $\langle P_L \rangle$ in Z' model for scenario-II

		$\langle P_L \rangle$ at $D_{LL} = 0$				$\langle P_L \rangle$ at $S_{LL} = 0$			
ϕ_{sb} in Degree	Decay Channel	S_{LL} −2.6		S_{LL} 0.2		D_{LL} −2.34		D_{LL} −1.6	
		B_{sb} = 2.05	2.35	2.05	2.35	2.05	2.35	2.05	2.35
−65°	$B \to K^* \mu^+ \mu^-$	-0.795	-0.780	-0.790	-0.788	-0.696	-0.675	-0.539	-0.537
	$B \to K^* \tau^+ \tau^-$	-0.437	-0.451	-0.531	-0.531	-0.535	-0.532	-0.539	-0.537
−79°	$B \to K^* \mu^+ \mu^-$	-0.754	-0.733	-0.793	-0.792	-0.689	-0.665	-0.736	-0.722
	$B \to K^* \tau^+ \tau^-$	-0.458	-0.434	-0.527	-0.526	-0.496	-0.488	-0.511	-0.507

figures 3.8a and 3.8b depict that for both $S1$ and $S2$ the $\langle P_N \rangle$ crosses zero and become positive at a particular value of S_{LL} which shift towards the lower value of S_{LL} when we increase the value of B_{sb}. One can also find from figs 3.8a (3.8b) that on setting the maximum values of Z' boson couplings the SM value -0.021 of $\langle P_N \rangle$ is reached up to +0.1 (+0.06) for $S1$ ($S2$). Therefore, the measurement of magnitude and sign of $\langle P_N \rangle$ is valuable to determine the exact values of Z' couplings.

- In the same way, we have also drawn the explicit dependence of $\langle P_N \rangle$ (when tauons are the final state leptons) on ϕ_{sb} for $S1$ and $S2$ in figs. 3.9a and 3.9b, respectively, where $S_{LL} = 0$ and D_{LL} is fixed to be its central value -6.7 for $S1$ and -2.5 for $S2$. It can be easily seen from these figures that in $S1$ ($S2$) the value of $\langle P_N \rangle$ is increased (decreased) when we decrease (increase) the value of new weak phase ϕ_{sb}. For instance at $\phi_{sb} = -65°$ ($-86°$) and $B_{sb} = 1.31 \times 10^{-3}$ (2.35×10^{-3}), the deviation in $\langle P_N \rangle$ from its SM value is about 62% (67%) for $S1$ (S2), while, the deviation in the value of $\langle P_N \rangle$ is not significant from its SM value when we take $\phi_{sb} = -79°$ ($-78°$). One last comment on $\langle P_N \rangle$ is that if we put $D_{LL} = 0$ and set S_{LL} to be non zero then $\langle P_N \rangle$ is not much sensitive to the value of new weak phase ϕ_{sb}. Thus, the normal polarization asymmetry when the tauons are the final state lepton is an interesting observable to constraint the Z' boson couplings as well as to determine the accurate value of new weak phase ϕ_{sb}.

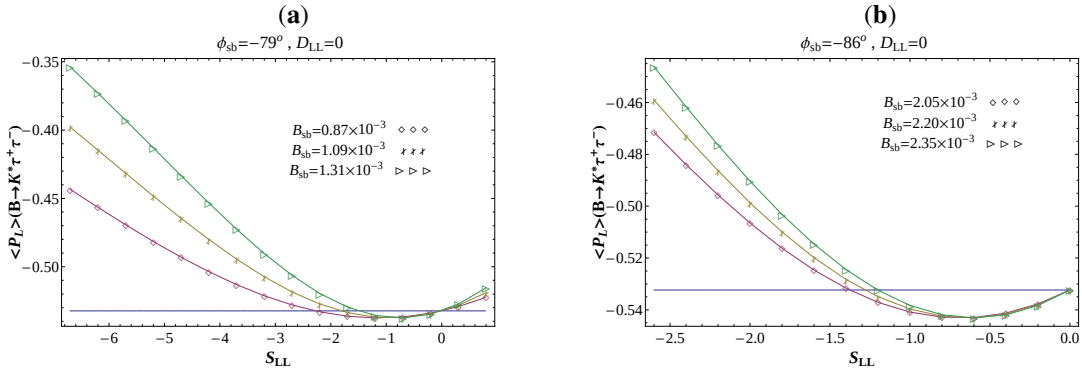

Figure 3.7: Legends are same as fig. 3.6 but for $B \to K^* \tau^+ \tau^-$.

- Average transverse polarization asymmetry $\langle P_T \rangle$ is depicted in figs. 3.10 and 3.11 only for $B \to K^* \tau^+ \tau^-$ since for the case of muons its SM value is too tiny to be measured and not become large enough to reach the visible range due to the influence of Z' boson contribution. In contrast to the case of $\langle P_L \rangle$ and $\langle P_N \rangle$ which

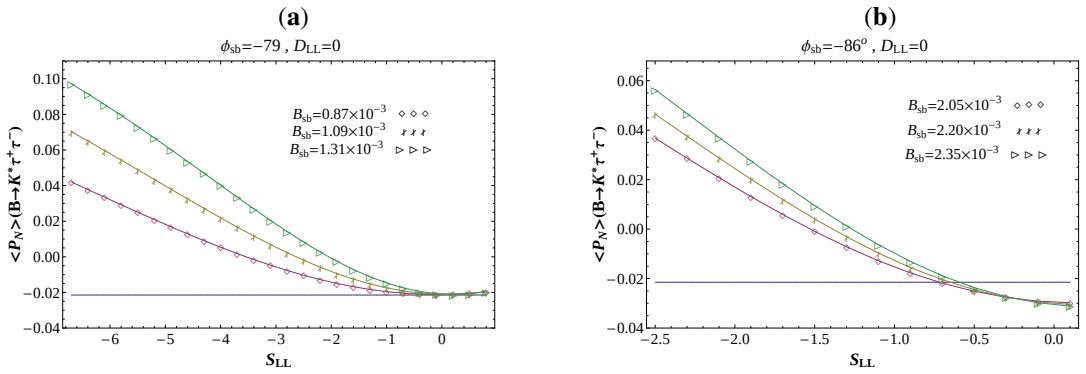

Figure 3.8: The average value of Normal Polarization Asymmetry P_N as a function of S_{LL} for $B \to K^*\tau^+\tau^-$ (a) for $S1$ and (b) for $S2$.

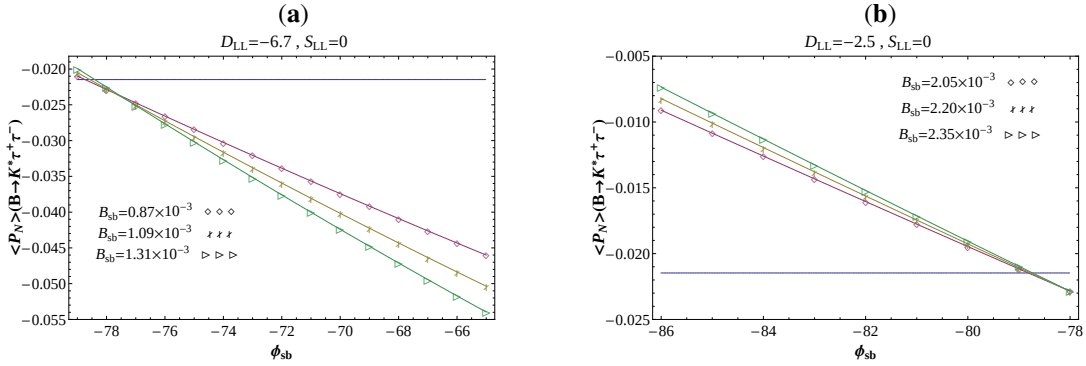

Figure 3.9: Legends are same as in fig. 3.8 but as a function of ϕ_{sb}.

are mildly effected by the variation in the value of D_{LL}, we have found that the value of $\langle P_T \rangle$ is sensitive to D_{LL}. Therefore, we have also shown the explicit dependence of $\langle P_T \rangle$ on D_{LL} in figure 3.11 along with the S_{LL} dependence which is shown in figure 3.10. One immediate look on these figures tells us that though the dependence of $\langle P_T \rangle$ on D_{LL} is not as strong as on S_{LL} but significantly enough to be observed. Furthermore, $\langle P_T \rangle$ is an increasing function of D_{LL} throughout the allowed region of D_{LL} for both $S1$ and $S2$. On the other hand for S_{LL} the $\langle P_T \rangle$ behavior is approximately similar to the $\langle P_N \rangle$ case but with the opposite sign which we have discussed above. However, $\langle P_T \rangle$ is insensitive to the new weak phase ϕ_{sb}.

Now we turn our attention to analysis of another interesting observable i.e. CP violation. As we have mentioned earlier in the introduction that for $b \to s\ell^+\ell^-$ transition the value of CP violation is negligible and any measurement of this observable is a clear sign of new physics. However, we have found that both the polarized and unpolarized CP violation asymmetries for $B \to K^*\mu^+\mu^-$ are suppressed in the SM and in the Z' model. Similarly, CP violation when one of the final state tauon is transversely polarized is also found to be suppressed and therefore, we do not include these asymmetries in our numerical discussion. The other CP asymmetries $\mathcal{A}_{CP}$ and $\mathcal{A}^i_{CP}$ (where $i = L, N$) for $B \to K^*\tau^+\tau^-$ are displayed in figs. 3.12 to 3.15 and their analysis is given in the following points.

- We have found that the value of direct unpolarized CP violation asymmetry $\mathcal{A}_{CP}$ is not significantly changed

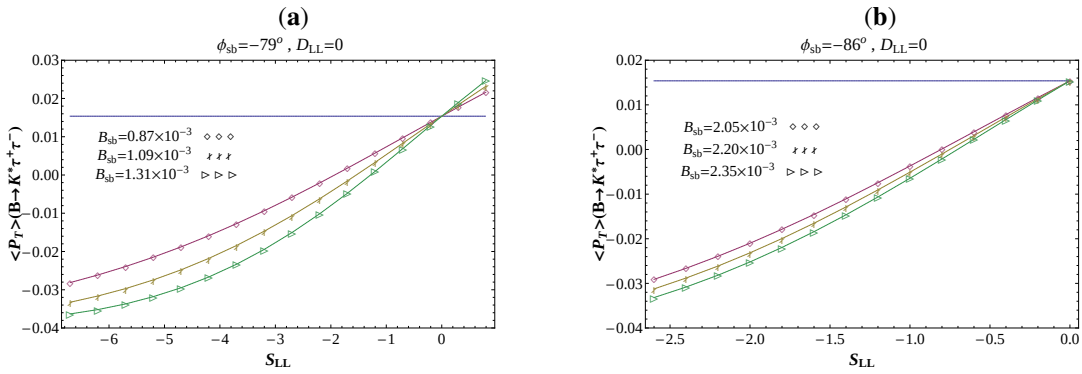

Figure 3.10: Legends are same as in fig. 3.8 but for $\langle P_T \rangle$.

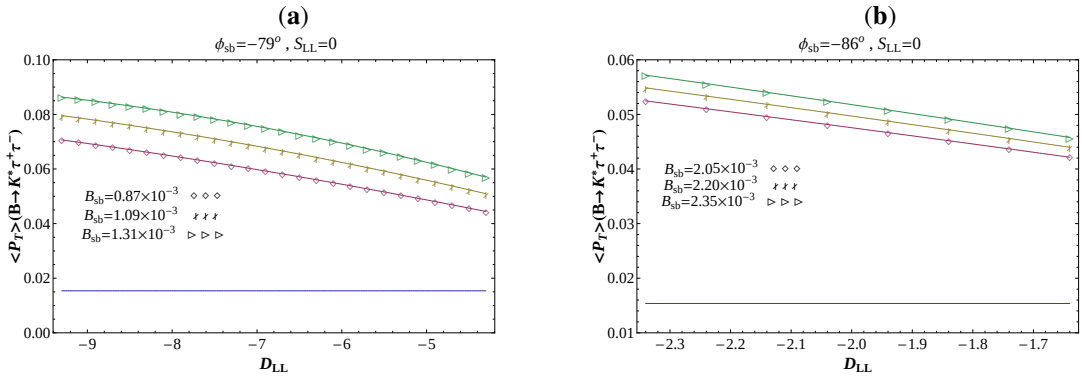

Figure 3.11: The average value of transverse polarization asymmetry $\langle P_T \rangle$ as a function of D_{LL} for $B \to K^*\tau^+\tau^-$ (a) for $S1$ and (b) for $S2$.

when we change the values of new weak phase ϕ_{sb} and D_{LL} but strongly depend on the value of S_{LL} and mildly depend on B_{sb} as can be seen from figs. 3.12a and 3.12b for $S1$ and $S2$, respectively. It is also noted from these figures that for both $S1$ and $S2$ the $\mathcal{A}_{CP}$ is an increasing function of S_{LL}.

- The longitudinally polarized CP asymmetry $\mathcal{A}_{CP}^{L}$ is drawn in figs 3.13a and 3.13b for $S1$ and $S2$, respectively. In contrast to the $\mathcal{A}_{CP}$ it is found that the $\mathcal{A}_{CP}^{L}$ is almost insensitive to the value of S_{LL} but sensitive to the values of D_{LL} and B_{sb}. It is also important to point out here that similar to the case of $\mathcal{A}_{CP}$, the value of $\mathcal{A}_{CP}^{L}$ is very mildly affected due to change in the value of ϕ_{sb}. Furthermore, the value of $\mathcal{A}_{CP}^{L}$ is increased with the increment in the values of D_{LL} and B_{sb}. For instance, from a closer look on fig 3.13a one can extract that at $B_{sb} = 0.87 \times 10^{-3}$ and $D_{LL} = -4.1$ the value of $\mathcal{A}_{CP}^{L}$ is approximately 0.035 which is enhanced up to 0.09 when we set $B_{sb} = 1.31 \times 10^{-3}$ and D_{LL} to be -9.3.

- In contrast to $\mathcal{A}_{CP}$ and $\mathcal{A}_{CP}^{L}$ the $\mathcal{A}_{CP}^{N}$ is sensitive for both S_{LL} and D_{LL}. The behavior of $\mathcal{A}_{CP}^{N}$ as a function of $S_{LL}(D_{LL})$ is depicted in figs. 3.14a (b) and 3.15a (b) for $S1$ and $S2$, respectively. These figures represent that the value of $\mathcal{A}_{CP}^{N}$ is positive when we put $S_{LL} = 0$ and negative when we put $D_{LL} = 0$; however, in both cases the $\mathcal{A}_{CP}^{N}$ is an increasing function of S_{LL} and D_{LL}.

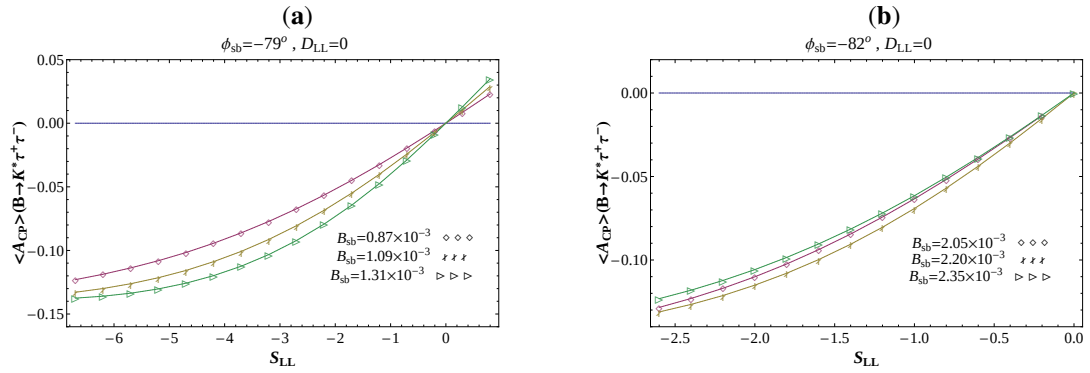

Figure 3.12: Unpolarized CP violation asymmetry $\mathcal{A}_{CP}$ as function of S_{LL} for $B \to K^*\tau^+\tau^-$ (a) for $S1$ and (b) for $S2$.

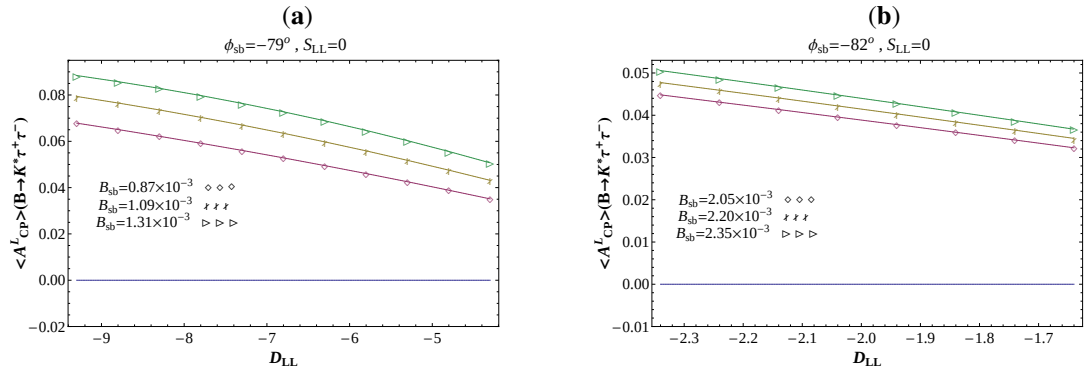

Figure 3.13: Longitudinally polarized CP violation asymmetry $\mathcal{A}^L_{CP}$ as a function of D_{LL} for $B \to K^*\tau^+\tau^-$ (a) for $S1$ and (b) for $S2$.

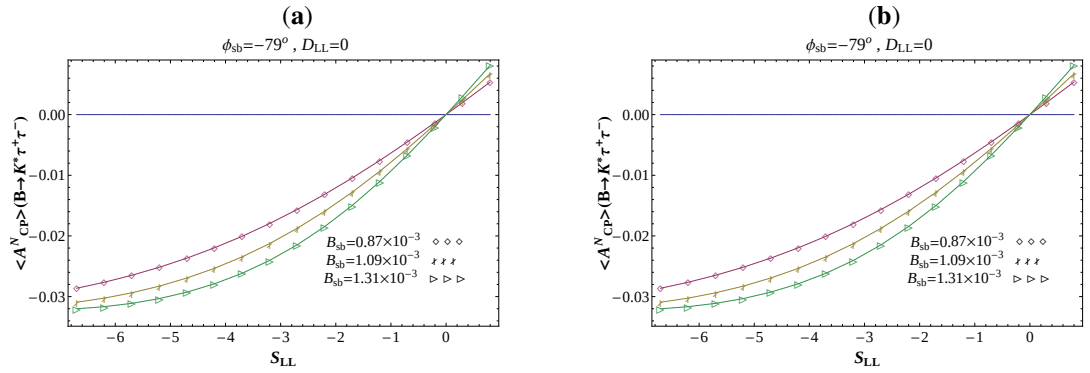

Figure 3.14: Normally polarized CP violation asymmetry for $B \to K^*\tau^+\tau^-$ in $S1$ (a) as a function of D_{LL} (b) as a function of S_{LL}.

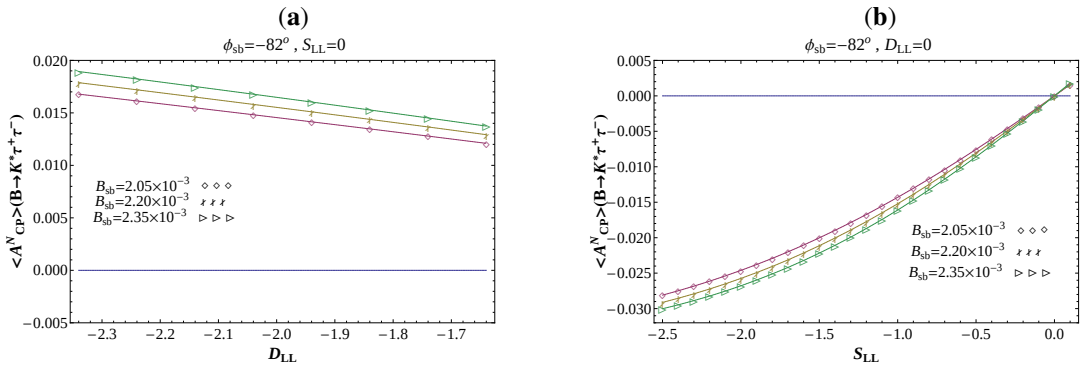

Figure 3.15: Legends are same as in fig. 3.14 but for $S2$.

3.5 Summary and Conclusion

In this chapter we have analyzed the influence of non-universal Z' model to the $B \to K^* \ell^+ \ell^-$ decay. For this purpose we have calculated CP violation and single lepton polarization asymmetries. To calculate the numerical values of these observables we rely on the LCSR form factors which are given in [73]. As we have mentioned in the introduction, the CP asymmetries for $b \to s\ell^+\ell^-$ are very tiny to be measurable experimentally, so, their measurements at current colliders would be clear indication of NP. In this context the unpolarized and polarized CP violation asymmetries are calculated for the above mentioned decay channel in Z' model. It is found that in this model the CP violation asymmetries $\mathcal{A}_{CP}$, $\mathcal{A}_{CP}^L$ and $\mathcal{A}_{CP}^N$ are considerably enhanced for the case when tauons are the final state leptons, while, for the case of muons CP asymmetries remain suppresed. It is also found that the unpolarized CP violation is not sensitive to the D_{LL} while its value is decreased when we increase the value of S_{LL} coupling of Z' . In contrast to the unpolarized CP violation, the longitudinally polarized CP violation $\mathcal{A}_{CP}^L$ is not much sensitive to the S_{LL} but sensitive to other couplings and similar to the case of unpolarized CP violation asymmetry its value is also increased when we increase the values of the couplings. On the other hand the value of $\mathcal{A}_{CP}^N$ is sensitive for all the couplings present in the Z' model. However, the dependence of these CP asymmetries on the value of new weak phase ϕ_{sb} is very mild.

Apart from the CP violation asymmetries, the single lepton polarization asymmetries are also analyzed in the presence of Z' boson. It is shown in this study that the values of P_i and $\langle P_i \rangle$ significantly deviate from their SM values where one can fix the parameters of Z' model. It is also shown that the longitudinal polarization asymmetry for both muons and tauons and the normal polarization only for tauons are sensitive to the new weak phase ϕ_{sb}. Therefore, the behavior of single lepton polarization asymmetries under the presence of Z' boson depict that precise measurements of these asymmetries may help to yield the accurate values of new weak phase ϕ_{sb} and its coupling with the fermions.

Finally, to measure the asymmetries of order 0.01 relative to the branching ratio of order 10^{-6} at 3σ level needs approximately 10^{10} to 10^{11} $B\bar{B}$ pairs (see last reference of [70]) and in LHC 10^8 to 10^{12} $B\bar{B}$ pairs are expected to be produced. Henceforth, the precise measurements of both the CP violation and lepton polarization asymmetries for $B \to K^* \ell^+ \ell^-$ would seen to be possible at LHC which are very promising handy tool to extract out the imprints of Z' boson at low energy level.

Chapter 4

Model Independent Analysis of the Forward-Backward Asymmetry for the $B \to K_1 \mu^+ \mu^-$ Decay

4.1 Introduction

As we have seen that in SM the decay $B \to K^* l^+ l^-$ is completely determined by the Wilson coefficients of only three operators Q_7, Q_9 and Q_{10} which are evaluated at the scale $\mu = m_b$ [74]. On the other hand the most general analysis of these decays needs other set of new operators which are based on the the general four-fermion interactions. In the literature, the model independent analysis of the quark level $b \to s l^+ l^-$ decay, in terms of 10 new types of local four fermion interactions, has been performed in Ref. [75, 76] which is then applied to the systematic study of $B \to (K, K^*) l^+ l^-$ [77].

Like $B \to K^* l^+ l^-$ the semileptonic decay $B \to K_1(1270) l^+ l^-$ is also governed by the quark level transition $b \to s l^+ l^-$. Analysis of this decay process will be a useful complement to the widely investigated analysis for the $B \to K^* l^+ l^-$ process, since the analysis probes the effective Hamiltonian in a similar but not identical way. Compared to $B \to K^* l^+ l^-$ the situation is complicated in the decay $B \to K_1(1270) l^+ l^-$, because the axial vector states $K_1(1270)$ and $K_1(1400)$ are the mixtures of ideal ${}^1P_1(K_{1A})$ and ${}^3P_1(K_{1B})$ orbital angular momentum states and current limit on the mixing angle is [78]

$$\theta = -(34 \pm 13)^o. \tag{4.1}$$

Recently, some studies have been made on $B \to K_1$ transitions both by incorporating the mixing angle as well as with out it [79]. Moreover, it is also shown in ref [80] that the zero position of the forward-backward asymmetry

mildly depend on the mixing angle for $B \to K_1(1270)l^+l^-$. Therefore, significant shift in the zero position of the forward-backward asymmetry would clearly give a signature of NP.

Regarding the experimental point of view the radiative decay $B \to K_1(1270)\gamma$ has already seen by Belle. The related decay with a lepton pair instead of a photon in the final state can also be expected to be observed at LHC [81] and SuperB factory [82]. In particular LHCb experiment at the LHC where estimates made in [81, 85] for LHCb collaboration show that with an integrated luminosity of $2fb^{-1}$, one may expect almost 8000 $B \to K^*l^+l^-$ events. As, the branching ratio of $B \to K_1(1270)l^+l^-$ is comparable to that of $B \to K^*l^+l^-$, therefore one can expect significant number of events for this decay and hence making analysis of FB asymmetry for this decay will be experimentally meaningful for comparison with the SM and the theories beyond it.

In this chapter, our aim is to analyze the possible new physics effects stemming from the new structures in the effective Hamiltonian [76] to the forward-backward asymmetry for the $B \to K_1(1270)l^+l^-$ decay. It is known that the forward-backward asymmetry becomes zero for a particular value of the dilepton invariant mass. In the SM, the zero position of the $\mathcal{A}_{FB}(q^2)$ appears in the low q^2 region, sufficiently away from the charm resonance region and is almost free from the hadronic uncertainties (i.e. the choice of form factors) as well as those from the mixing angle. Now this zero position of $\mathcal{A}_{FB}$ an important tool to search for physics beyond the SM. The organization of the chapter is as follows: In section 4.2 we introduce the model independent effective Hamiltonian and obtain the transition matrix elements in terms of form factors of the $B \to K_1(1270)l^+l^-$. Section 4.3 describes the formulas that can be used to determine the zero position of the FBA. In Sec. 4.4 we present our numerical analysis and Sec. 4.5 summarizes our conclusion.

4.2 Model Independent Effective Hamiltonian and Matrix Elements

The exclusive $B \to K_1(1270)l^+l^-$ decay involves the hadronic matrix elements of quark operators given in Eq. (2.9) and Eq. (2.23) which one can be parametrize in terms of the form factors as follows:

$$\begin{aligned}
\left\langle K_1(k,\varepsilon)\left|V_\mu\right|B(p)\right\rangle &= \varepsilon_\mu^*\left(M_B + M_{K_1}\right)V_1(s) \\
&\quad -(p+k)_\mu\left(\varepsilon^*\cdot q\right)\frac{V_2(s)}{M_B + M_{K_1}} \\
&\quad -q_\mu\left(\varepsilon\cdot q\right)\frac{2M_{K_1}}{s}\left[V_3(s) - V_0(s)\right] \qquad (4.2)\\
\left\langle K_1(k,\varepsilon)\left|A_\mu\right|B(p)\right\rangle &= \frac{2i\epsilon_{\mu\nu\alpha\beta}}{M_B + M_{K_1}}\varepsilon^{*\nu}p^\alpha k^\beta A(s) \qquad (4.3)
\end{aligned}$$

where $V_\mu = \bar{s}\gamma_\mu b$ and $A_\mu = \bar{s}\gamma_\mu\gamma_5 b$ are the vectors and axial vector currents respectively. Also $p(k)$ are the momentum of the $B(K_1)$ meson and ε_μ^* is the polarization of the final state axial vector K_1 meson. In Eq.(4.2) we have

$$V_3(s) = \frac{M_B + M_{K_1}}{2M_{K_1}}V_1(s) - \frac{M_B - M_{K_1}}{2M_{K_1}}V_2(s) \qquad (4.4)$$

with

$$V_3(0) = V_0(0)$$

Further, there is also a contribution from the Penguin form factors that can be written as

$$\begin{aligned}\left\langle K_1(k,\varepsilon)\left|\bar{s}i\sigma_{\mu\nu}q^\nu b\right|B(p)\right\rangle &= \left[\left(M_B^2 - M_{K_1}^2\right)\varepsilon_\mu - (\varepsilon\cdot q)(p+k)_\mu\right]F_2(s) \\ &\quad +(\varepsilon^*\cdot q)\left[q_\mu - \frac{s}{M_B^2 - M_{K_1}^2}(p+k)_\mu\right]F_3(s) \end{aligned} \tag{4.5}$$

$$\left\langle K_1(k,\varepsilon)\left|\bar{s}i\sigma_{\mu\nu}q^\nu\gamma_5 b\right|B(p)\right\rangle = -i\epsilon_{\mu\nu\alpha\beta}\varepsilon^{*\nu}p^\alpha k^\beta F_1(s) \tag{4.6}$$

By contracting Eq. (4.2) with q_μ and making use of the equation of motions

$$q^\mu(\bar{\psi}_1\gamma_\mu\psi_2) = (m_2 - m_1)\bar{\psi}_1\psi_2 \tag{4.7}$$

$$q^\mu(\bar{\psi}_1\gamma_\mu\gamma_5\psi_2) = -(m_1 + m_2)\bar{\psi}_1\gamma_5\psi_2 \tag{4.8}$$

we have

$$\langle K_1(k,\varepsilon)|\bar{s}(1\pm\gamma_5)b|B(p)\rangle = \frac{1}{m_b + m_s}\left\{\mp 2iM_{K_1}(\varepsilon^*\cdot q)V_0(s)\right\} \tag{4.9}$$

The form factors for $B \to K_1(1270)$ transition are the non-perturbative quantities and are needed to be calculated using different approaches (both perturbative and non-perturbative) like Lattice QCD, QCD sum rules, Light Cone sum rules, etc. As the zero position of the forward-backward asymmetry depends on the short distance contribution i.e. the Wilson coefficients and is independent from the long distance contribution (Form factors) [83] as well as on the mixing angle between $^1P_1$ and $^3P_1$ states. We will consider the form factors that were calculated using Ward Identities in Ref. [83] which can be summarized as follows:

$$\begin{aligned} A(s) &= \frac{A(0)}{(1 - s/M'^2_{B_S})(1 - s/M'^2_{B_{SA}})} \\ V_1(s) &= \frac{V_1(0)}{(1 - s/M^2_{B_A^*})(1 - s/M'^2_{B_A^*})}\left(1 - \frac{s}{M_B^2 - M_{K_1}^2}\right) \\ V_2(s) &= \frac{\tilde{V}_2(0)}{(1 - s/M^2_{B_A^*})(1 - s/M'^2_{B_A^*})} - \frac{2M_{K_1}}{M_B - M_{K_1}}\frac{V_0(0)}{(1 - s/M_B^2)(1 - s/M'^2_B)} \end{aligned} \tag{4.10}$$

with

$$\begin{aligned} V_0(0) &= 0.36 \pm 0.03 \\ A(0) &= -(0.52 \pm 0.05) \end{aligned} \tag{4.11}$$

$$
\begin{aligned}
V_1(0) &= -(0.24 \pm 0.02) \\
\tilde{V}_2(0) &= -(0.39 \pm 0.05)
\end{aligned}
\tag{4.12}
$$

4.3 Forward backward asymmetry for $B \to K_1(1270) l^+ l^-$

In this section, we are going to perform the calculation of the forward-backward asymmetry. From Eq. (2.22) and by using the matrix elements given in Eqs. (4.2-4.9), it is straightforward to obtain the decay amplitude for $B \to K_1(1270) l^+ l^-$ as

$$
\mathcal{M}_{B\to K_1(1270)l^+l^-} = \frac{G_F \alpha}{4\sqrt{2}\pi} V_{tb} V_{ts}^* M_B \left\{ \begin{array}{c} T_\mu^1 \bar{l}\gamma^\mu l + T_\mu^2 \bar{l}\gamma^\mu\gamma^5 l + T^3 \bar{l} l + T^4 \bar{l}\gamma^5 l \\ +8C_T(\bar{l}\sigma^{\mu\nu} l)(-2F_1(\hat{s})\,\varepsilon^{*\mu}(\hat{p}_B + \hat{p}_{K_1})^\mu + J_1' \varepsilon^{*\mu}\widehat{q}^\nu - J_2'(\varepsilon^* \cdot \widehat{q})\,\hat{p}_{K_1}^\mu \widehat{q}^\nu) \\ +2iC_{TE}\epsilon_{\mu\nu\alpha\beta}(\bar{l}\sigma^{\mu\nu} l)(-2F_1(\hat{s})\,\varepsilon^{*\alpha}(\hat{p}_B + \hat{p}_{K_1})^\beta + J_1' \varepsilon^{*\alpha}\widehat{q}^\beta - J_2'(\varepsilon^* \cdot \widehat{q})\,\hat{p}_{K_1}^\alpha \widehat{q}^\beta) \end{array} \right\}
\tag{4.13}
$$

where the functions T_μ^1, T_μ^2, T^3 and T^4 interms of auxiliary functions are given by

$$
\begin{aligned}
T_\mu^1 &= iA'(\hat{s})\epsilon_{\mu\rho\alpha\beta}\epsilon^{*\rho}\hat{p}_B^\alpha \hat{p}_{K_1}^\beta - B'(\hat{s})\epsilon_\mu^* + C'(\hat{s})(\varepsilon^* \cdot \hat{p}_B)\hat{p}_{h\mu} + D'(\hat{s})(\varepsilon^* \cdot \hat{p}_B)\hat{q}_\mu \\
T_\mu^2 &= iE'(\hat{s})\epsilon_{\mu\rho\alpha\beta}\epsilon^{*\rho}\hat{p}_B^\alpha \hat{p}_{K_1}^\beta - F'(\hat{s})\epsilon_\mu^* + G'(\hat{s})(\varepsilon^* \cdot \hat{p}_B)\hat{p}_{h\mu} + H'(\widehat{s})(\varepsilon^* \cdot \hat{p}_B)\widehat{q}_\mu \\
T^3 &= iI'(\varepsilon^* \cdot \widehat{q}) \\
T^4 &= iJ'(\varepsilon^* \cdot \widehat{q})
\end{aligned}
\tag{4.14}
$$

By using the combination of the Wilson Coefficients

$$
\begin{aligned}
C_{RR}^{(+)} &= C_{RR} + C_{RL},\ C_{RR}^{(-)} = C_{RR} - C_{RL}, \\
C_{LL}^{(+)} &= C_{LL} + C_{LR},\ C_{LL}^{(-)} = C_{LL} - C_{LR}, \\
C_{RLLR}^{(+)} &= C_{LRRL} - C_{RLRL},\ C_{RLLR}^{(+)} = C_{RLLR} + C_{LRLR}
\end{aligned}
\tag{4.15}
$$

where $\hat{s} = s/M_B^2$, $\hat{p}_{K_1} = p_{K_1}/M_B$, $\hat{p}_B = p_B/M_B$

The auxiliary functions appearing in Eqs. (4.14) are defined as follows:

$$
\begin{aligned}
A'(\hat{s}) &= -\frac{2}{1+\hat{M}_{K_1}}[C_9^{eff} + \frac{1}{2}(C_{RR}^{(+)} + C_{LL}^{(+)})]A(\hat{s}) + \frac{2\hat{m}_b}{\hat{s}} C_7^{eff} F_1(\hat{s}) \\
B'(\hat{s}) &= (1+\hat{M}_{K_1})(C_9^{eff} + \frac{1}{2}(C_{LL}^{(+)} - C_{RR}^{(-)}))V_1(\widehat{s}) + \frac{2\hat{m}_b}{\hat{s}}(1-\hat{M}_{K_1}^2) C_7^{eff} F_2(\widehat{s}) \\
C'(\hat{s}) &= \frac{1}{(1-\hat{M}_{K_1}^2)}\left[((1-\hat{M}_{K_1})(C_9^{eff} + \frac{1}{2}(C_{LL}^{(+)} - C_{RR}^{(+)})))V_2(\hat{s}) + 2\hat{m}_b C_7^{eff}(F_3(\hat{s}) - (1-\hat{M}_{K_1}^2)/\hat{s})F_2(\hat{s})\right] \\
D'(\hat{s}) &= \frac{1}{\widehat{s}}\left[((1+\hat{M}_{K_1})V_1(\hat{s}) - (1-\hat{M}_{K_1})V_2(\hat{s}) - 2\hat{M}_{K_1}V_0(\hat{s}))(C_9^{eff} + \frac{1}{2}(C_{LL}^{(+)} - C_{RR}^{(+)})) - 2\hat{m}_b C_7^{eff} F_3(\hat{s})\right]
\end{aligned}
$$

$$
\begin{aligned}
E'(\hat{s}) &= \frac{-2}{1+\hat{M}_{K_1}}[C_{10}+\frac{1}{2}(C_{RR}^{(-)}-C_{LL}^{(-)})]A(\hat{s}) \\
F'(\hat{s}) &= (1+\hat{M}_{K_1})[C_{10}-\frac{1}{2}(C_{LL}^{(-)}+C_{RR}^{(-)}]V_1(\hat{s}) \\
G'(\hat{s}) &= -\frac{1}{\left(1+\hat{M}_{K_1}\right)}[C_{10}-\frac{1}{2}(C_{LL}^{(-)}+C_{RR}^{(-)}]V_2(\hat{s}) \\
H'(\hat{s}) &= \frac{1}{\hat{s}}\left[((1-\hat{M}_{K_1})V_2(\widehat{s})-(1+\hat{M}_{K_1})V_1(\widehat{s})+2\hat{M}_{K_1}V_0(\widehat{s}))(C_{10}-\frac{1}{2}(C_{RR}^{(-)}+C_{LL}^{(-)})\right] \\
I'(\hat{s}) &= \frac{2\hat{M}_{K_1}}{\widehat{m}_b}V_0(\widehat{s})[C_{RLLR}^{(+)}+C_{LRRL}^{(+)}] \\
J'(\hat{s}) &= \frac{2\hat{M}_{K_1}}{\hat{m}_b}V_0(\hat{s})[C_{RLLR}^{(+)}-C_{LRRL}^{(+)}] \\
J_1'(\hat{s}) &= 2\left(1-\hat{M}_{K_1}^2\right)\frac{F_1(\hat{s})-F_2(\hat{s})}{\hat{s}} \\
J_2'(\hat{s}) &= \frac{4M_B^2}{\hat{s}}\left(F_1(\hat{s})-F_2(\hat{s})-\frac{\hat{s}}{1-\hat{M}_{K_1}^2}F_3(\hat{s})\right)
\end{aligned}
\tag{4.16}
$$

where, the auxiliary functions A', B', C', D', E', F', G', H' corresponds to VA interactions where as I', J', J_1', J_2' are relevant for SP and T interactions.

To calculate the forward-backward asymmetry of the final state leptons, one needs to know the differential decay width of $B \to K_1(1270)l^+l^-$, which in the rest frame of B meson can be written as

$$
\frac{d\Gamma(B\to K_1(1270)l^+l^-)}{ds} = \frac{1}{(2\pi)^3}\frac{1}{32M_B}\int_{u_{min}}^{u_{max}}|\mathcal{M}_{B\to K_1(1270)l^+l^-}|^2du, \tag{4.17}
$$

where $u = (k+p_{l^-})^2$ and $s = (p_{l^+}+p_{l^-})^2$; k, p_{l^+} and p_{l^-} are the four-momenta vectors of $K_1(1270)$, l^+ and l^- respectively; $|\mathcal{M}_{B\to K_1(1270)l^+l^-}|^2$ is the squared decay amplitude after integrating over the angle between the lepton l^- and $K_1(1270)$ meson. The upper and lower limits of u are given by

$$
\begin{aligned}
u_{max} &= (E^*_{K_1(1270)}+E^*_{l^-})^2-(\sqrt{E^{*2}_{K_1(1270)}-m^2_{K_1(1270)}}-\sqrt{E^{*2}_{l^-}-m^2_{l^-}})^2, \\
u_{min} &= (E^*_{K_1(1270)}+E^*_{l^-})^2-(\sqrt{E^{*2}_{K_1(1270)}-m^2_{K_1(1270)}}+\sqrt{E^{*2}_{l^-}-m^2_{l^-}})^2;
\end{aligned}
\tag{4.18}
$$

where $E^*_{K_1(1270)}$ and $E^*_{l^-}$ are the energies of $K_1(1270)$ and l^- in the rest frame of lepton pair and can be determined as

$$
E^*_{K_1(1270)} = \frac{m_B^2-m^2_{K_1(1270)}-s}{2\sqrt{s}}, \qquad E^*_l = \frac{s}{2\sqrt{s}}. \tag{4.19}
$$

The differential FBA of final state lepton for the said decay can be written as

$$
\frac{dA_{FB}(s)}{ds} = \int_0^1 d\cos\theta\frac{d^2\Gamma(s,\cos\theta)}{ds d\cos\theta} - \int_{-1}^0 d\cos\theta\frac{d^2\Gamma(s,\cos\theta)}{ds d\cos\theta} \tag{4.20}
$$

and

$$
A_{FB}(s) = \frac{\int_0^1 d\cos\theta\frac{d^2\Gamma(s,\cos\theta)}{ds d\cos\theta} - \int_{-1}^0 d\cos\theta\frac{d^2\Gamma(s,\cos\theta)}{ds d\cos\theta}}{\int_0^1 d\cos\theta\frac{d^2\Gamma(s,\cos\theta)}{ds d\cos\theta} + \int_{-1}^0 d\cos\theta\frac{d^2\Gamma(s,\cos\theta)}{ds d\cos\theta}}. \tag{4.21}
$$

Now putting everything together in hat notation i.e. $q^2 = s = \hat{s}m_B^2$ we have

$$\frac{dA_{FB}}{d\hat{s}} = \frac{G_F^2\alpha^2 m_B^5}{2^{10}\pi^5}\left|V_{ts}^* V_{tb}\right|^2 u(\hat{s})\left[X_{VA} + X_{SP} + X_T + X_{VA-SP} + X_{VA-T} + X_{SP-T}\right] \tag{4.22}$$

where

$$\begin{aligned} u(\hat{s}) &= \sqrt{\lambda(1, \hat{M_{K_1}}, \hat{s})(1 - 4\frac{\hat{m}_l^2}{\hat{s}})} \\ \lambda(1, \hat{M}_{K_1}^2, \hat{s}) &= 1 + \hat{M}_{K_1}^4 + \hat{s}^2 - 2\hat{s} - 2\hat{M}_{K_1}^2(1 + \hat{s}) \end{aligned}$$

and

$$\begin{aligned} X_{VA} &= M_B\hat{s}\hat{M}_{K_1}\Re[A'^* F' + B'^* E'] \\ X_{SP} &= 0 \\ X_T &= 0 \\ X_{SP-VA} &= \hat{m}_l\left[\left(\hat{M}_{K_1}^2 + \hat{s} - 1\right)\Re(B'^* I') + M_B^2\lambda\Re(I'^* C')\right] \\ X_{SP-T} &= M_B\hat{M}_{K_1}^2\,\Re[2I'^* C_T + J'^* C_{TE})\left(2J_1'(\hat{M}_{K_1}^2 + \hat{s} - 1) + J_2' M_B^2\lambda + 4F_1(\hat{s})(3\hat{M}_{K_1}^2 - \hat{s} + 1)\right) \\ X_{VA-T} &= \hat{m}_l[2\Re(F'^* C_{TE})\left(2J_1'(\hat{M}_{K_1}^2 + \hat{s} - 1) + J_2' M_B^2\lambda + F_1(\hat{s})(4\hat{M}_{K_1}^2 - 4\hat{s} + 4)\right) \\ &\quad -2\Re(G'^* C_{TE})M_B^2\begin{pmatrix} 2J_1'(\hat{M}_{K_1}^2\hat{s} - \hat{s}^2 + \hat{s} + \lambda) + J_2' M_B^2(\hat{M}_{K_1}^2 - 1)\lambda \\ +4F_1(\hat{s})(5\hat{M}_{K_1}^2\hat{s} + 4\hat{M}_{K_1}^2 - 3\hat{s}^2 + 7\hat{s} + 3\lambda - 4) \end{pmatrix} \\ &\quad +2\Re(H'^* C_{TE})M_B^2\hat{M}_{K_1}^2\left(2J_1'(\hat{M}_{K_1}^2 + \hat{s} - 1) + J_2' M_B^2\lambda + 4F_1(\hat{s})(3\hat{M}_{K_1}^2 - \hat{s} + 1)\right) \\ &\quad -64\Re(E'^* C_T)M_B^2\left(J_1\hat{M}_{K_1}^2\hat{s} + 2F_1(\hat{s})\left(\hat{M}_{K_1}^2\hat{s} + \hat{s} - (\hat{s} - 1)^2 + \lambda\right)\right)] \end{aligned} \tag{4.23}$$

From experimental point of view the normalized forward-backward asymmetry is more useful, defined as

$$\frac{d\bar{\mathcal{A}}_{FB}}{d\hat{s}} = \frac{d\mathcal{A}_{FB}}{d\hat{s}} \Big/ \frac{d\Gamma}{d\hat{s}}$$

4.4 Numerical Analysis

In this following section, we examine the lepton forward-backward asymmetry and study the sensitivity of its zero position to New Physics operators. We consider different Lorentz structures of NP, as well as their combinations and take all the NP couplings to be real.

Switching off all New Physics Operators

By switching off all the new physics operators one will get the SM result of the lepton forward-backward asymmetry for $B \to K_1(1270)\mu^+\mu^-$ which was earlier calculated by Paracha et al. [83] and has been shown by solid line in all the figures shown below. The zero position lies at $\hat{s} = 0.16$ ($s = 4.46$ GeV^{-2}) and is almost

independent of the choice of form factors and also from the uncertainties arising from different input parameters like form factors, CKM matrix elements, etc. In the subsequent analysis we will ignore these uncertanities.

The study of the $B \to K^*$ done in reference [84] showed that the presence of the tensor and the scalar type interactions will have very mild effect on the zero position of forward-backward asymmetry ($\mathcal{A}_{FB}$) and they have ignored it in their analysis. However, recently the discrepancy has been observed in the lepton forward-backward asymmetry in the exclusive $B \to K^*\mu^+\mu^-$ decay [86, 87]. To explain the experimental results, Kumar et al. [88] has done a systematic study $B \to K^*\mu^+\mu^-$ decay by using the most general model independent Hamiltonian. They have shown that though the scalar and tensor operators are not important to study the lepton forward-backward asymmetry but the interference of these two is important and is not ignorable. Therefore, keeping this in view we will not ignore these scalar and tensor type couplings in our analysis of $B \to K_1(1270)$ decay. In order to see the effect of the new vector type Wilson coefficients ($C_X = C_{LL}, C_{LR}, C_{RR}, C_{RL}, C_{LRLR},\ C_T,\ C_{TE}$), we have plotted the dependence of $\mathcal{A}_{FB}$ on $\hat{s}$ by using different values of C_X, which can be summarized as follows.

Switching on only C_{LL} and C_{LR} along with SM operators

Considering the constraints provided by Kumar et al. [88] we took broad range of the values of different VA couplings. Fig. 4.1(a, b) shows the dependence of $\mathcal{A}_{FB}$ on $\hat{s}$ when all the $\mathbf{C}_{LL}$ and C_{LR} are present. When $C_{LL(LR)} = -C_{10}$, $C_{LL(LR)} = C_{10}$, $C_{LL(LR)} = -0.7 \times C_{10}$, $C_{LL(LR)} = 0.7 \times C_{10}$ (and all other Wilson coefficients are set to zero) the corresponding curves of $\mathcal{A}_{FB}$ are denoted by dashed double dotted, dashed triple dotted, dashed and dashed dotted lines respectively. The solid line corresponds to the SM result. One can deduce from here that there is a significant shift in the zero position of the forward-backward asymmetry and the position of zero is gradually shifted to the left for positive values of C_{10} and to the right for negative values of C_{10} compared to the SM value. This is contrary to the $B \to K^*\mu^+\mu^-$ decay process where for the positive values of $C_{LL}(LR)$ the zero position of A_{FB} shifts to the right and for negative value of these new coefficients the shift in the zero position is to the left [90]. This difference is due to the axial vector nature of the $K_1(1270)$. For different values of NP coefficients, the location of the zero of the $\mathcal{A}_{FB}$ varies from $\hat{s} =$ 0.12 to 0.23.

Switching on $\mathbf{C}_{RR}$ and C_{RL} along with SM operators

In Fig. 4.2(a, b) we have shown the dependence of forward-backward asymmetry on C_{RR} and C_{RL}. Fig. 4.2a give the plot of the $\mathcal{A}_{FB}$ with $\hat{s}$ by using different values of C_{RR} and setting all the other Wilson Coefficients to zero. By varying the C_{RR} from $-C_{10}$ to C_{10} in the same way as we did for the C_{LL} in Fig. 4.1, we have plotted the $\mathcal{A}_{FB}$ with $\hat{s}$ in Fig. 4.2a where, the legends of the curves are the same as in Fig. 4.1. One can clearly see that the zero position of the forward-backward asymmetry is less sensitive to C_{RR} compares to the C_{LL} and C_{LR} and the position of the zero shifts left to the SM value from $\hat{s} = 0.16$ to 0.12 when C_{RR} is changed from $-C_{10}$ to C_{10}. Again this is contrary to the $B \to K^*\mu^+\mu^-$ case where the shift of zero position of A_{FB} is on the other way.

Similarly Fig. 4.2b shows the dependency of the zero position of forward backward asymmetry on different values of C_{RL}. It can be seen that when C_{RL} vary from $-C_{10}$ to C_{10}, the zero position of the $\mathcal{A}_{FB}$ shifts gradually right to the SM value from $\hat{s} = 0.16$ to 0.21 .

(a) (b)

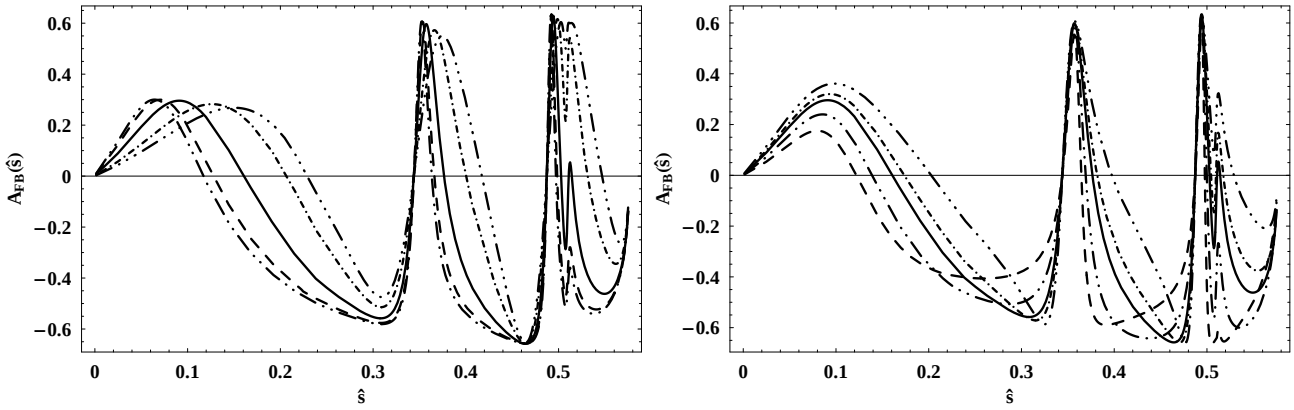

Figure 4.1: Forward-backward asymmetry for the $B \to K_1\mu^+\mu^-$ decays as functions of $\hat{s}$ for different values of $C_{LL(LR)}$. Solid line correspond to SM value, dashed line is for $C_{LL(LR)} = -C_{10}$, dashed-dot-dot is for $C_{LL(LR)} = -0.7C_{10}$, dashed dotted line is for $C_{LL(LR)} = C_{10}$, dashed-triple-dotted is for $C_{LL(LR)} = 0.7C_{10}$. The coefficients of the other interactions are all set to zero.

Switching only Scalar- Psudoscalar (C_{LRLR}, C_{RLLR}, C_{LRRL}, C_{RLRL})**operators along with SM operators**

Fig. (4.3) shows the behavior of the lepton forward-backward asymmetry for different NP scalar operators. In the graph we took the values of the scalar operators to be $-C_{10}$ and $+C_{10}$. Now such a large value of SP couplings has been excluded by the $\bar{B}_s^0 \to \mu^+\mu^-$ decay but these are still in the range of the weak limits provided by $\bar{B} \to X_s\mu^+\mu^-$ [88]. It is clear from the Eq. (4.23) that the contribution from the scalar operators alone is zero. This is quite clear in the graph where the value of $\mathcal{A}_{FB}$ overlap with that of the SM value and this is due to the interference between the NP scalar operators and that of the SM operators (i.e their coefficients).

Switching on only Tensor-Axial Tensor(C_T, C_{TE})**operators along with SM operators**

This is the case where only NP tensor operators are added. It is expected from Eq. (4.23) that the contribution from the tensor operators alone to $\mathcal{A}_{FB}$ is zero and Fig. (4.4) reflects this scenario. Just like the scalar operators, the non zero value of the forward-backward asymmetry is due to the interference between the tensor type operator and those of the SM operators but these are $\hat{m}_l$ suppressed (c. f. Eq. (4.23)). The allowed values of new tensor type operators are restricted to be [88]

$$|C_T|^2 + 4\,|C_{TE}|^2 \leqslant 1.3 \tag{4.24}$$

In Fig. 4.4 one can see the $\hat{m}_l$ suppression (which is not negligible) of the value of $A_{FB}(\hat{s})$ in the low $\hat{s}$ region. Though the value is suppressed but still the shift in the zero position is quite significant in the low $\hat{s}$ region, which is due to the mixing of Tensor and SM interactions.

Combination of SP, VA and T operators

Apart from the individual contribution of NP operators and their interference with the SM operators there is a also a mixing between NP operators by itself. By looking at the term X_{SP-VA} in Eq. (4.23) one can see that it is $\hat{m}_l$ suppressed but with the second term there is a factor of M_B^2 which will over come this suppression. This will not

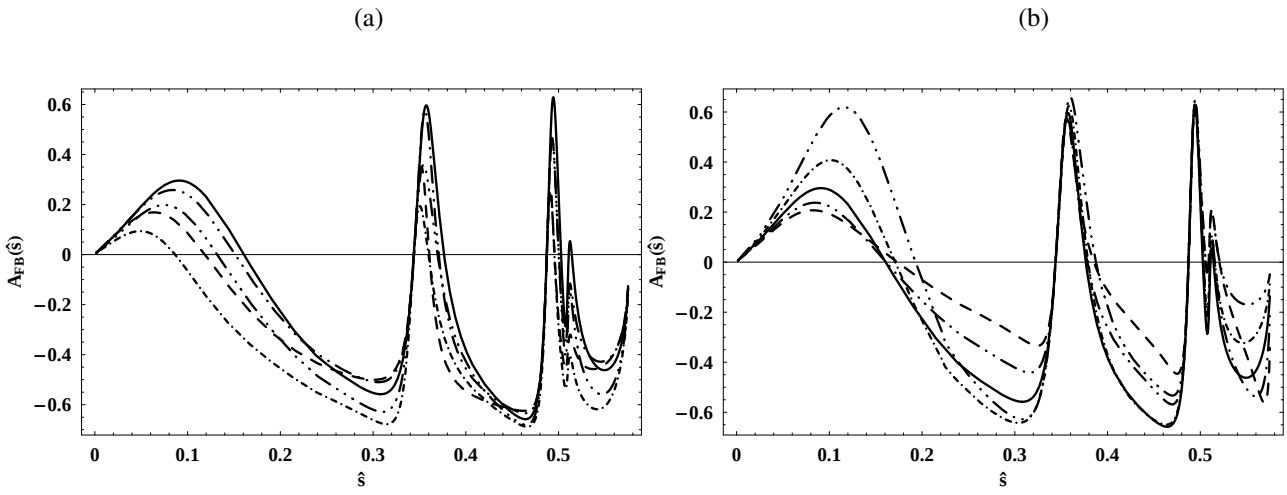

Figure 4.2: Forward-backward asymmetry for the $B \to K_1\mu^+\mu^-$ decays as functions of $\hat{s}$ for different values of $C_{RR(RL)}$. Solid line correspond to SM value, dashed line is for $C_{RR(RL)} = -C_{10}$, dashed-dot-dot is for $C_{RR(RL)} = -0.7C_{10}$, dashed dotted line is for $C_{RR(RL)} = C_{10}$, dashed-triple-dotted is for $C_{RR(RL)} = 0.7C_{10}$. The coefficients of the other interactions are all set to zero.

only change the zero position of A_{FB} but also increases or decreases its value compared to SM value depending on the size and sign of NP couplings. In Fig. 4.5, we have shown this dependence by taking the value of all NP coupling to be $+C_{10}$ or $-C_{10}$.

Among different mixing terms the most important is the SP and T term. Though the individual contribution of SP and T to the A_{FB} are not very significant but their interference term is quite promising. One can see this from X_{SP-T} term in Eq. (4.23) in which there is no lepton mass suppression. In Fig. 4.6, we have shown the dependencies of the zero position of forward-backward asymmetry for different values of SP couplings. The value of tensor couplings is chosen to be $|C_T|^2 + 4\,|C_{TE}|^2 \leqslant 1.3$.

Finally, the contribution from the mixing terms of VA and T is suppressed by $\hat{m}_l$ which can be seen in X_{VA-T} term of Eq. 4.23.

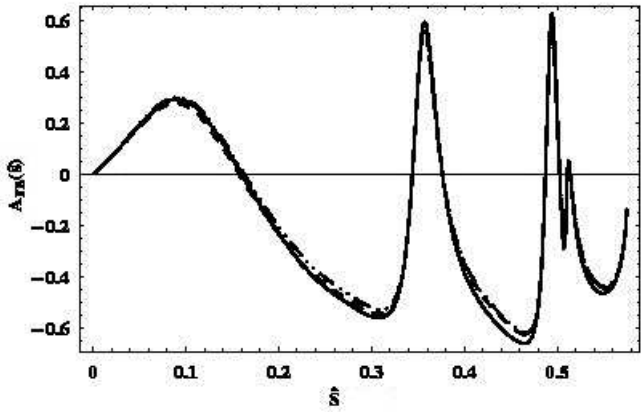

Figure 4.3: Forward-backward asymmetry for the $B \to K_1\mu^+\mu^-$ decays as functions of $\hat{s}$ for different values of Scalar and Psudoscalar operators. Solid line correspond to SM value, dashed line is for $(C_{LRLR}, C_{RLLR}, C_{LRRL}, C_{RLRL})=-C_{10}$, dashed-dot-dot is for $(C_{LRLR}, C_{RLLR}, C_{LRRL}, C_{RLRL})=C_{10}$. The coefficients of the other NP interactions are all set to zero.

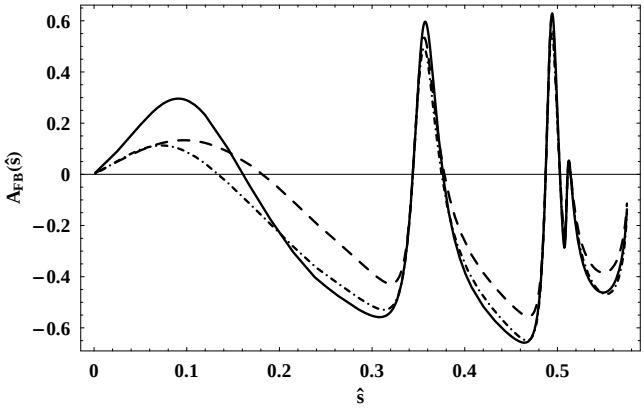

Figure 4.4: Forward-backward asymmetry for the $B \to K_1\mu^+\mu^-$ decays as functions of $\hat{s}$ for different values of Scalar and Psudoscalar operators. Solid line correspond to SM value,dashed line is for $|C_T|^2 + 4\,|C_{TE}|^2$=1.3, dashed-dot is for $|C_T|^2 + 4\,|C_{TE}|^2$=0.9. The coefficients of the other NP interactions are all set to zero.

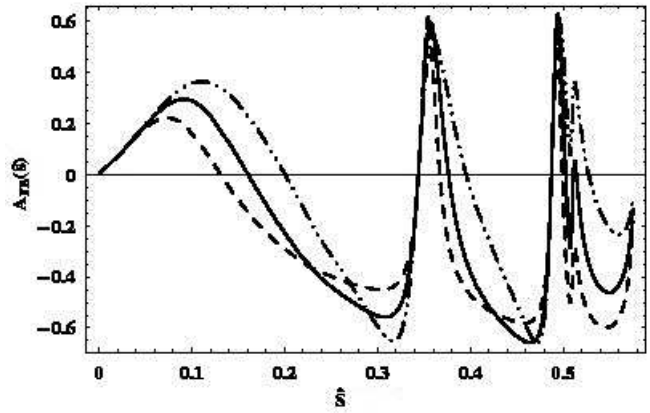

Figure 4.5: Forward-backward asymmetry for the $B \to K_1\mu^+\mu^-$ decays as functions of $\hat{s}$ for different values of Scalar, Psudoscalar, Vector and Axialvector operators. Solid line correspond to SM value, dashed and dashed-dot-dot lines are for all New Physics SP and VA couplings where SP coupling correspond to $+C_{10}$ and $-C_{10}$ and VA correspond to $+0.3C_{10}$ and $-0.3C_{10}$. The coefficients of the other NP interactions are all set to zero.

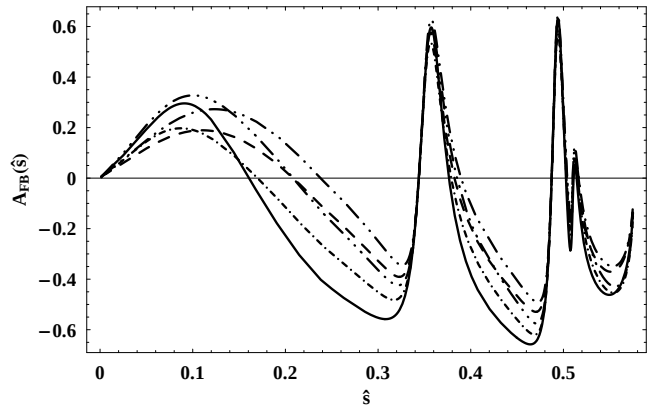

Figure 4.6: Forward-backward asymmetry for the $B \to K_1\mu^+\mu^-$ decays as functions of $\hat{s}$ for different values of Scalar and Psudoscalar operators. Solid line correspond to SM value,dashed line is for SP coupling to be $-C_{10}$, dashed-dot-dot is for SP couplings to be $-0.7C_{10}$, dashed dot is for SP couplings to be $+C_{10}$ and dashed-triple dotted is for SP couplings to be $0.7C_{10}$. Here $|C_T|^2 + 4\,|C_{TE}|^2 = 1.3$. The coefficients of the VA NP interactions are all set to zero.

4.5 Conclusion

The sensitivity of the zero position of the forward backward asymmetry to the new physics effects is studied here. We showed that the position of the zero of the forward backward asymmetry shifts significantly from its Standard Model value both for the size and sign of the vector-vector new physics operators which are the opposite chirality part of the corresponding SM operators. The scalar-scalar four fermion interactions have very mild effects on the zero of the forward-backward asymmetry. The tensor type interactions shifts the zero position of the forward-backward asymmetry but these are $\hat{m}_l$ suppressed. However, the interference of SP and T operators gives significant change in the zero position of $\mathcal{A}_{FB}$.

In short, our results provide, just as in case of the $B \to K^* l^+ l^-$ process, an opportunity for the straightforward comparison of the basic theory with the experimental results, which may be expected in near future for this process.

Chapter 5

Model independent Analysis of $B \to K_2^*(1430)\mu^+\mu^-$ Decay

5.1 Introduction

As mentioned in the introduction, in general there are two ways to search NP which in the experimental measurements. One is the direct search which can be achieved by increasing the energies of colliders and find the predicted new particles but these particles are quite massive and therefore hard to produced. The other one is indirect search which is comparatively easier i.e to see how much different observables are affected by these new particles. The indirect searches require precise measurement of the observables for the channel under consideration as well as need rigorous complementary studies. Furthermore, as we do not know the exact form of new physics, more and more analysis of different observables for different decay channels are required to cast the form of the new physics [89]. Therefore, it seems to be indispensable to study the decay channels other than the $\bar{B} \to \bar{K}^*\mu^+\mu^-$.

With this motivation, the $B \to K_2^*\ell^+\ell^-$ channel, where K_2^* is the excited state of K^* with spin parity 2^+, provides the same testing ground to study the effects of the NP as in $\bar{B} \to \bar{K}^*\mu^+\mu^-$ decay. The exclusive $B \to K_2^*(1430)\ell^+\ell^-$ decay has been studied in the SM and some approaches beyond SM [92, 93, 94, 95, 96, 97, 98, 99, 100]. For example, in refs. [92, 64] the form factors for $B \to K_2^*\ell^+\ell^-$ are calculated using perturbative QCD and LCSR approaches. The analysis of different physical observable for this decay is studied in various beyond SM scenarios, like SM4, non-universal Z' model, Universal Extra dimension model and a model with the flipped sign of C_7^{eff} [94, 95, 96, 99]. The analysis of lepton polarization asymmetries of $B \to K_2^*\ell^+\ell^-$ in the presence of new right-handed currents is done in [97, 98]. The analysis of polarized decay width and forward-backward asymmetry by considering beyond SM operator basis is given in [100]. These studies show that, like $B \to K^*\ell^+\ell^-$ decay, this channel is quite promising in finding NP and will provide us some independent tests of the physics of the SM and beyond.

In this chapter we perform the study of $B \to K_2^*(1430)\mu^+\mu^-$ on the lines of ref. [37] and study the NP effects without restricting ourselves to any specific model. Contrary to $B \to K^*\mu^+\mu^-$, the decay $B \to K_2^*(1430)\mu^+\mu^-$ is not yet experimentally observed. We have taken into account the constraints from the different B decay modes such as $B_s \to \mu^+\mu^-$, $B \to X_s\mu^+\mu^-$ and $\bar{B} \to \bar{K}^*\mu^+\mu^-$ on different NP operator couplings allowed by the most general lorentz structure of transition matrix elements. In this chapter we also incorporate bounds on the input parameters coming from the recent A_{FB} measurements at LHCb experiment for the decay $\bar{B} \to \bar{K}^*(892)\mu^+\mu^-$ [91]. With these new bounds we obtain better understanding of how these new physics operators affect branching ratio, zero-position of forward-backward asymmetry, different lepton polarization asymmetries and the helicity fractions of final state meson.

The effects of these new operators couplings (VA,SP,T) are significant to the zero position of $A_{FB}(q^2)$ as well as on its magnitude. In addition to A_{FB}, these NP operators also give significant effects on decay rate, lepton polarization asymmetries and longitudinal and transverse helicities of final state $K_2^*(1430)$ meson. We hope that in the coming years, the LHCb experiment will collect around $6.4k$ events in the full range of q^2 for an integrated luminosity of $2fb^{-1}$ [37]. This would allow us to observe the $B \to K_2^*(1430)\mu^+\mu^-$ in the SM and would also permit many of the additional tests of NP.

The chapter is organized as follows: In Sec. 5.2 the necessary hadronic inputs, namely, new physics operators and form factors and constraints on the NP parameters are collected. Sec. 5.3 contains the analytic formulas for differential decay rates, forward backward asymmetry, different polarizations (longitudinal, normal and transverse) and the helicity fractions of the final state $K_2^*(1430)$ meson. Sec. 5.4 deals with the numerical analysis and then conclusions are summarized in Sec. 5.5.

5.2 Parametrization of Matrix Elements and Form Factors

The exclusive $B \to K_2^*(1430)l^+l^-$ decay involves the hadronic matrix elements of quark operators, which can be parameterized in terms of form factors. These matrix elements are written as

$$\left\langle K_2^*(k,\epsilon)\left|\bar{s}\gamma^\mu b\right|\overline{B}(p)\right\rangle = -\frac{2V(q^2)}{m_B+m_{K_2^*}}\epsilon^{\mu\nu\rho\sigma}\frac{\varepsilon^*_{\nu\alpha}p^\alpha}{m_B}p_\rho k_\sigma \tag{5.1}$$

$$\begin{aligned}\left\langle K_2^*(k,\epsilon)\left|\bar{s}\gamma^\mu\gamma^5 b\right|\overline{B}(p)\right\rangle &= \frac{2im_{K_2^*}A_0(q^2)}{q^2}\frac{\varepsilon^*_{\nu\alpha}p^\alpha}{m_B}q^\nu q^\mu + \frac{i(m_B+m_{K_2^*})A_1(q^2)}{m_B}\left[g^{\mu\nu}\varepsilon^*_{\nu\alpha}p^\alpha - \frac{1}{q^2}\varepsilon^*_{\nu\alpha}p^\alpha q^\nu q^\mu\right]\\ &\quad -iA_2(q^2)\frac{\varepsilon^*_{\nu\alpha}p^\alpha q^\nu}{m_B(m_B+m_{K_2^*})}\left[(p^\mu+k^\mu)-\frac{m_B^2-m_{K_2^*}^2}{q^2}q^\mu\right]\end{aligned} \tag{5.2}$$

$$\left\langle K_2^*(k,\epsilon)\left|\bar{s}\sigma^{\mu\nu}q_\nu b\right|\overline{B}(p)\right\rangle = -2iT_1(q^2)\epsilon^{\mu\nu\rho\sigma}\frac{\varepsilon^*_{\nu\alpha}p^\alpha}{m_B}p_\rho k_\sigma \tag{5.3}$$

$$\left\langle K_2^*(k,\epsilon)\left|\bar{s}\sigma^{\mu\nu}\gamma^5 q_\nu b\right|\overline{B}(p)\right\rangle = T_2(q^2)\left[(m_B^2-m_{K_2^*}^2)g^{\mu\nu}\varepsilon^*_{\nu\alpha}p^\alpha - \varepsilon^*_{\nu\alpha}p^\alpha q^\nu(p^\mu+k^\mu)\right]\frac{1}{m_B}$$

$$+T_3(q^2)\frac{\varepsilon^*_{\nu\alpha}p^\alpha}{m_B}q^\nu\left[q^\mu-\frac{q^2}{m_B^2-m_{K_2^*}^2}(p^\mu+k^\mu)\right] \tag{5.4}$$

$$\left\langle K_2^*(k,\epsilon)\left|\bar{s}b\right|\overline{B}(p)\right\rangle = \frac{2V(q^2)}{(m_B+m_{K_2^*})(m_b-m_s)}\epsilon^{\mu\nu\rho\sigma}\frac{\varepsilon^*_{\nu\alpha}p^\alpha}{m_B}p_\rho k_\sigma \tag{5.5}$$

$$\left\langle K_2^*(k,\epsilon)\left|\bar{s}\gamma^5 b\right|\bar{B}(p)\right\rangle = \frac{2im_{K_2^*}A_0(q^2)}{q^2}\frac{\varepsilon^*_{\nu\alpha}p^\alpha}{m_B(m_b+m_s)}q^\nu q^\mu \tag{5.6}$$

$$\left\langle K_2^*(k,\epsilon)\left|\bar{s}\sigma^{\mu\nu}b\right|\overline{B}(p)\right\rangle = -2T_1(q^2)\epsilon^{\mu\nu\rho\sigma}\frac{\varepsilon^*_{\nu\alpha}p^\alpha}{m_B}p_\rho k_\sigma \tag{5.7}$$

where $p(k)$ is the momentum of the $B(K_2^*)$ meson and $\varepsilon^*_{\nu\alpha}$ is the polarization of the final state $K_2^*(1430)$ meson. In case of the tensor meson the polarization sum is given by [92]

$$P_{\mu\nu\alpha\beta}=\sum\varepsilon_{\mu\nu}(p)\varepsilon^*_{\alpha\beta}(p)=\frac{1}{2}\left(\theta_{\mu\alpha}\theta_{\nu\beta}+\theta_{\mu\beta}\theta_{\nu\alpha}\right)-\frac{1}{3}\left(\theta_{\mu\nu}\theta_{\alpha\beta}\right) \tag{5.8}$$

with

$$\theta_{\mu\nu}=-g_{\mu\nu}+\frac{k_\mu k_\nu}{m_{K_2^*}^2} \tag{5.9}$$

Defining

$$\varepsilon^*_\nu=\varepsilon^*_{\nu\alpha}p^\alpha/m_B \tag{5.10}$$

the resulting matrix elements for $B\to K_2^*(1430)$ look just like those for $B\to V$ (e.g. K^* meson) transitions. The form factors for $B\to K_2^*(1430)$ transition are the non-perturbative quantities and are needed to be calculated using different approaches (both perturbative and non-perturbative) like Lattice QCD, QCD sum rules, Light Cone sum rules, etc. Here, we consider the form factors calculated in the LCSR approach [93] and their evolution with q^2 is given by:

$$F(q^2)=\frac{F(0)}{1-a(q^2/m_B^2)+b(q^2/m_B^2)^2} \tag{5.11}$$

where the value of different parameters is given in Table 5.1.

Table 5.1: $B\to K_2^*$ form factors in the light cone sum rules approach. $F(0)$ denotes the value of form factors at $q^2=0$ while a and b are the parameters in the parameterizations shown in Eq. (5.11)[93]

$F(q^2)$	$F(0)$	a	b
$V(q^2)$	$0.16^{+0.02}_{-0.02}$	2.08	1.5
$A_0(q^2)$	$0.25^{+0.04}_{-0.04}$	1.57	0.1
$A_1(q^2)$	$0.14^{+0.02}_{-0.02}$	1.23	0.49
$A_2(q^2)$	$0.05^{+0.02}_{-0.02}$	1.32	14.9
$T_1(q^2)$	$0.14^{+0.02}_{-0.02}$	2.07	1.5
$T_2(q^2)$	$0.14^{+0.02}_{-0.02}$	1.22	0.34
$T_3(q^2)$	$0.01^{+0.01}_{-0.02}$	9.91	276

The errors in the values of the form factors arise from number of input parameters involved in their calculation

in LCSR such as variations in the Boral parameters, fluctuation of threshold parameters, errors in the b quark mass, corrections from the decay constants of involved mesons and from the Gengenbauer moments in the distribution amplitudes.

It is worth mentioning here that it is possible to study this mode with the help of QCD factorization. Besides the factorizable contribution of form factors which has been used here, there are in principle non-factorizable contributions to matrix elements as well [101]. QCD factorization not only reduces the number of independent parameters in heavy quark limit but also help us to compute the non-factorizable corrections to B meson decays with the help of light-cone distribution amplitudes and hard scattering kernel [106, 107]. Especially if the factorization approach discussed in [101] is taken into account, it leads to significant shift towards right in the zero position of the forward backward asymmetry.

5.3 Numerical Constraints on NP Parameters

The constraints on NP parameters can be obtained from the branching ratios of $\bar{B}_s^0 \to \mu^+\mu^-$, $\bar{B}_s^0 \to X_s\mu^+\mu^-$ and $\bar{B}_d^0 \to \bar{K}\mu^+\mu^-$[108, 109, 110, 111, 112]. Due to the large hadronic uncertainties, the constraints obtained from the exclusive decay modes are somewhat weaker compared to the inclusive ones. The branching ratio of inclusive decay mode $\bar{B} \to X_s\mu^+\mu^-$ has been measured by Babar [111] and Belle [112] and their measurements in low-q^2 ($1\text{GeV}^2 \leq q^2 \leq 6\text{GeV}^2$) and high-$q^2$ ($14.4\text{GeV}^2 \leq q^2 \leq 25\text{GeV}^2$) regions can be summarized as:

$$
\begin{aligned}
B(\bar{B} \to X_s\mu^+\mu^-)_{\text{low } q^2} &= (1.49 \pm 0.50^{+0.41}_{-0.32}) \times 10^{-6} && \text{(Belle)}, \\
&= (1.8 \pm 0.7 \pm 0.50) \times 10^{-6} && \text{(BaBar)} \qquad (5.12) \\
&= (1.60 \pm 0.50) \times 10^{-6} && \text{(Average)} \\
B(\bar{B} \to X_s\mu^+\mu^-)_{\text{high } q^2} &= (0.42 \pm 0.12^{+0.07}_{-0.07}) \times 10^{-6} && \text{(Belle)}, \\
&= (0.50 \pm 0.25^{+0.07}_{-0.08}) \times 10^{-6} && \text{(BaBar)} \qquad (5.13) \\
&= (0.44 \pm 0.12) \times 10^{-6} && \text{(Average)} \\
& && \qquad (5.14)
\end{aligned}
$$

where q^2 is the invariant mass squared of two muons and low-q^2 region corresponds to $1\text{GeV}^2 \leq q^2 \leq 6\text{GeV}^2$ and high-q^2 region corresponds to $q^2 \geq 14.4\text{GeV}^2$.

Now we discuss the constraints on the new physics couplings which are defined in eq. (2.17). The constraints on the new VA couplings come mainly from $\bar{B}_d^0 \to X_s\mu^+\mu^-$ and $\bar{B}_d^0 \to \bar{K}\mu^+\mu^-$ [113]. It has been shown in Ref. [113] that if $R_{V,A}$ couplings are present only, the constraints on these couplings from above decays is

$$
1.0 \leq \frac{|R_V + 3.6|^2}{(4.7)^2} + \frac{|R_A - 4.0|^2}{(4.8)^2}, \frac{|R_V + 2.8|^2}{(6.5)^2} + \frac{|R_A - 4.1|^2}{(6.6)^2} \leq 1 \qquad (5.15)
$$

Similarly when we have only $R'_{V,A}$ couplings, the constraints on them from the same decay will become [113]

$$2.2 \leq |R'_V + 3.6|^2 + |R'_A - 4.0|^2 \leq 56.6, |R'_V|^2 + |R'_A|^2 \leq 17 \tag{5.16}$$

These constraints are weekend when both $R_{V,A}$ and $R'_{V,A}$ couplings are present at the same time. In this case these new physics couplings are restricted to be

$$\frac{|R_V + 2.8|^2}{(6.5)^2} + \frac{|R_A - 4.1|^2}{(6.6)^2} \leq 1 \tag{5.17}$$

and

$$|R'_V|^2 + |R'_A|^2 \leq 40. \tag{5.18}$$

The limits on couplings corresponding to scalar-pseudoscalar (SP) operators comes from the upper bound on $\bar{B}^0_s \to \mu^+\mu^-$ which provides the limit

$$|R_S - R'_S|^2 + |R_P - R'_P|^2 \leq 0.44. \tag{5.19}$$

This puts a sever constraint on the NP couplings if only $R_{S,P}$ or $R'_{S,P}$ are present. However, under the condition where both types of operators are present, $R_{S,P}$ and $R'_{S,P}$, these bounds can be relaxed due to cancelation between the $R_{S,P}$ and $R'_{S,P}$. In this case $\bar{B}^0_d \to X_s\mu^+\mu^-$ and $\bar{B}^0_d \to \bar{K}\mu^+\mu^-$ can still bound these couplings and the stronger bound is obtained from the measurement of later quantity, which yields

$$|R_S|^2 + |R_P|^2 \leq 9, \qquad R_S \approx R'_S, \qquad R_S \approx R'_P. \tag{5.20}$$

Now the constraint on the NP tensor type couplings comes entirely from the inclusive $\bar{B}^0_d \to X_s\mu^+\mu^-$ decay. In case when only tensor type operators are present, the limits on tensor type couplings are[113]:

$$|C_T|^2 + |C_{TE}|^2 \leq 1.0. \tag{5.21}$$

In the present study we will examine $B \to K^*_2(1430)\mu^+\mu^-$ decays by using these NP constraints.

5.4 Decay Rate, Forward-Backward Asymmetry and Lepton Polarization Asymmetries for $B \to K^*_2(1430)\mu^+\mu^-$ decay

In this section, we perform the calculations of some interesting quantities like the decay rate, the forward-backward asymmetry, the polarization asymmetries of the final state lepton and the helicity fractions of the final state $K^*_2(1430)$ meson. By using Eq. (2.22) with matrix elements given in section 5.2, the decay amplitude for

$B \to K_2^*(1430)\mu^+\mu^-$ can be written as

$$\begin{aligned}\mathcal{M}(\bar{B} \to K_2^*(1430)\mu^+\mu^-) = \quad & -\frac{G_F\alpha}{2\sqrt{2}\pi}V_{tb}V_{ts}^*\Big[T_V^\mu \bar{l}\gamma_\mu l + T_A^\mu \bar{l}\gamma_\mu\gamma_5 l \\ & + T_S\bar{l}l + T_P\bar{l}\gamma^5 l + T_T^{\mu\nu}\bar{l}\sigma^{\mu\nu}l + iT_E^{\mu\nu}\epsilon^{\mu\nu\alpha\beta}\bar{l}\sigma_{\alpha\beta}l\Big] \end{aligned} \tag{5.22}$$

with

$$\begin{aligned} T_V^\mu &= -\mathcal{F}_1\epsilon^{\mu\nu\alpha\beta}\varepsilon_\nu^* p_{K^*\alpha}q_\beta + i\mathcal{F}_2\varepsilon^{*\mu} + i\mathcal{F}_3\varepsilon^*\cdot q(p_B+p_{K^*})^\mu + i\mathcal{F}_4\varepsilon^*\cdot q q^\mu \\ T_A^\mu &= -\mathcal{F}_5\epsilon^{\mu\nu\alpha\beta}\varepsilon_\nu^* p_{K^*\alpha}q_\beta + i\mathcal{F}_6\varepsilon^{*\mu} + i\mathcal{F}_7\varepsilon^*\cdot q(p_B+p_{K^*})^\mu + i\mathcal{F}_8\varepsilon^*\cdot q q^\mu \\ T_S &= i\mathcal{F}_9\varepsilon^*\cdot q \\ T_P &= i\mathcal{F}_{10}\varepsilon^*\cdot p_B \\ T_T^{\mu\nu} &= C_T\left(i\mathcal{F}_{11}\epsilon^{\mu\nu\alpha\beta}\varepsilon_\alpha^*(p_B+p_{K^*})_\beta + i\mathcal{F}_{12}\epsilon^{\mu\nu\alpha\beta}\varepsilon_\alpha^* q_\beta - i\mathcal{F}_{13}\epsilon^{\mu\nu\alpha\beta}\varepsilon^*\cdot q p_{\alpha K^*}q_\beta\right) \\ T_E^{\mu\nu} &= C_{TE}\left(i\mathcal{F}_{11}\epsilon^{\mu\nu\alpha\beta}\varepsilon_\alpha^*(p_B+p_{K^*})_\beta + i\mathcal{F}_{12}\epsilon^{\mu\nu\alpha\beta}\varepsilon_\alpha^* q_\beta - i\mathcal{F}_{13}\epsilon^{\mu\nu\alpha\beta}\varepsilon^*\cdot q p_{\alpha K^*}q_\beta\right) \end{aligned} \tag{5.23}$$

The auxiliary functions $\mathcal{F}_1\cdots\mathcal{F}_{13}$ appearing in Eq. (5.23) are defined as follows:

$$\begin{aligned} \mathcal{F}_1 &= \left[\frac{2V(q^2)}{m_B+m_{K^*}}(C_9^{eff}+R_V+R_V') + \frac{4m_b}{q^2}C_7^{eff}T_1(q^2)\right], \\ \mathcal{F}_2 &= -\left[(m_B+m_{K^*})A_1(q^2)(C_9^{eff}+R_V-R_V') + \frac{2m_b}{q^2}C_7^{eff}T_1(q^2)(m_B^2-m_{K^*})\right], \\ \mathcal{F}_3 &= \left[\frac{A(q^2)}{m_B+m_{K^*}}(C_9^{eff}+R_V-R_V') + \frac{2m_b}{q^2}C_7^{eff}\left(T_1(q^2)+\frac{q^2T_3(q^2)}{m_B^2-m_{K^*}}\right)\right], \\ \mathcal{F}_4 &= \left[\frac{2m_{K^*}}{q^2}(C_9^{eff}+R_V-R_V')(A_3(q^2)-A_0(q^2)) - \frac{2m_b}{q^2}C_7^{eff}T_3(q^2)\right], \\ \mathcal{F}_5 &= \left[\frac{2V(q^2)}{m_B+m_{K^*}}(C_{10}^{eff}+R_A+R_A')\right], \\ \mathcal{F}_6 &= -\left[(m_B+m_{K^*})A_1(q^2)(C_{10}^{eff}+R_A-R_A')\right], \\ \mathcal{F}_7 &= \left[\frac{A(q^2)}{m_B+m_{K^*}}(C_{10}^{eff}+R_A-R_A')\right], \\ \mathcal{F}_8 &= \left[\frac{2m_{K^*}}{q^2}(C_{10}^{eff}+R_A-R_A')(A_3(q^2)-A_0(q^2))\right], \\ \mathcal{F}_9 &= \left[-2(R_S-R_S')\frac{m_{K^*}}{m_b}A_0(q^2)\right], \\ \mathcal{F}_{10} &= \left[2(R_P-R_P')\frac{m_{K^*}}{m_b}A_0(q^2)\right], \\ \mathcal{F}_{11} &= -2T_1(q^2), \\ \mathcal{F}_{12} &= \left[\frac{2(m_B^2-m_{K^*}^2)}{q^2}(T_1(q^2)-T_2(q^2))\right], \\ \mathcal{F}_{13} &= \left[\frac{4}{q^2}\left(T_1(q^2)-T_2(q^2)-\frac{q^2T_3(q^2)}{m_B^2-m_{K^*}^2}\right)\right] \end{aligned} \tag{5.24}$$

5.4.1 Differential Decay Rate

Collecting everything together, one can write the general expression of the differential decay rate for $B \to K_2^*(1430)\mu^+\mu^-$ by using the formula given in Eq. (4.17) as

$$\begin{aligned}
\frac{d\Gamma}{dq^2} &= \frac{G_F^2\alpha^2}{2^{11}\pi^5 m_B^3}\left|V_{tb}V_{ts}^*\right|^2 \frac{u(q^2)\lambda}{18 m_l^2 m_T^4 q^2}\Big\{3\mathcal{F}_1^2 m_{K_2^*}^2 q^2\lambda + 2\mathcal{F}_2^2 m_B^4(\lambda + 10m_T^2 q^2) \\
&+2\mathcal{F}_3^2\lambda^2\Big]\left(2m_l^2 + q^2\right) - \left[3\mathcal{F}_5^2 m_{K_2^*}^2 - 3\mathcal{F}_9^2 m_B^2\right]K_2 q^2\lambda + 12\mathcal{F}_8^2 m_l^2 q^4\lambda \\
&+2\mathcal{F}_6^2 m_B^4\left[2\left(\lambda - 20m_T^2 q^2\right)m_l^2 + q^2\left(\lambda + 10m_T^2 q^2\right)\right] + 3\mathcal{F}_{10}^2 m_B^2 q^4\lambda \\
&+2\mathcal{F}_7^2\lambda\left[2\left(\lambda - 3q^4 + 6m_T^2 q^2\right)m_{K_2^*}^2 + q^2\lambda\right] - 4\mathcal{F}_2\mathcal{F}_3 m_B^4\left(2m_l^2 + q^2\right)K_1\lambda^2 \\
&-4\mathcal{F}_6\mathcal{F}_7 m_B^2\lambda\left[2\left(K_1 + 3q^2\right)m_l^2 + K_1 q^2\right] - 24\mathcal{F}_6\mathcal{F}_8 m_l^2 m_B^2 q^2\lambda - 12\mathcal{F}_{10}\mathcal{F}_6 m_l m_B^3 q^2\lambda \\
&+24\mathcal{F}_7\mathcal{F}_8 m_l^2 K_0 q^2\lambda + 12\mathcal{F}_{10}\mathcal{F}_7 m_l m_B K_0 q^2\lambda + 8\mathcal{F}_{11}\mathcal{F}_{12} q^2(\lambda + 10m_T^2 m_B^2 - 10m_T^4)K_3 \\
&-4\mathcal{F}_{11}\mathcal{F}_{13}(K_1 + 4m_T^2)\lambda q^2 K_3 - 72\mathcal{F}_1\mathcal{F}_{11} m_l m_{K_2^*}^2 q^2\lambda C_T \\
&+48\mathcal{F}_{11}\mathcal{F}_2 m_l m_B^2 q^2(\lambda + 10m_T^2 m_B^2 - 10m_T^4)C_{TE} - 4\mathcal{F}_{12}\mathcal{F}_{13}K_1\lambda q^2 K_3 \\
&+48\mathcal{F}_{12}\mathcal{F}_2 m_l m_B^2 q^2\left(\lambda + 10m_T^2 q^2\right)C_{TE} - 48\mathcal{F}_{12}\mathcal{F}_3 m_l q^2 K_1 C_{TE}\lambda \\
&-24\mathcal{F}_{13}\mathcal{F}_2 m_l m_B^2 K_1\lambda q^2 C_{TE} + 24\mathcal{F}_{13}\mathcal{F}_3 m_l q^2 C_{TE}\lambda^2\Big\}
\end{aligned} \tag{5.25}$$

where m_l is the mass of final state muon and

$$\lambda = \lambda\left(m_B^2, m_{K_2^*}^2, q^2\right) \equiv m_B^4 + m_{K_2^*}^4 + q^4 - 2m_{K_2^*}^2 m_B^2 - 2q^2 m_B^2 - 2m_{K_2^*}^2 q^2. \tag{5.26}$$

$$K_0 = (m_B^2 - m_{K_2^*}^2),\ K_1 = \left(m_B^2 - m_{K_2^*}^2 - q^2\right),\ K_2 = q^2 - 4m_l^2,$$

$$K_3 = q^2 C_T^2 - 4m_l^2\left(C_T^2 - 36C_{TE}^2\right). \tag{5.27}$$

and the auxiliary functions are the same as defined in Eq.(5.24).

5.4.2 Forward-Backward Asymmetry

Now we are in a position to explore the forward-backward asymmetry of final state leptons in the $B \to K_2^*(1430)\mu^+\mu^-$, which is an essential observable sensitive to the new physics effects. Making use of the formula of forward-backward asymmetry which is given in Eq. (4.21), one can easily get the expression for the forward-backward asymmetry for $B \to K_2^*(1430)\mu^+\mu^-$ as follows:

$$\frac{dA_{FB}(q^2)}{dq^2} = \frac{G_F^2\alpha^2}{2^{11}\pi^5 m_B^3}\left|V_{tb}V_{ts}^*\right|^2 \frac{u(q^2)\lambda}{6 m_B m_T^4}\left[A_{FB}^{VA} + A_{FB}^{SP} + A_{FB}^{TSP} + A_{FB}^{T}\right] \tag{5.28a}$$

$$A_{FB}^{VA} = -3(\mathcal{F}_2\mathcal{F}_5 + \mathcal{F}_1\mathcal{F}_6)q^2 m_B^2 m_{K_2} \tag{5.28b}$$

$$A_{FB}^{SP} = 2\mathcal{F}_9 m_l m_B\left(\mathcal{F}_3\lambda + \mathcal{F}_2 m_B^2\left[q^2 - m_B^2 + m_{K_2}^2\right]\right) \tag{5.28c}$$

$$
\begin{aligned}
A_{FB}^{TSP} &= -q^2\left(\mathcal{F}_{10}C_T + 2\mathcal{F}_9 C_{TE}\right) m_B \left(2\mathcal{F}_{12}\left(m_B^2 - m_{K_2}^2 - q^2\right)\right. && (5.28d)\\
&\quad \left. -\mathcal{F}_{13}\lambda + 2\mathcal{F}_{11}\left(m_B^2 + 3m_{K_2}^2 - q^2\right)\right)\\
A_{FB}^{T} &= -2m_l\left(12\mathcal{F}_{12}\mathcal{F}_5 q^2 C_{TE} m_{K_2}^2 + 12\mathcal{F}_{11}\mathcal{F}_5 C_{TE} m_{K_2}^2\left(m_B^2 - m_{K_2}^2\right)\right. && (5.28e)\\
&\quad +\mathcal{F}_{13}\lambda C_T\left((\mathcal{F}_6 - \mathcal{F}_7)m_B^2 - \mathcal{F}_8 q^2 + \mathcal{F}_7 m_{K_2}^2\right)\\
&\quad -2\mathcal{F}_{12}C_T\left(m_B^2 - m_{K_2}^2 - q^2\right)\left((\mathcal{F}_6 - \mathcal{F}_7)m_B^2 - \mathcal{F}_8 q^2 + \mathcal{F}_7 m_{K_2}^2\right)\\
&\quad \left. -2\mathcal{F}_{11}C_T\left(\mathcal{F}_6 m_B^2\left(m_B^2 + 9m_{K_2}^2 - q^2\right) - \left(m_B^2 + 3m_{K_2}^2 - q^2\right)\left(\mathcal{F}_8 q^2 + \mathcal{F}_7\left(m_B^2 - m_{K_2}^2\right)\right)\right)\right)
\end{aligned}
$$

and the expression of the differential decay rate is given in Eq. (5.25).

5.4.3 Lepton Polarization asymmetries

By using Eqs. (3.14-3.18), we can obtain the expressions for longitudinal, normal and transverse polarizations for $B \to K_2^*(1430)\mu^+\mu^-$ decays and one collected below. The longitudinal lepton polarization can be written as:

$$
\begin{aligned}
\mathcal{P}_L &\propto \frac{1}{36m_B^2 m_T^4} 4u(q^2)\sqrt{\lambda}\left[P_L^{VA} + P_L^{SP} + P_L^{T}\right], && (5.29a)\\
P_L^{VA} &= m_l\left(2\lambda F_2\left(\mathcal{F}_6 - \mathcal{F}_7\right)m_B^4 + \left(3\lambda F_1\mathcal{F}_5 q^2 + 2F_2 m_B^2\left(10q^2\mathcal{F}_6 m_B^2 + \lambda F_7\right)\right)m_{K_2^*}^2\right.\\
&\quad \left. +2\lambda F_3\left(\mathcal{F}_6\left(q^2 - m_B^2 + m_{K_2^*}^2\right)m_B^2 + \lambda F_7\right)\right), && (5.29b)\\
P_L^{SP} &= 3m_l\lambda\mathcal{F}_9 m_B\left(-2m_l\mathcal{F}_8 q^2 - \mathcal{F}_{10}m_B q^2 + 2m_l\left(\left(\mathcal{F}_6 - \mathcal{F}_7\right)m_B^2 + \mathcal{F}_7 m_{K_2^*}^2\right)\right), && (5.29c)\\
P_L^{T} &= m_l^2\mathcal{F}_{11}\left(24\left(C_{TE}F_1 - C_T F_5\right)m_{K_2^*}^2\lambda + 4C_T\lambda F_3\left(m_B^2 + 3m_{K_2^*}^2 - q^2\right)\right.\\
&\quad +4m_B^2\left(4C_{TE}\mathcal{F}_6 - C_T\mathcal{F}_2\right)\left(10\left(m_B^2 - m_{K_2^*}^2\right)m_{K_2^*}^2 + \lambda\right)\\
&\quad +m_l^2\mathcal{F}_{12}\left(4m_B^2\left(4C_{TE}\mathcal{F}_6 - C_T\mathcal{F}_2\right)\left(10q^2 m_{K_2^*}^2 + \lambda\right) - 4C_T\mathcal{F}_3\left(q^2 - m_B^2 + m_{K_2^*}^2\right)\right)\\
&\quad \left. +m_l^2\mathcal{F}_{13}\left(2C_T\lambda - 4C_T\mathcal{F}_2 m_B^2\left(m_B^2 - m_{K_2^*}^2 - q^2\right) - 2C_T\lambda^2\mathcal{F}_3\right)\right). && (5.29d)
\end{aligned}
$$

Similarly, the normal lepton polarization is

$$
\begin{aligned}
\mathcal{P}_N &\propto -\frac{\pi u(q^2)t}{(12m_B^2 m_T^4}\left(\frac{\lambda}{t}\right)^{3/2}\left[P_N^{VA} + P_N^{SP} + P_N^{T}\right], && (5.30a)\\
P_N^{VA} &= 2m_l\left(\mathcal{F}_2\left(\mathcal{F}_8 q^4 - \left(\left(\mathcal{F}_6 - \mathcal{F}_7 + \mathcal{F}_8\right)m_B^2 + \left(-3\mathcal{F}_1 + \mathcal{F}_7 - \mathcal{F}_8\right)m_{K_2^*}^2\right)q^2 + \left(m_B^2 - m_{K_2^*}^2\right)\right. \right. && (5.30b)\\
&\quad \left.\left. m_B^2\left(\left(\mathcal{F}_6 - \mathcal{F}_7\right)m_B^2 + \mathcal{F}_7 m_{K_2^*}^2\right)\right) + \lambda\mathcal{F}_3\left(\mathcal{F}_8 q^2 - \mathcal{F}_6 m_B^2 + \mathcal{F}_7\left(m_B^2 - m_{K_2^*}^2\right)\right)\right)\right),\\
P_N^{SP} &= m_B\lambda\left(\mathcal{F}_3\mathcal{F}_{10}q^2 + \left(q^2 - 4m_l^2\right)\mathcal{F}_7\mathcal{F}_9\right) - \left(\mathcal{F}_2\mathcal{F}_{10}q^2 + \left(q^2 - 4m_l^2\right)\mathcal{F}_6\mathcal{F}_9\right)m_B^3\left(m_B^2 - m_{K_2^*}^2 - q^2\right), && (5.30c)\\
P_N^{T} &= \mathcal{F}_{13}\left(8m_l^2\lambda C_{TE}\left(\mathcal{F}_8 q^2 - \mathcal{F}_6 m_B^2 - \mathcal{F}_7\left(m_{K_2^*}^2 - m_B^2\right)\right) + 4m_l m_B\lambda C_{TE}\mathcal{F}_{10}q^2\right)\\
&\quad +\mathcal{F}_{12}\left(16m_l^2 C_{TE}\left(\mathcal{F}_6 m_B^2 - \mathcal{F}_7\left(m_B^2 - m_{K_2^*}^2\right) - \mathcal{F}_8 q^2 - \frac{m_B}{2m_l}\mathcal{F}_{10}q^2\right)\left(m_B^2 - m_{K_2^*}^2 - q^2\right)\right.\\
&\quad +6\left(4m_l^2 + q^2\right)C_{TE}\mathcal{F}_1 q^2 m_{K_2^*}^2 + 3\left(q^2 - 4m^2\right)C_T\mathcal{F}_5 q^2 m_{K_2^*}^2\Big)\\
&\quad +\mathcal{F}_{11}\left(-16m_l^2 C_{TE}\left(\mathcal{F}_8 q^2 + \mathcal{F}_7\left(m_B^2 - m_{K_2^*}^2\right) + \frac{m_B}{2m_l}\mathcal{F}_{10}q^2\right)\left(m_B^2 + 3m_{K_2^*}^2 - q^2\right)\right.
\end{aligned}
$$

$$+6m_{K_2^*}^2\left(4m_l^2+q^2\right)\left(C_{TE}\mathcal{F}_1\left(m_B^2-m_{K_2^*}^2\right)-C_T\mathcal{F}_2m_B^2\right)+3\left(4m_l^2-q^2\right)C_T\mathcal{F}_5m_{K_2^*}^2\left(m_{K_2^*}^2-m_B^2\right)$$
$$+4C_{TE}\mathcal{F}_6m_B^2\left(4m_l^2\left(m_B^2+6m_{K_2^*}^2-q^2\right)-3q^2m_{K_2^*}^2\right)\Big)\Big). \tag{5.30d}$$

and the transverse one is given by

$$\begin{aligned}\mathcal{P}_T \propto\ & \frac{i\pi\lambda q^2u(q^2)}{12m_Bm_{K_2^*}^2}\Big\{\lambda C_{TE}\mathcal{F}_{13}\left(4\mathcal{F}_2m_B^2-3\mathcal{F}_5m_{K_2^*}^2+\mathcal{F}_3\left(q^2-5m_B^2+m_{K_2^*}^2\right)\right)\\
&-2\mathcal{F}_{12}\Big(2C_{TE}\Big(\left(8\mathcal{F}_3m_B^2-(2\mathcal{F}_3+3\mathcal{F}_5)\,m_{K_2^*}^2\right)q^2+4\mathcal{F}_2m_B^2\left(2m_B^2+m_{K_2^*}^2-2q^2\right)\\
&-\left(m_B^2-m_{K_2^*}^2\right)\left(8\mathcal{F}_3m_B^2+(4\mathcal{F}_3+3\mathcal{F}_5)\,m_{K_2^*}^2\right)\Big)-3C_T\mathcal{F}_1m_{K_2^*}^2\left(q^2-3m_B^2+3m_{K_2^*}^2\right)\Big)\\
&+2\mathcal{F}_{11}\Big(2C_{TE}\left(3\mathcal{F}_5m_{K_2^*}^2\left(3m_B^2+m_{K_2^*}^2-q^2\right)-4\mathcal{F}_2\left(2m_B^2+3m_{K_2^*}^2-2q^2\right)m_B^2\right.\\
&\left.+2\mathcal{F}_3\left(7m_{K_2^*}^2q^2-4q^4+6\lambda+4m_B^2\left(q^2+5m_{K_2^*}^2\right)\right)\right)-3C_T\mathcal{F}_1m_{K_2^*}^2\left(3m_B^2+m_{K_2^*}^2-q^2\right)\Big\}\end{aligned} \tag{5.31}$$

5.4.4 Helicity Fractions

Helicity fraction is an observable associated with polarization of the out going meson that is almost free of hadronic uncertainties. The spin-2 polarization tensor, which satisfies $\epsilon_{\mu\nu}k^\nu=0$ with k being the momentum, is symmetric and traceless. It can be constructed by the vector polarization ϵ_μ as

$$\begin{aligned}\epsilon_{\mu\nu}(\pm2) &= \epsilon_\mu(\pm)\epsilon_\nu(\pm),\ \epsilon_{\mu\nu}(\pm1)=\frac{1}{\sqrt{2}}[\epsilon_\mu(\pm)\epsilon_\nu(0)+\epsilon_\mu(0)\epsilon_\nu(\pm)],\\
\epsilon_{\mu\nu}(0) &= \frac{1}{\sqrt{6}}[\epsilon_\mu(+)\epsilon_\nu(-)+\epsilon_\mu(-)\epsilon_\nu(+)]+\sqrt{\frac{2}{3}}\epsilon_\mu(0)\epsilon_\nu(0).\end{aligned} \tag{5.32}$$

Using the definition

$$\varepsilon_{T\nu}(n)=\frac{\varepsilon_{\nu\alpha}(n)p^\alpha}{m_B},$$

the above relations simplify to

$$\varepsilon_{T\nu}(\pm2)=0,\ \varepsilon_{T\nu}(\pm1)=\frac{\epsilon(0).p}{\sqrt{2}m_B}\epsilon_\mu(\pm),\ \varepsilon_{T\nu}(0)=\sqrt{\frac{2}{3}}\frac{\epsilon(0).p}{m_B}\epsilon_\mu(0)$$

The physical expressions for helicity fractions are given by

$$f_i(q^2)=\frac{d\Gamma_i/dq^2}{d\Gamma/dq^2},i=L,T \tag{5.33}$$

Here L and T refer to longitudinal and transverse helicity fractions. The explicit expression of the longitudinal helicity fraction for the decay $B\to K_2^*(1430)l^+l^-$ is

$$\begin{aligned}\frac{d\Gamma_L}{dq^2} &= \frac{G_F^2\alpha^2}{2^{11}\pi^5m_B^3}\frac{\left|V_{tb}V_{ts}^*\right|^2u(q^2)}{36m_{K_2^*}^4m_B^2q^2}\Big(4F_2^2m_B^4\left(2m^2+q^2\right)K_1^2+4F_3^2(2m^2+t)\lambda^2\\
&+6F_9^2q^2\lambda m_B^2\left(q^2-4m\right)+6F_{10}^2q^4\lambda m_B^2+4F_6^2m_B^4\left(q^2K_1^2+2m^2\left(\lambda-8q^2m_{K_2^*}^2\right)\right)\end{aligned}$$

$$
\begin{aligned}
&+4F_7^2\lambda\left(2m^2\left(4q^2\left(m_B^2+m_{K_2^*}^2\right)+K_0^2-2q^4\right)+q^2\lambda\right)+24F_8^2m^2q^4\lambda\\
&-8F_6F_7\lambda m_B^2\left(2m^2\left(K_0+2q^2\right)+q^2K_1\right)-8F_2F_3\lambda m_B^2\left(2m^2+q^2\right)K_1-8F_{12}F_{13}q^2\lambda K_1K_3\\
&+48F_7F_8m^2q^2\lambda K_0+8F_{11}^2q^2K_4^2K_3+8F_{12}^2q^2K_1^2K_3+2F_{13}^2q^2\lambda^2K_3+16F_{11}F_{12}q^2K_1K_4K_3\\
&-8F_{11}F_{13}\lambda\left(4C_T^2m^2\left(\lambda-K_0K_1\right)+144m^2q^2C_{TE}^2K_4+3m^2C_T^2m_{K_2^*}^2\right)+48F_3F_{13}mq^2\lambda^2C_{TE}\\
&-48F_2F_{13}mq^2\lambda m_B^2C_{TE}K_1-96F_3F_{12}mq^2\lambda C_{TE}K_1+96F_2F_{12}mq^2m_B^2C_{TE}K_1^2\\
&+96F_2F_{11}mq^2m_B^2C_{TE}K_1K_4-48F_2F_{13}mq^2\lambda m_B^2C_{TE}K_1-96F_3F_{12}mq^2\lambda C_{TE}K_1\\
&+8F_{11}^2q^2K_4^2K_3+8F_{12}^2q^2K_1^2K_3+2F_{13}^2q^2\lambda^2K_3-8F_{12}F_{13}q^2\lambda K_1K_3+16F_{11}F_{12}q^2K_1K_4K_3\\
&-8F_{11}F_{13}\lambda\left(4C_T^2m^2\left(\lambda-K_0K_1\right)+144m^2q^2C_{TE}^2K_4+3m^2C_T^2m_{K_2^*}^2\right)\\
&+96F_2F_{12}mq^2m_B^2C_{TE}K_1^2+48F_3F_{13}mq^2\lambda^2C_{TE}+96F_2F_{11}mq^2m_B^2C_{TE}K_1K_4\Big)
\end{aligned}
\tag{5.34}
$$

As the sum of the longitudinal and transverse helicity amplitudes is equal to unity i.e. $f_L(q^2)+f_T(q^2)=1$ for each value of q^2, therefore, the expression of transverse helicity fraction of final state meson is quite obvious.

5.5 Numerical Analysis

In this section we will examine the physical observables derived above and analyze the effects of model independent(MI) parameters on these observables. As $B\to K_2^*(1430)\mu^+\mu^-$ is not yet observed, therefore the purpose of this study is not to get constraints on NP parameters but is to use the constraints on MI parameters defined in Sec. 5.3. which comes from different B meson decays. We consider different Lorentz structures of NP, as well as their combinations and examine their implications on differential decay rate, the forward-backward asymmetry, the lepton polarization asymmetries and the helicity fractions of the final state $K_2^*(1430)$ meson. Here we varied the strength of individual NP couplings such that they lie inside the bounds given by different flavor decays (c.f. Sec. 5.3). In all the figures the band correspond to the uncertainties in different input parameters where form factors (c.f. Table 5.1) are the major contributors. The same type of lines correspond to the same set of NP parameters and all the NP curves are plotted for the central values of the form factors and other input parameters. To make the quantitative analysis complete the numerical values of input parameters that we have used are given in Table 3.1 and 3.2.

From the point of view of probing physics beyond the standard model there are a large number of observables which are accessible in the above mentioned B-meson decay. For instance, the branching ratio, in general for semi-leptonic decays like $B\to K_2^*(1430)\mu^+\mu^-$, is prune to many sources of uncertainties. The major source of uncertainty originate from the $B\to K_2^*(1430)$ transition form factors calculated using the LCSR approach, as shown in Table 5.1, and can give $20-30\%$ uncertainty to the differential branching ratio. Thus the differential branching ratio is not a suitable observable to look for the NP effects unless these effects are very drastic. It is therefore valuable to look for the observables where hadronic uncertainties almost have no effect. In this

regard the most important observables are the zero position of the forward-backward asymmetry, different lepton polarization asymmetries and the helicity fractions of the final state meson. These observables are almost free from the hadronic uncertainties and serve as an important probe to look for NP.

The SM predicts the zero crossing of $A_{FB}(q^2)$ at a well determined position which is free from the hadronic uncertainties at the leading order (LO) in strong coupling α_s [102, 103, 104]. This zero position of A_{FB}, which is independent of form factors, is an important observable in the search of new physics. The short distance relation between the Wilson coefficients and the zero position of A_{FB} is given by [105, 101]

$$\Re[C_9^{eff}(q_0^2)] = \frac{2m_b m_B}{q_0^2} C_7^{eff} \tag{5.35}$$

where q_0^2 is the zero position (ZP) of the A_{FB}. Recently LHCb has published its results on $A_{FB}(\bar{B} \to \bar{K}^* \mu^+ \mu^-)$ that are quite close to SM predictions [91]. The LHCb result shows, with small error bars, that the zero position of $A_{FB}(\bar{B} \to \bar{K}^* \mu^+ \mu^-)$ is close to the SM's zero position. Like $\bar{B} \to \bar{K}^* \mu^+ \mu^-$ decay, the semileptonic decay $B \to K_2^*(1430)\mu^+\mu^-$ also occurs through the quark level transition $b \to s\mu^+\mu^-$. Therefore, the future measurements of the $A_{FB}(B \to K_2^*(1430)\mu^+\mu^-)$ will shed more light on NP in the flavor sector.

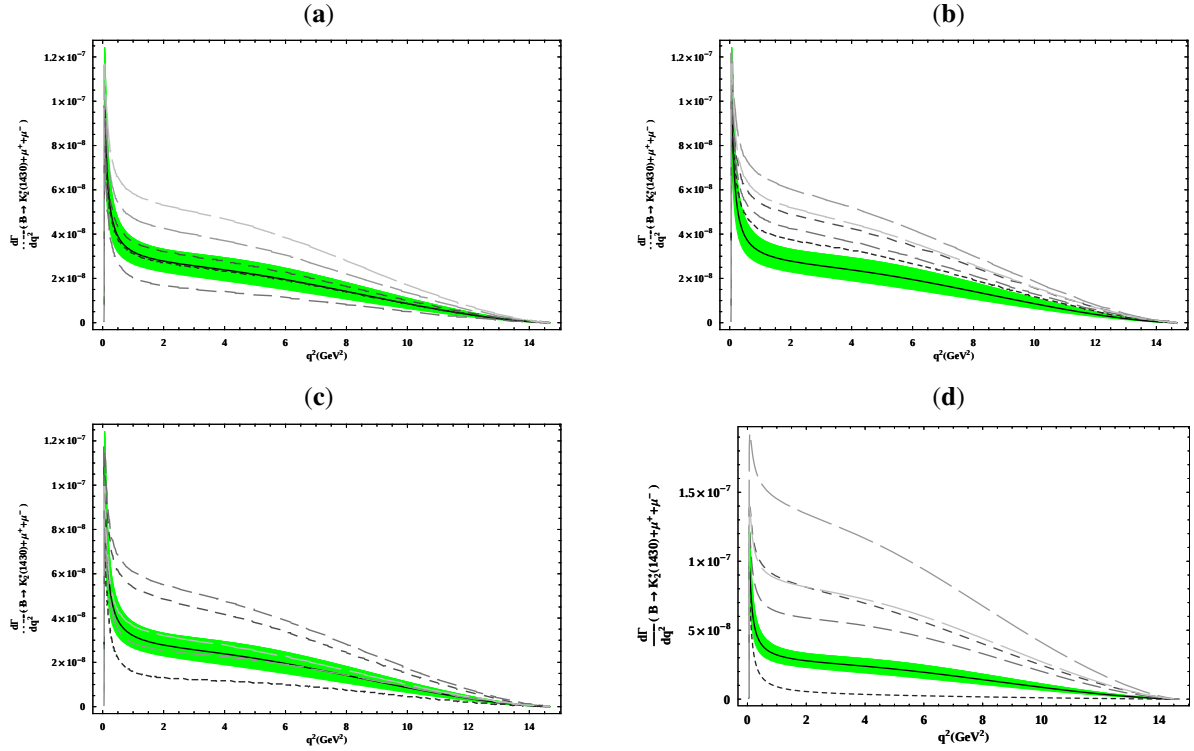

Figure 5.1: The dependence of decay rate for $B_0 \to K_2^*(1430)\mu^+\mu^-$ on q^2 where different curves correspond to different choices of the values of VA couplings inside their allowed region. In Fig(a) only R_V and R_A are present, Fig(b) when only R'_V and R'_A are present, Fig(c), Fig(d) when both R_V, R'_V and R_A, R'_A are present and in all figures the solid line represent the SM with light green shaded region as uncertainty in SM.

The polarization of the final state leptons can shed light on the helicity structure of the electroweak interactions. The longitudinal and normal lepton polarization asymmetry are also very good observables to look for NP

effects. As in the case of forward-backward asymmetry the long distance effects are also canceled out in these asymmetries. Hence, they provide a good tool to test the various new physics extensions of the SM. In the present numerical analysis, we have taken the NP couplings to be real. The transverse lepton polarization asymmetry as given in Eq. (5.31) involves the imaginary part of the auxiliary functions, and hence for real couplings its value comes out to be negligibly small. In this numerical study we will discuss the results of transverse lepton polarization asymmetry in the presence of all NP operators at the very end.

Another interesting observable is the study of the spin effects of the final state meson which for our case is the $K_2^*(1430)$ meson. A detailed discussion about the effects of NP operators on the longitudinal and transverse helicity fractions of final state meson will also be done in the forthcoming numerical analysis.

A model independent numerical analysis of this decay channel $B \to K_2^*(1430)\mu^+\mu^-$ is presented in this section, where we will analyze the effects of different NP operator couplings (VA,SP,T) on different physical observables. A similar NP study was presented in [100] where the observables studied were polarized branching ratios as function of NP couplings and forward backward asymmetry. The observables we have presented in this chapter are different than the ones presented in [100]. For example we have studied differential observables(that are functions of q^2) like branching ratio, forward backward asymmetry, lepton polarization asymmetries and helicity fractions of the final state meson. We have also incorporated the old bounds [113, 114] as well as the new LHCb bound [91] on different NP couplings. We will study the effects of these NP couplings one by one as follows.

5.5.1 *VA* new-physics operators

In this section, we shall consider the scenarios when (a) only $R_{V,A}$ couplings are present, (b) only $R'_{V,A}$ couplings are present, and (c) both types of couplings are present.

Figs. 5.1-5.5 display the results when the only vector-axial vector *VA* NP couplings ($R_{V,A}$ and $R'_{V,A}$) are present. In the case of differential branching ratio it can be seen that its value increases for certain range of parameters while it decreases for another range of parameters. The increase in differential branching ratio is up to 4 time its SM value for the case when both type of NP couplings are present simultaneously (c.f. Fig. 5.1(c,d)).

As can be seen in Fig. 5.2 that the $A_{FB}(q^2)$ is very sensitive to the NP effects. The zero crossing is also disturbed significantly by the VA couplings. The short distance relation Eq. (5.35) is modified with the inclusion of new VA couplings which now takes the form

$$\Re(C_9^{eff}(q_0^2)) + R_V - \frac{R'_V R'_A}{C_{10}} = \frac{2m_b m_B}{q_0^2} C_7^{eff} \tag{5.36}$$

The experimental results that came in from measurement of $A_{FB}(\bar{B} \to \bar{K}^*\mu^+\mu^-)$ at LHCb can put stringent bound on the NP coupling constants. In the measurement of the zero position of $A_{FB}(\bar{B} \to \bar{K}^*\mu^+\mu^-)$ at LHCb, the experimental error bar in this zero position is roughly 30 percent. When this error bar uncertainty is plugged in Eq. 5.36 we get a new bound on the VA coupling constants

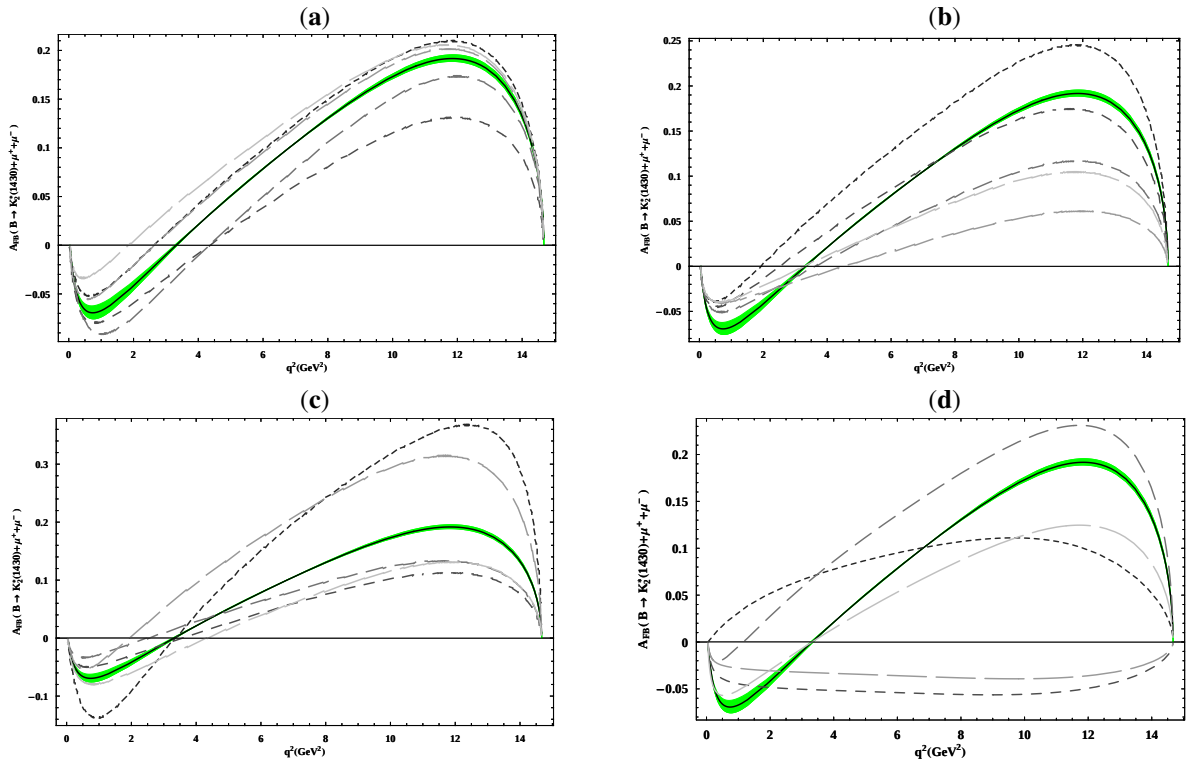

Figure 5.2: The dependence of forward-backward asymmetry for $B \to K_2^*(1430)\mu^+\mu^-$ on q^2 for different values of VA couplings. The caption for the above figures are the same as Fig. 5.1.

$$-1 < R_V - \frac{R'_V R'_A}{C_{10}} < 3.2 \tag{5.37}$$

When this bound is taken into consideration then the zero position (ZP) stays in the vicinity of Standard Model's ZP (see Figs. 5.2(a,b,c)). But if we ignore this new bound then the effects on forward backward asymmetry become very drastic (see Fig. 5.2d). These effects increase when all the couplings $R_{V,A}$ and $R'_{V,A}$ are present (Figs. 5.2(c,d)). The zero crossing shifts quite significantly and it even disappears for certain values of $R_{V,A}$ and $R'_{V,A}$ (Fig. 5.2d).

Figs. 5.3 and 5.4 depict the effects on lepton polarization asymmetries coming from $R_{V,A}$ and $R'_{V,A}$ couplings. The effects are quite obvious in the case of longitudinal lepton polarization asymmetry. The magnitude of P_L decrease in most cases and when $R'_{V,A}$ is present the effects get more amplified. This asymmetry even vanishes (Fig. 5.3b) in some values of $R'_{V,A}$ couplings. When both $R_{V,A}$ and $R'_{V,A}$ are present, P_L even changes sign for some values of couplings (see Figs. 5.3(c,d)). As can be seen in Eq. (5.29b) the VA effects are only m_l suppressed compared to other NP contributions that are m_l^2 suppressed. Qualitatively, these effects are large because of large numerical values and different signs of the new VA couplings. The normal lepton polarization asymmetry is also sensitive to NP effects, as it develops a zero crossing which is not present in SM. Still, the effects are suppressed by m_l (see Eq. 5.30b) hence in Fig. 5.4 all curves show nearly the same behavior.

The longitudinal and transverse helicity fractions are depicted in Figs. 5.5. The deviation from the SM results

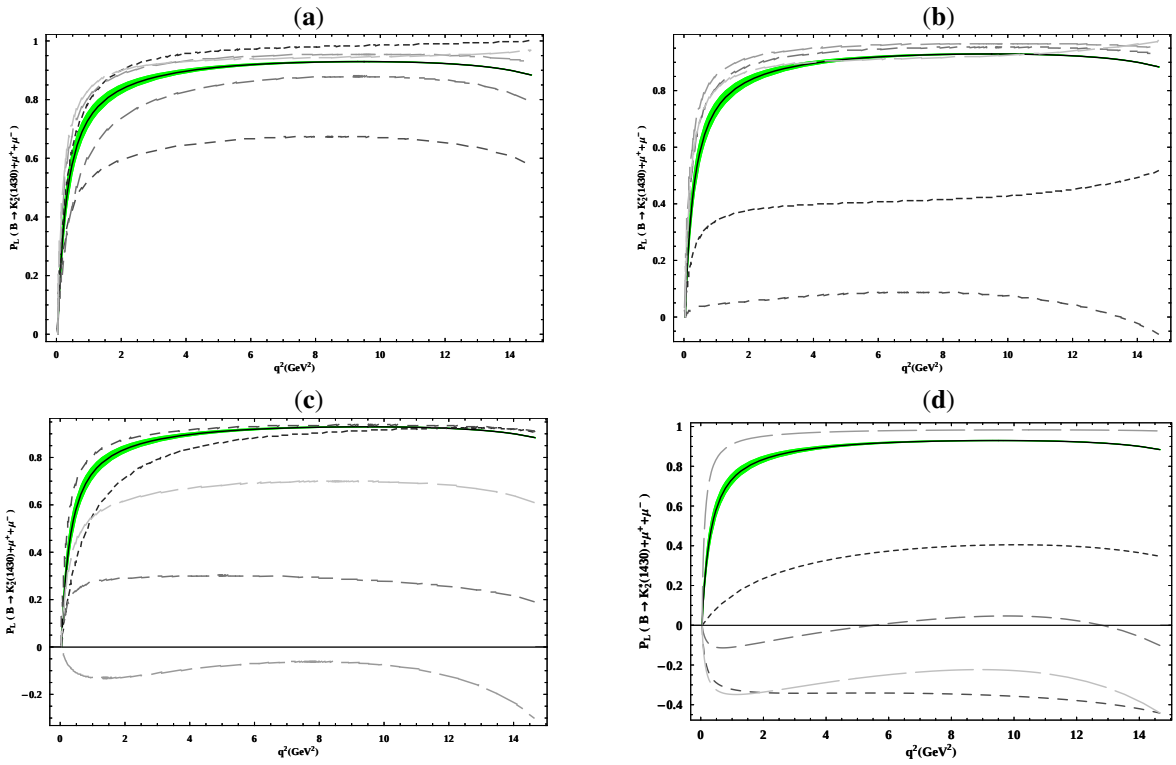

Figure 5.3: The dependence of Longitudinal lepton polarization asymmetry for $B \to K_2^*(1430)\mu^+\mu^-$ on q^2 for different values of VA couplings. The caption for the above figures are the same as Fig. 5.1.

are fairly large that arise from the effects of different VA couplings. When both $R_{V,A}$ and $R'_{V,A}$ couplings are present (see Figs. 5.5(c,d,g,h)) the traits become even more conspicuous.

5.5.2 SP new-physics operators

In this section, we consider the scenarios when (a) only R_S and R'_S couplings are present, (b) only R_P and R'_P couplings are present, and (c) both types of couplings are present.

The differential branching ratio in Fig. 5.6 shows that it is slightly disturbed by the different values of SP parameters. Fig. 5.7 depicts that the lepton forward-backward asymmetry is not very sensitive to the NP arising form SP operators. There is a slight shift in the zero position of the $A_{FB}(q^2)$ towards left or right. These mild effects can also be inferred from the Eq. (5.28c) that SP effects on forward-backward asymmetry are m_l suppressed.

Fig. 5.8 displays the plots of the longitudinal lepton asymmetry in the presence of SP operator couplings. The S and P couplings separately (Figs. 5.8(a,b)) have a mild effect on the longitudinal lepton polarization asymmetry, while the effects increase three folds when both the couplings are present, Fig. 5.8(c). The dominant contribution comes from the $\mathcal{F}_9\mathcal{F}_{10}$ term in Eq. (5.29c) which is enhanced by a factor of $m_B q^2$.

The normal lepton polarization asymmetry is very sensitive to the S and P couplings. In SM this asymmetry takes only negative values and there is no zero crossing, but as S and P couplings are introduced the curves are scattered in both positive and negative regimes (Fig 5.9). When both SP couplings are present the effects are even more enhanced. The Eq. (5.30c) clearly shows that SP contribution is not m_l suppressed like other VA

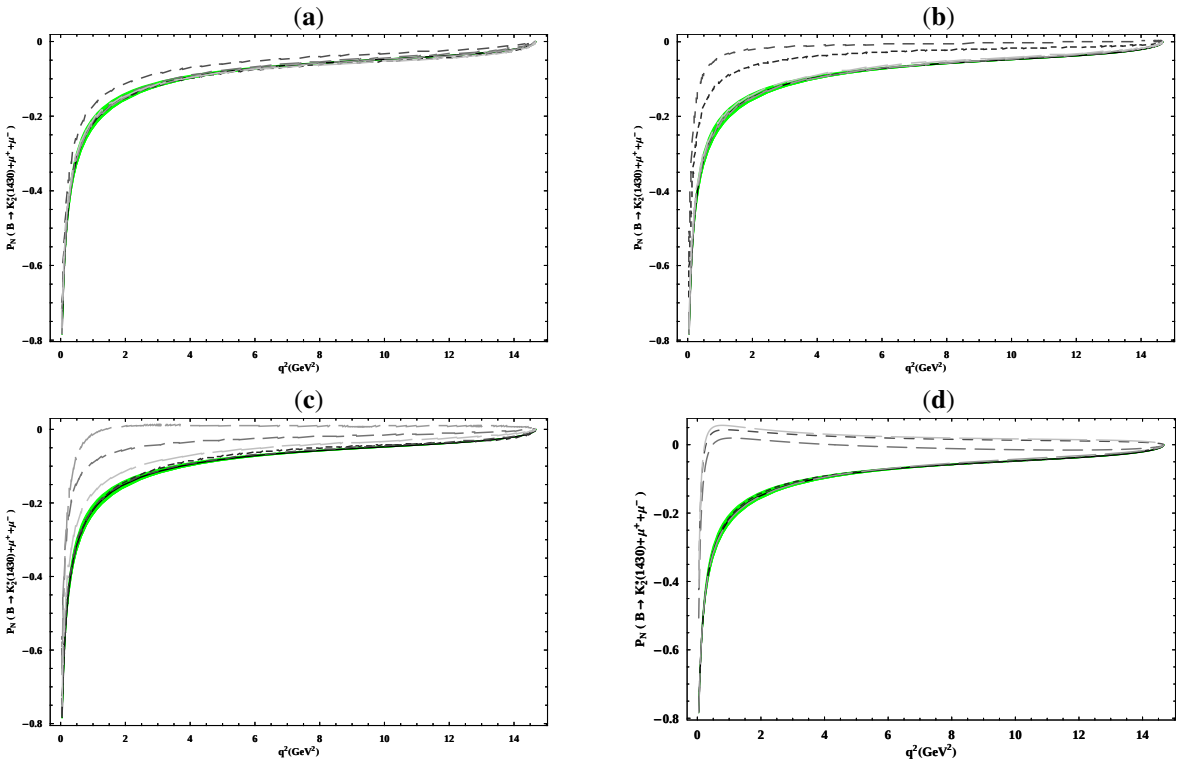

Figure 5.4: The dependence of Normal lepton polarization asymmetry for $B \to K_2^*(1430)\mu^+\mu^-$ on q^2 for different values of VA couplings. The caption for the above figures are the same as Fig. 5.1.

contributions to the normal polarization asymmetry. So the normal lepton polarization asymmetry is a very good tool to constraint the values of the SP couplings.

In case of SP couplings the longitudinal and transverse helicity fractions are shown in Fig. 5.10. The effects in this case are quite subtle especially in the large q^2 region as seen in Fig 5.10. The deviation from SM amplifies when both S and P couplings are present (see Figs. 5.10(c,f)).

5.5.3 T operators and interference of SP and T operators

In this section, we shall consider the scenarios when (a) only C_T and C_{TE} couplings are present, (b) when S, C_T and C_{TE} couplings are present, and (c) when P, C_T and C_{TE} couplings are present.

The differential branching ratio shown in Fig. 5.11 indicates that its value increases for most values T coupling parameters. These T type coupling also effects the zero crossing of the $A_{FB}(q^2)$ which can be seen in Fig. 5.12. By looking at the Eq. (5.28) one can see that the contribution from the T couplings is m_l suppressed (c.f. Eq. (5.28e)) but after including SP operators along with T operators it is no more m_l suppressed. It is therefore expected that the value of $A_{FB}(q^2)$ in this scenario will be large compared to T coupling only, but the sever constraints on the SP couplings do not allow $A_{FB}(q^2)$ to become significantly more than the SM in magnitude. Also there is some parameter space of couplings where $A_{FB}(q^2)$ is negative every where, i.e. there is no zero crossing (Fig. 5.12(b,c)).

In Fig. 5.13(a) the longitudinal lepton asymmetry is shown in the presence of T operator couplings. From Eq. (5.29b) we can observe that the effect of the T couplings are m_l^2 suppressed and therefore we expect the small

variation of longitudinal lepton polarization asymmetry unless the value of T couplings is large and this can also be inferred from Fig. 5.13. When SP couplings are also included the results hardly change (Fig. 5.13(b,c)) since their effect is also m_l suppressed compared to SM results.

The normal lepton polarization asymmetry (Fig 5.14(a)) develops a zero crossing when only T operator couplings are incorporated. Adding the SP operators change the plots as well. The zero crossing of the normal lepton polarization asymmetry is shifted when the SP couplings are introduced along with C_T and C_{TE}.

The longitudinal and transverse helicity fractions in the presence of T operator couplings are plotted in Fig. 5.15. Here, the response to the different values of T couplings are visible both in the high and low q^2 regimes. The effects are more distinct when C_T coupling is present compared to when only C_{TE} coupling is present. When SP couplings are added along with the T couplings the results are an emulsion of the effects coming from T as well as high q^2 effects of SP (Figs. 5.15(b,c,e,f)).

5.5.4 All NP operators together

In the presence of all new physics operator couplings of V, A, S, P and T the results as expected are pretty drastic. The combination of all these couplings have most of the attributes of each individual type of coupling. The branching ratio plots as shown in Fig. 5.16 increases by a factor of two and depending upon the values of coupling this increase is four times compared to the SM branching ratio (Fig. 5.16(b)).

The forward backward asymmetry gets scrambled results, the zero crossing vanishes for most values of NP couplings when new bound Eq. (5.37) is neglected (Fig 5.17b). If this new bound is incorporated then the zero position does not vanish but the shift in ZP is significantly in both directions.

The longitudinal lepton polarization varies a lot and takes on both positive and negative values (Fig. 5.18). The normal lepton polarization crosses the zero and become positive for some values of the NP couplings (Fig. 5.19) showing us the presence of SP couplings.

The longitudinal and transverse helicity fractions are shown in Fig. 5.20 for the case when all couplings are present. The deviation from SM values, as expected, are large since now all couplings are present.

Finally, the transverse lepton polarization asymmetry P_T acquires non-zero values when T couplings are present (see Eq. (5.31)). In the SM this asymmetry is negligibly small since all Wilson coefficients are predominantly real. The transverse lepton polarization asymmetry will be imaginary if all couplings are real(c.f. Eq. (3.19)), but for imaginary values of C_T, C_{TE} couplings it will become a real observable. Fig. 5.21 shows P_T for different values of imaginary tensor couplings while all other couplings are taken to be real. It can be seen that for certain values of NP couplings the value of transverse lepton polarization is significant. It is therefore expected that its experimental observation in future will help us to get constraints on C_T, C_{TE} couplings. In Fig. 5.21a only C_T, C_{TE} couplings are present and in Figs. 5.21(b,c) all other couplings are present too, hence the values of P_T become large.

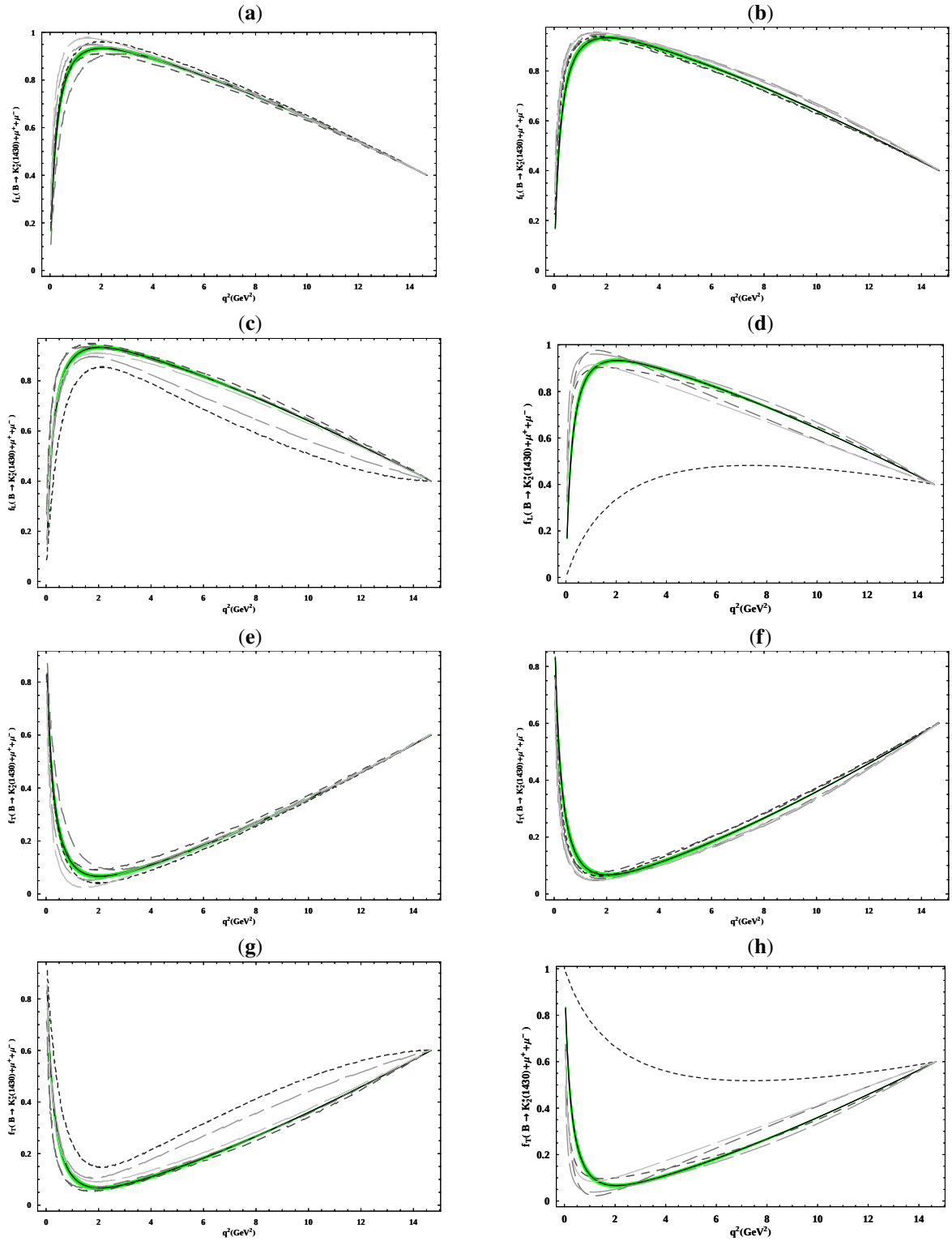

Figure 5.5: The dependence of Longitudinal and Transverse helicity fractions for $B \to K_2^*(1430)\mu^+\mu^-$ on q^2 for different values of VA couplings. The caption for the above figures are the same as Fig. 5.1.

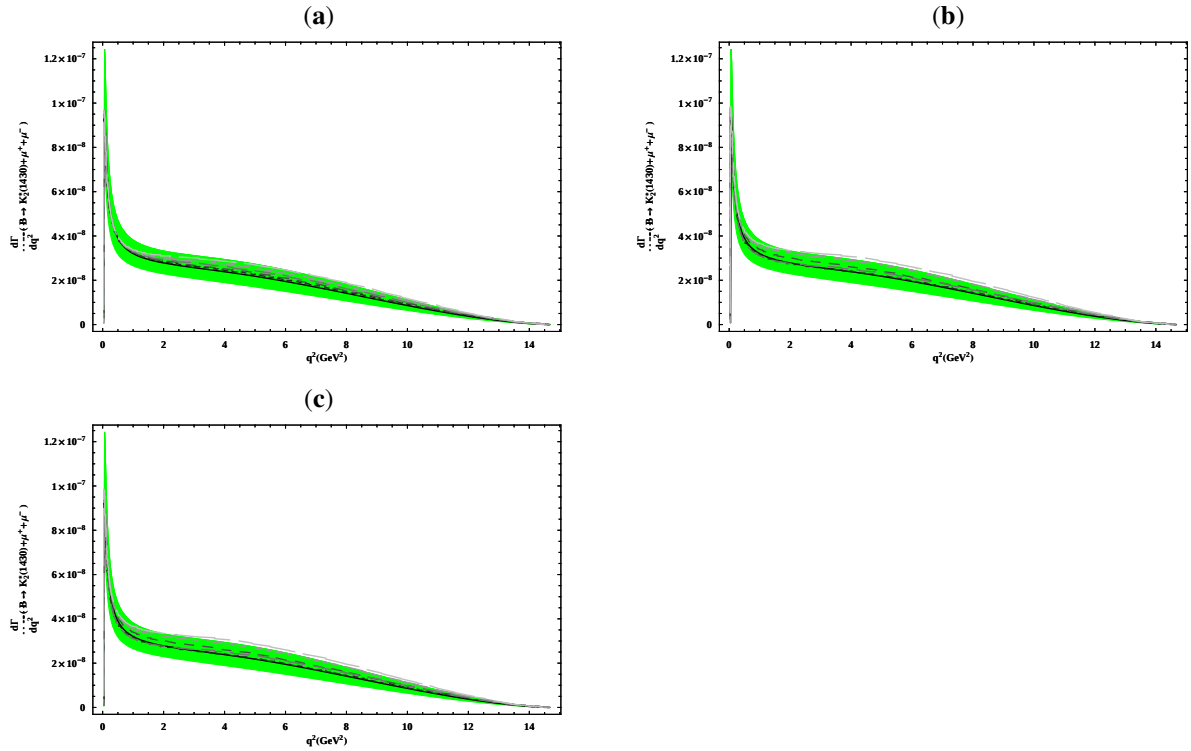

Figure 5.6: The dependence of decay rate for $B_0 \to K_2^*(1430)\mu^+\mu^-$ on q^2 where different curves correspond to different choices of the values of SP couplings inside their allowed region. In Fig(a) only R_S and R_P are present, Fig(b) when only R'_S and R'_P are present, Fig(c) when both R_S, R'_S and R_P, R'_P are present and in all figures the solid line represent the SM with light green shaded region as uncertainty in SM.

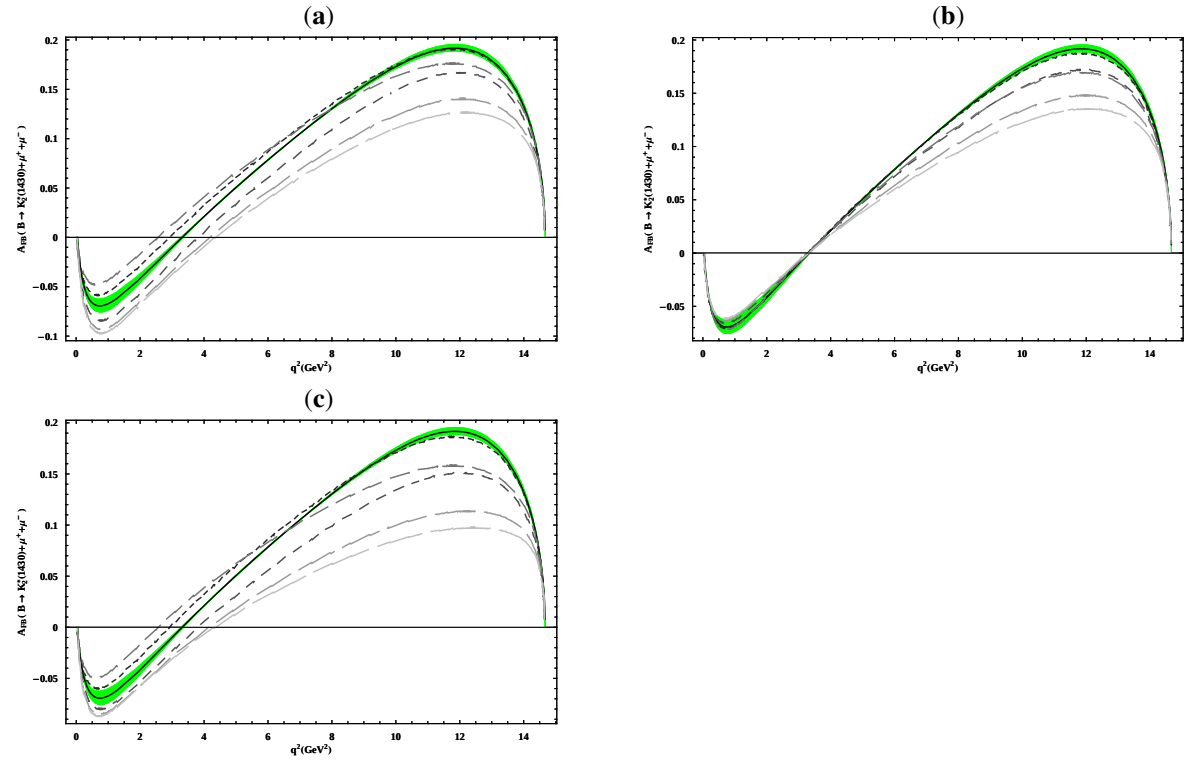

Figure 5.7: The dependence of forward-backward asymmetry for $B \to K_2^*(1430)\mu^+\mu^-$ on q^2 for different values of SP couplings. The caption for the above figures are the same as Fig. 5.6.

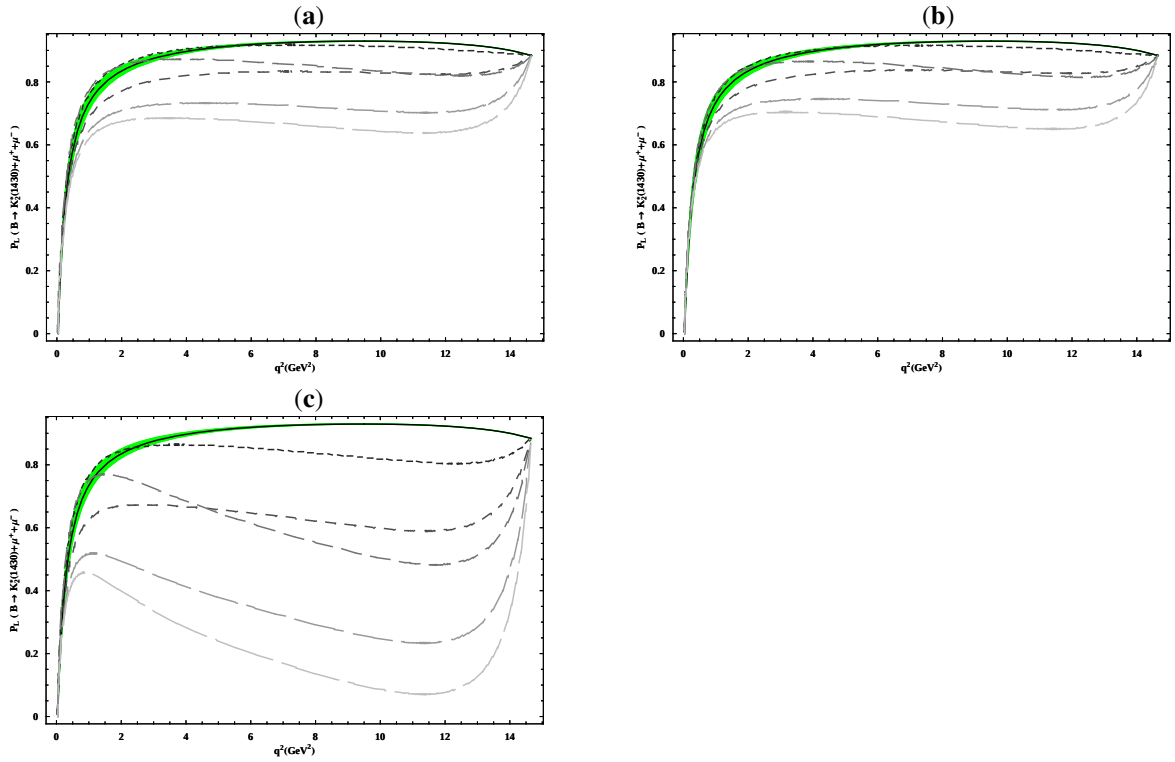

Figure 5.8:

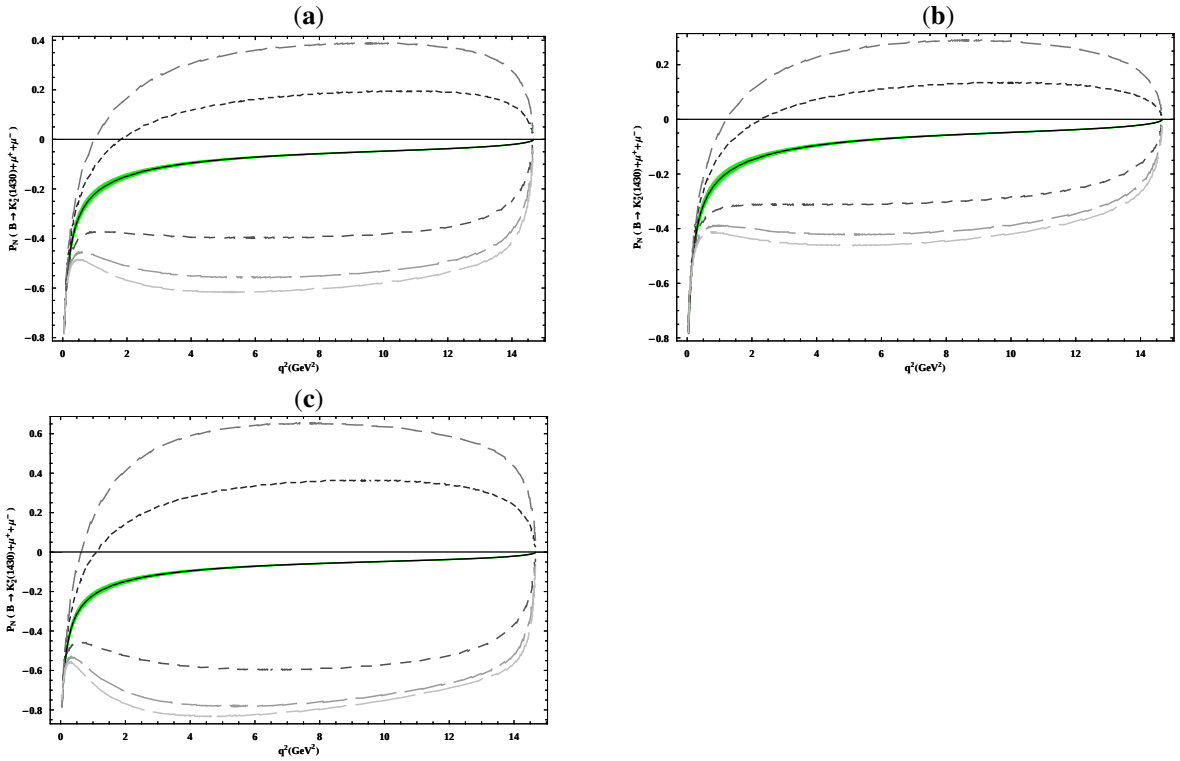

Figure 5.9: The dependence of Longitudinal and Normal lepton polarization asymmetry for $B \to K_2^*(1430)\mu^+\mu^-$ on q^2 for different values of SP couplings. The caption for the above figures are the same as Fig. 5.6.

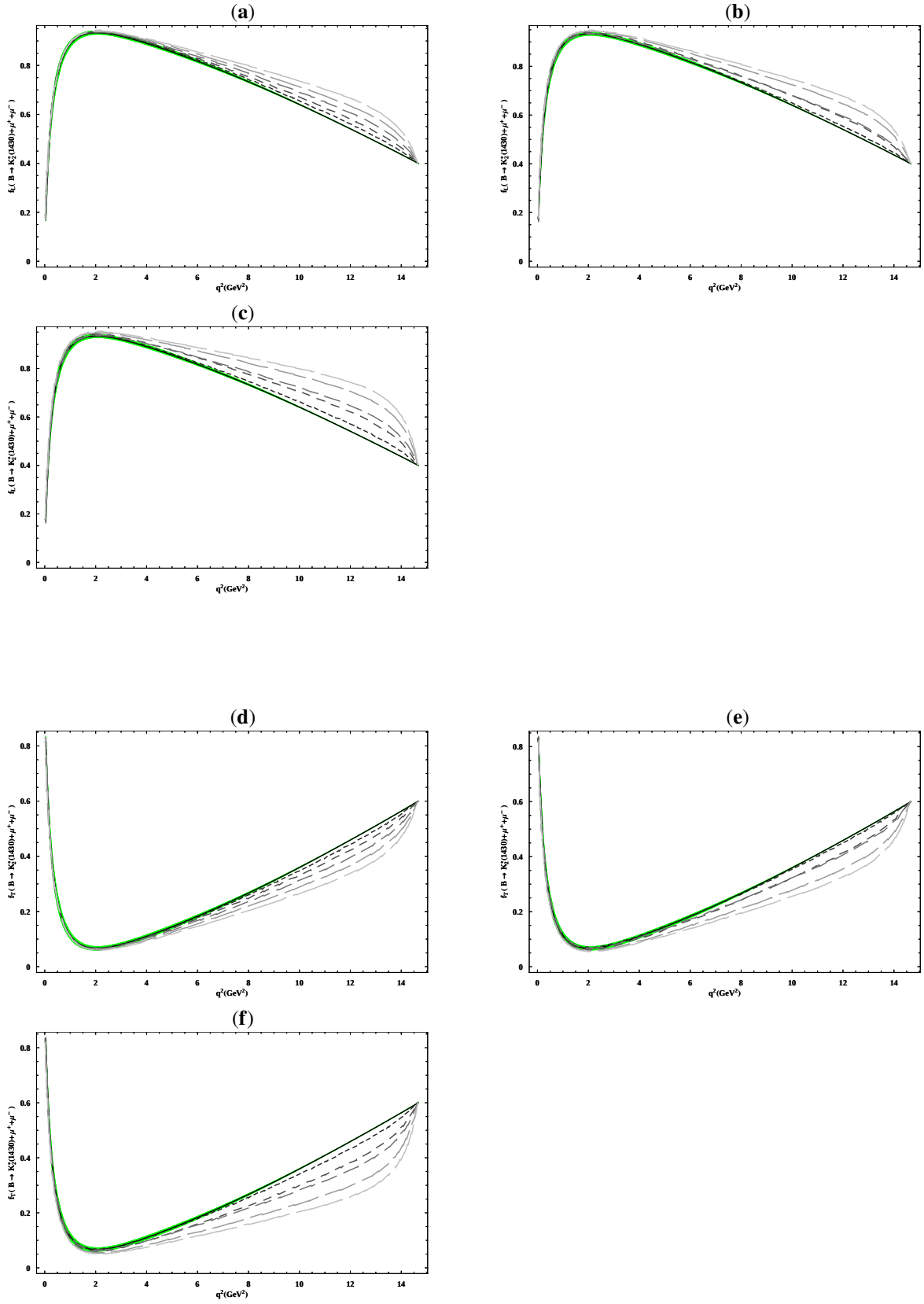

Figure 5.10: The dependence of Longitudinal and Transverse helicity fractions for $B \to K_2^*(1430)\mu^+\mu^-$ on q^2 for different values of SP couplings. The caption for the above figures are the same as Fig. 5.6.

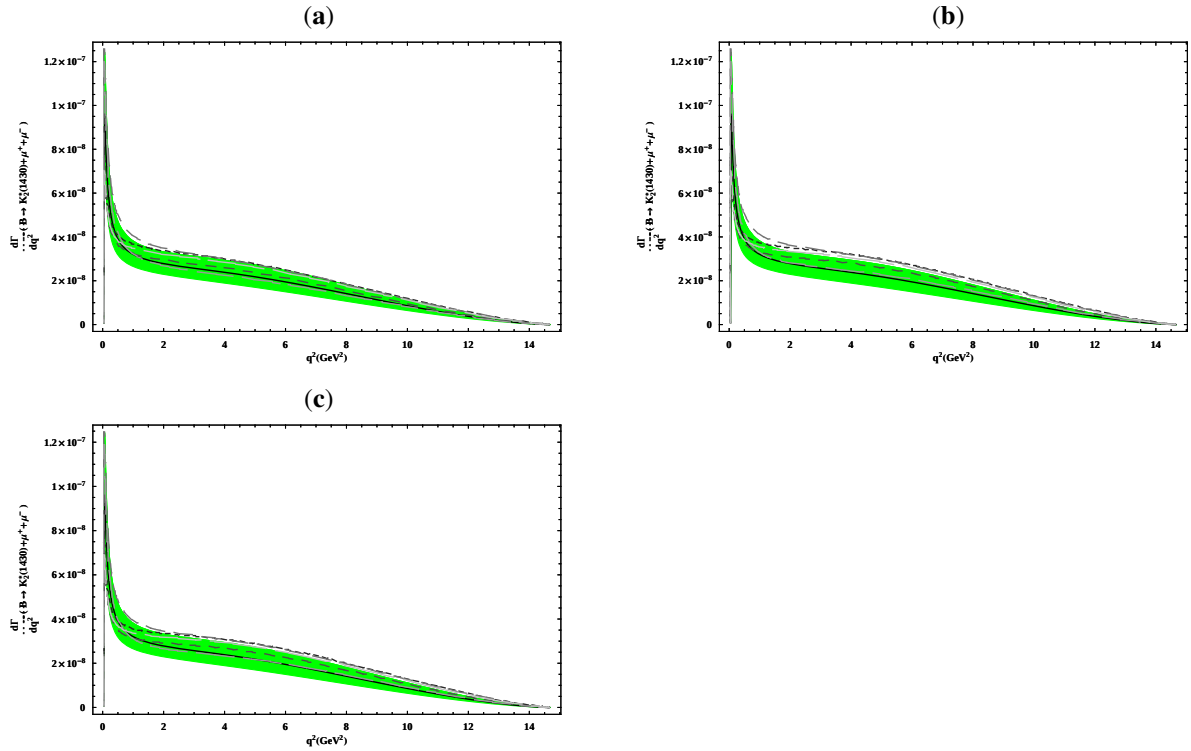

Figure 5.11: The dependence of decay rate for $B_0 \to K_2^*(1430)\mu^+\mu^-$ on q^2 where different curves correspond to different choices of the values of T-SP couplings inside their allowed region. In Fig(a) only C_T and C_{TE} are present, Fig(b) when only C_T, C_{TE}, R_S and R'_S are present, Fig(c) when only C_T, C_{TE}, R_P and R'_P are present and in all figures the solid line represent the SM with light green shaded region as uncertainty in SM.

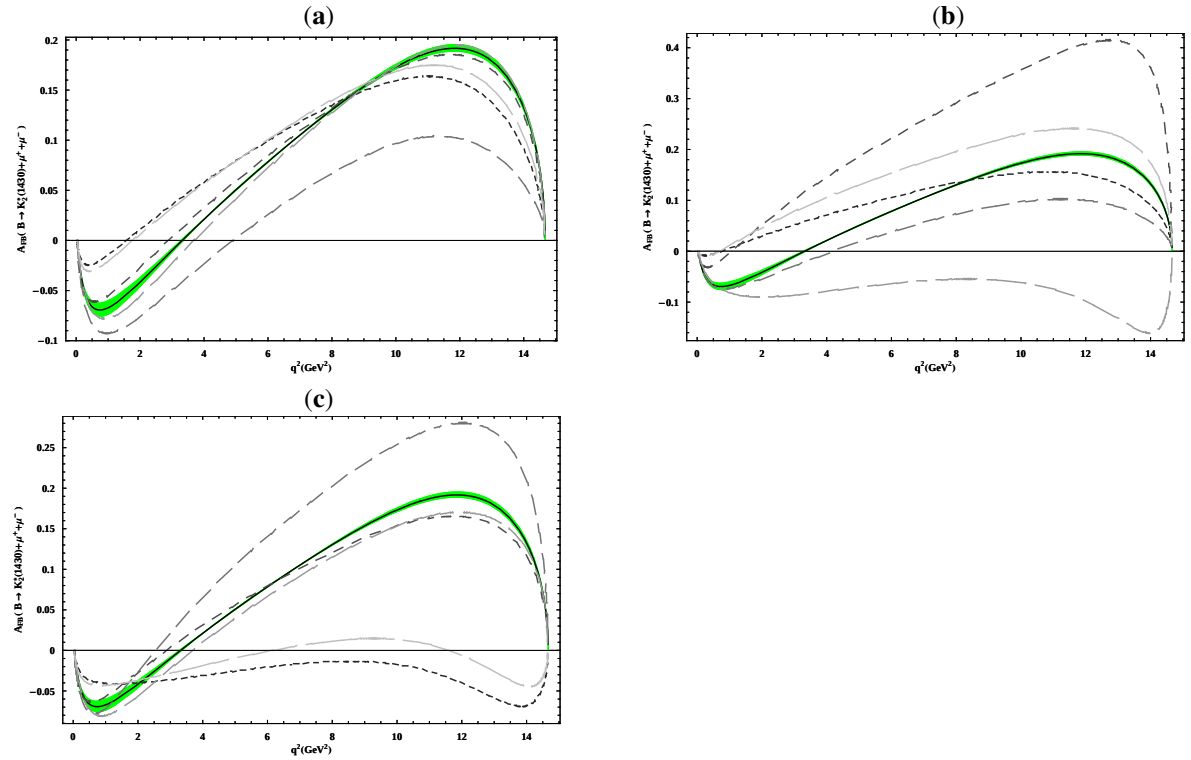

Figure 5.12: The dependence of forward-backward asymmetry for $B \to K_2^*(1430)\mu^+\mu^-$ on q^2 for different values of T-SP couplings. The caption for the above figures are the same as Fig. 5.11.

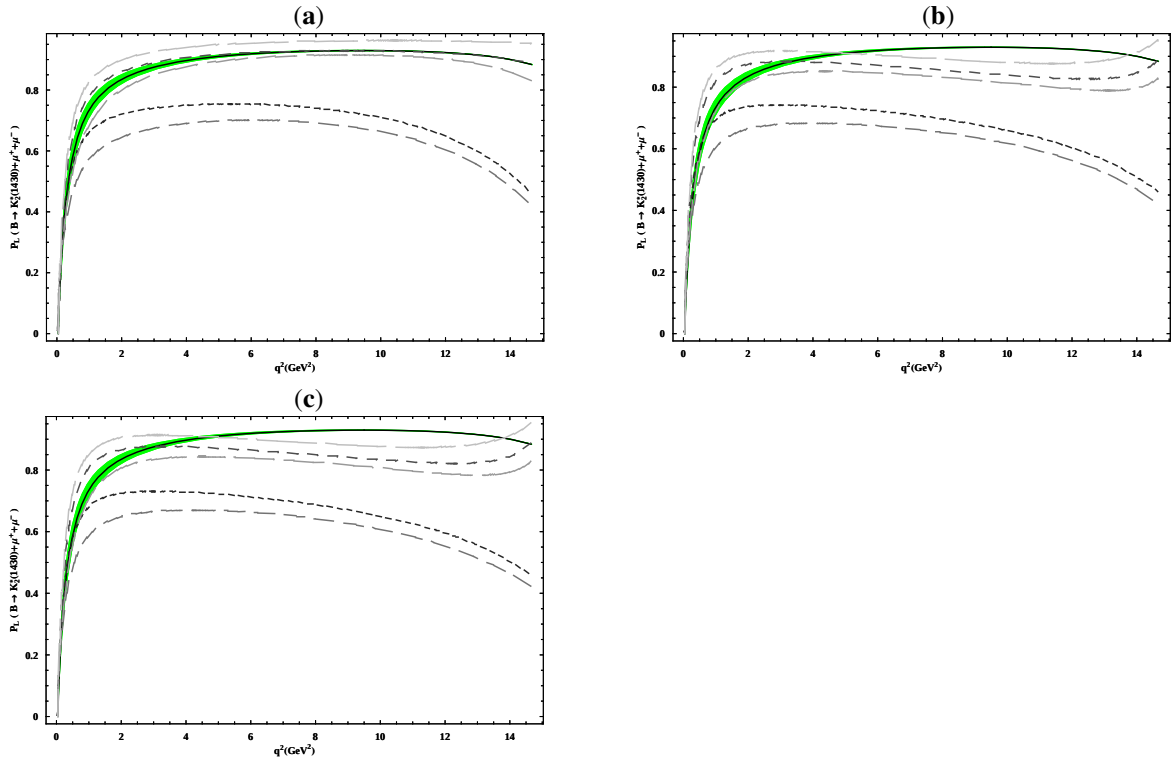

Figure 5.13:

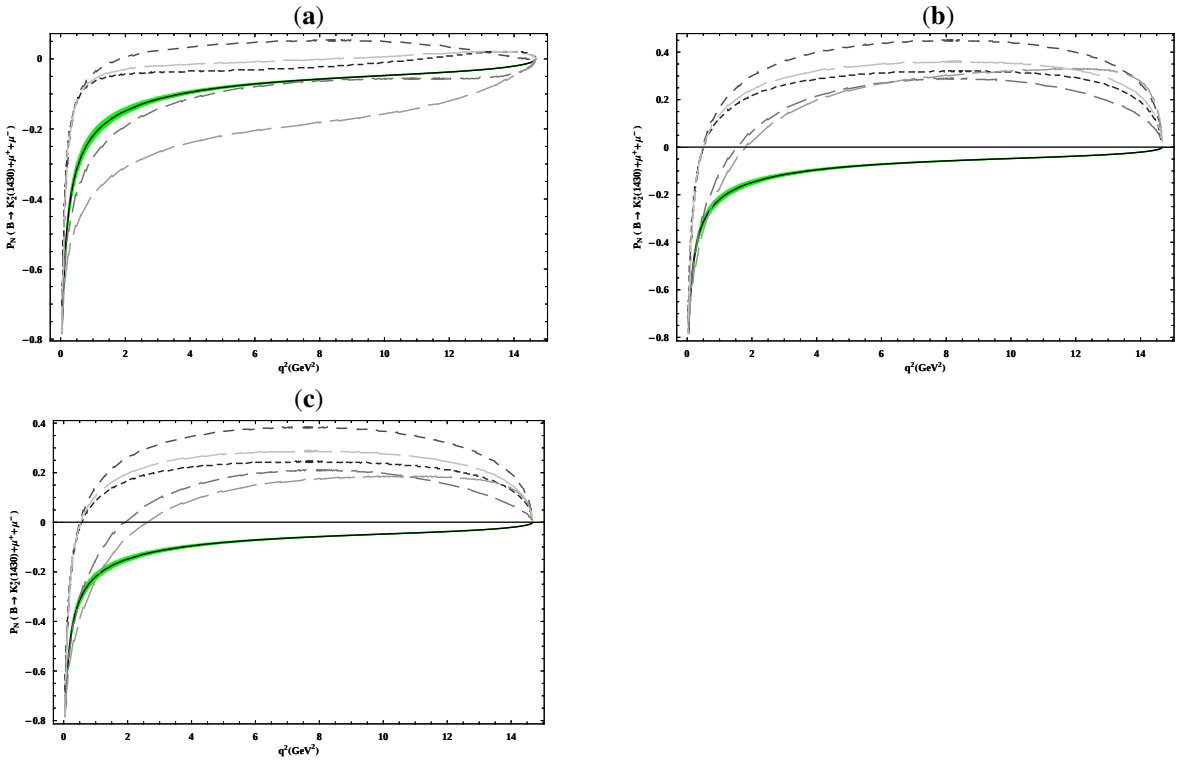

Figure 5.14: The dependence of Longitudinal and Normal lepton polarization asymmetry for $B \to K_2^*(1430)\mu^+\mu^-$ on q^2 for different values of T-SP couplings. The caption for the above figures are the same as Fig. 5.11.

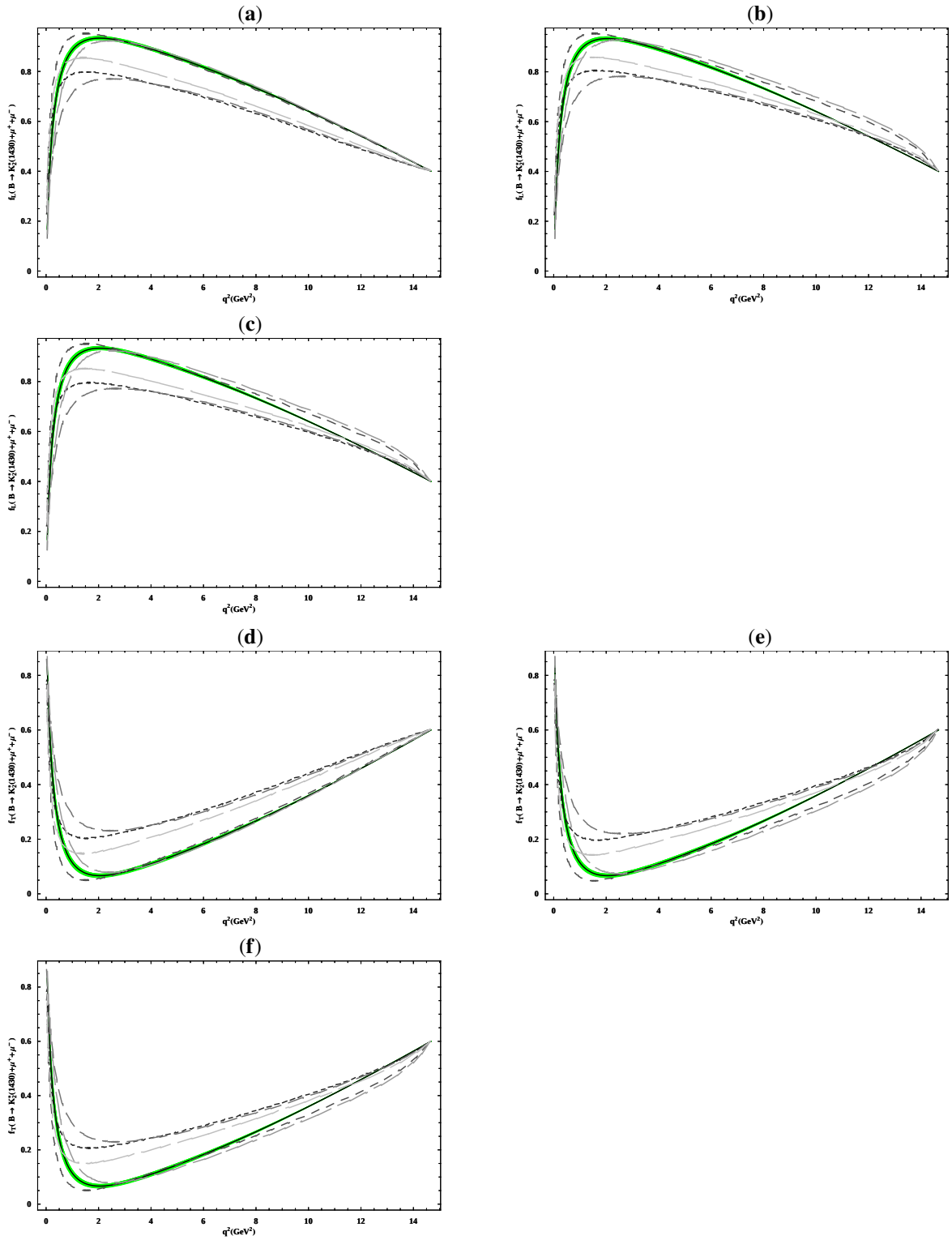

Figure 5.15: The dependence of Longitudinal and Transverse helicity fractions for $B \to K_2^*(1430)\mu^+\mu^-$ on q^2 for different values of T-SP couplings. The caption for the above figures are the same as Fig. 5.11.

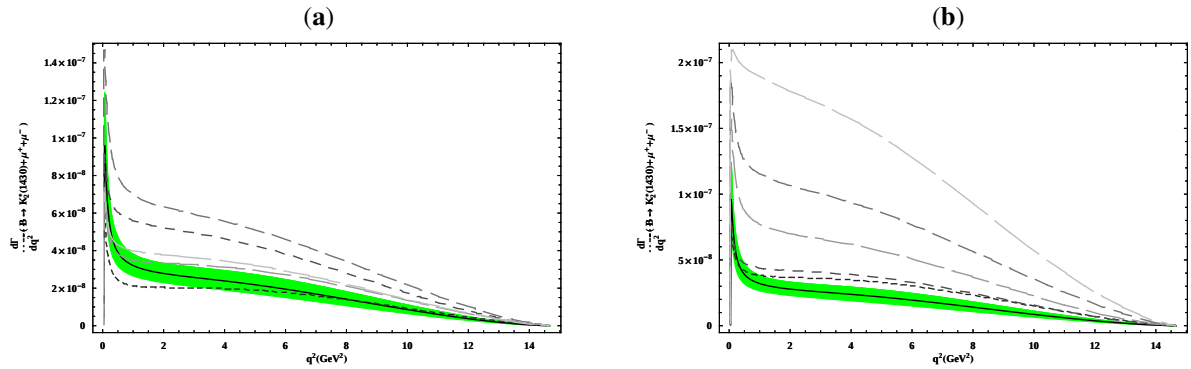

Figure 5.16: The dependence of decay rate for $B_0 \to K_2^*(1430)\mu^+\mu^-$ on q^2 where different curves correspond to different choices of the values of all couplings are taken into account inside their allowed region. In all figures the solid line represent the SM with light green shaded region as uncertainty in SM.

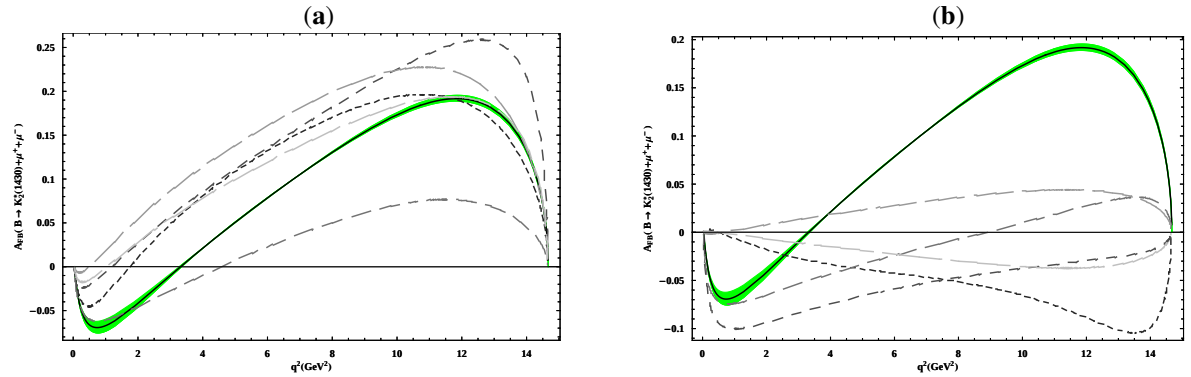

Figure 5.17: The dependence of forward-backward asymmetry for $B \to K_2^*(1430)\mu^+\mu^-$ on q^2 for different values of All couplings. The caption for the above figures are the same as Fig. 5.16.

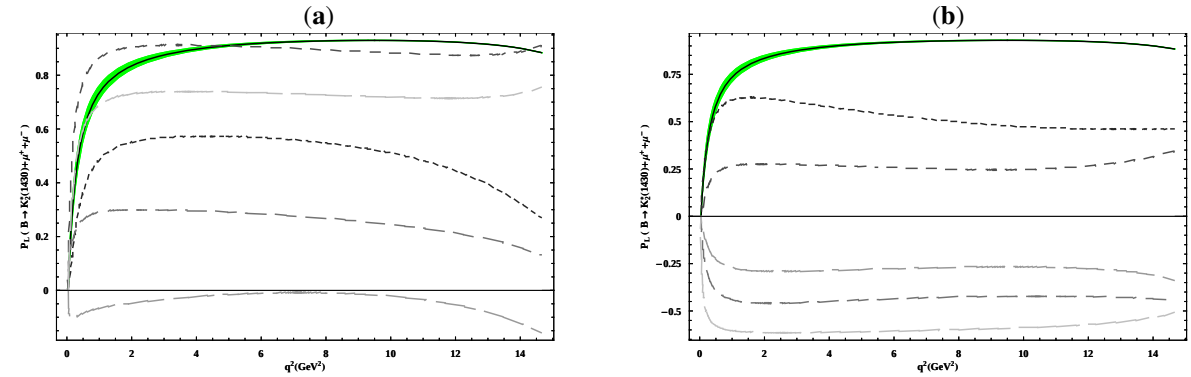

Figure 5.18:

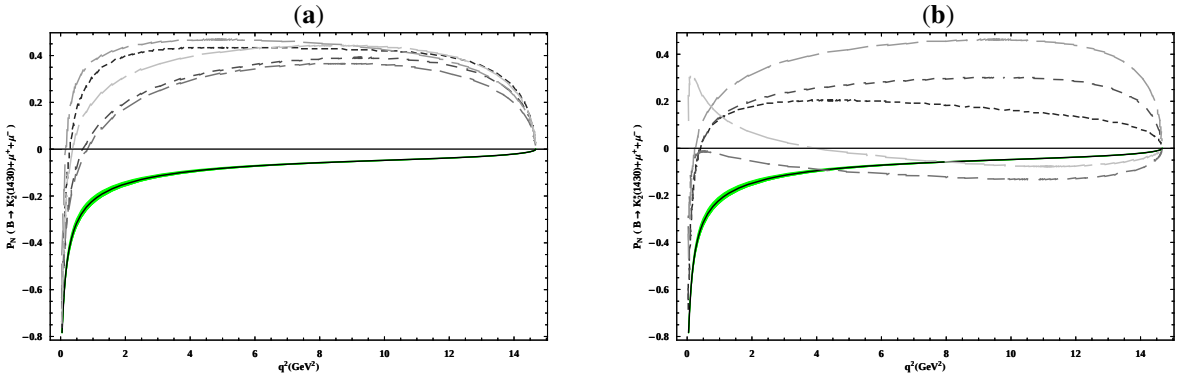

Figure 5.19: The dependence of Longitudinal and Normal lepton polarization asymmetry for $B \to K_2^*(1430)\mu^+\mu^-$ on q^2 for different values of All couplings. The caption for the above figures are the same as Fig. 5.16.

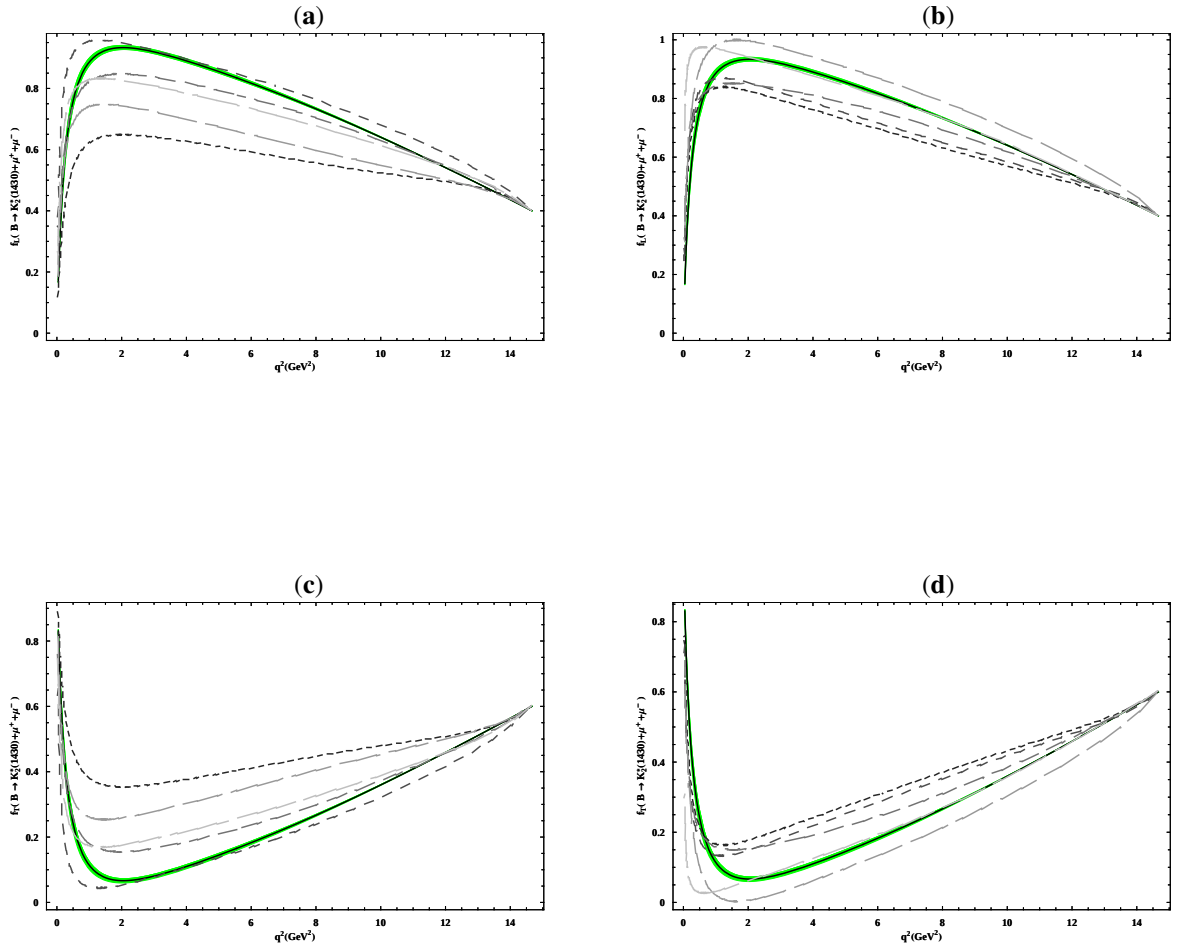

Figure 5.20: The dependence of Longitudinal and Transverse helicity fractions for $B \to K_2^*(1430)\mu^+\mu^-$ on q^2 for different values of All couplings. The caption for the above figures are the same as Fig. 5.16.

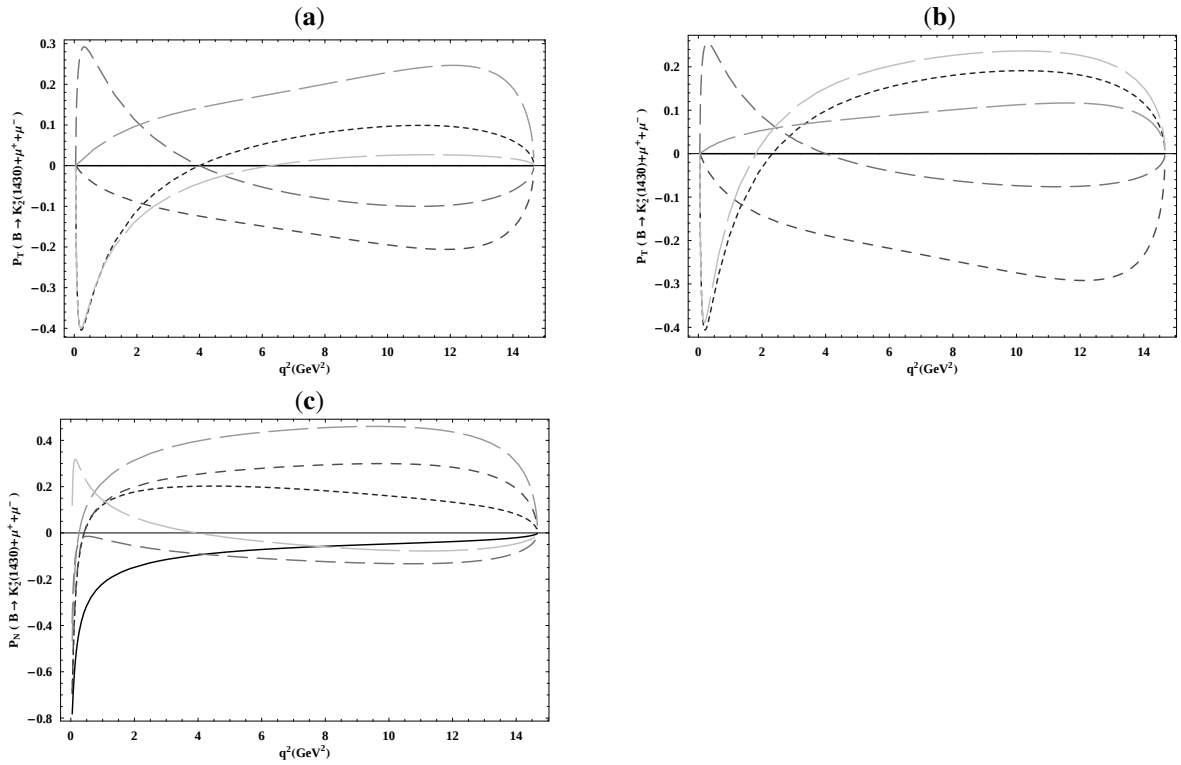

Figure 5.21: The dependence of transverse lepton polarization asymmetry for $B_0 \to K_2^*(1430)\mu^+\mu^-$ on q^2 where different curves correspond to different choices of the values of all couplings inside their allowed region and the flat solid line at $P_T = 0$ represent the SM with no uncertainty region. In Fig(a) only tensor type couplings are present, Fig(b,c) when all couplings are present.

5.6 Conclusions

We carried out the study of the decay $B \to K_2^*(1430)\mu^+\mu^-$ in the presence of new physics (NP) operators beyond SM. We have performed a schematic model-independent analysis, allowing for new vector-axial vector (VA), scalar-pseudoscalar (SP) and tensor (T) operator couplings. We analyzed the effects on different physical observables for this channel in the presence of these NP operator couplings. To conclude this study we summarize the important out comes as follows

- The differential branching ratios generally increase for most of the parameter space of NP couplings. For VA couplings the BR increases considerably particularly when both $R_{V,A}$ and $R'_{V,A}$ are involved the BR is enhanced by more than a factor of 4 and the reason is that the new VA couplings are not m_l suppressed compared to other NP couplings. On the other hand the BR for case of SP and T couplings fall mainly in uncertainty region of SM. The reason behind this lies in the fact that SP and T operator couplings are severely constrained by the upper bound on $B(B_s \to \mu^+\mu^-)$ as well as their contribution is m_l suppressed.

- The forward-backward asymmetry of the final state leptons deviates sizable in the presence of VA couplings. When the new bound given in Eq 5.37 is ignored the zero crossing even disappears and its values become all positives or all negative. Similar kind of trend was also witnessed for the decay $B \to K^*(892)\mu^+\mu^-$. If we consider the recent measurement of A_{FB} for $B \to K^*(892)\mu^+\mu^-$ decay at LHCb [91] we can see that

new VA couplings get constrained within a narrow band given in Eq 4.3. However, the new SP couplings contribute delicately to the shifting of the zero position of A_{FB} for both decays $B \to K^*(892)\mu^+\mu^-$ [114] and $B \to K_2^*(1430)\mu^+\mu^-$. SP operators couplings particularly S coupling shift the zero crossing both towards left as well as towards right. When T coupling is added to the scene the zero shifting is enhanced and it even disappears for certain values of $SP - T$ couplings. Qualitatively the A_{FB} in presence of SP and T couplings separately are m_l suppressed while $SP - T$ couplings together are not m_l suppressed and hence show large NP effects on the decay under consideration.

- The longitudinal lepton polarization asymmetry (P_L) is also an important tool to look for physics beyond SM. Again the P_L is very sensitive to VA couplings, its values sway between the positive SM value to negative maximum value for defined range of $R_{V,A}$ and $R'_{V,A}$ couplings. The effects on P_L are still mild when S and P couplings are introduced individually but the effects are magnified when both SP couplings are present. The T couplings also disturb the values of P_L and the effects get added up when both SP and T couplings are in combination.

- The normal lepton polarization asymmetry is not as sensitive to VA operator couplings like the other observables. The VA effects on P_N are more dominant in the low q^2 region while in high q^2 regime they all asymptotically converge to zero. The normal lepton polarization provides an ideal testing ground to test the existence of SP new physics operators. The distinct behavior of P_N in the presence of SP couplings is very important to test the existence of SP as well as $SP - T$ operators.

- The longitudinal and transverse helicity fractions of the final state meson $K_2^*(1430)$ are also efficient tool to look for the NP effects. In case of VA operators there is a noticeable change in helicity fractions of the final state meson. For SP operator couplings the effects are more prominent in the high q^2 regime. The tensor couplings C_T and C_{TE} also allow the helicity fractions to deviate significantly from their SM values.

We hope that these results will be tested one some ongoing and future experiments like LHCb and super B factories.

Chapter 6

Exclusive charm B meson decays in universal extra dimensions

6.1 Introduction

The charmed B_c meson is a bound state of two heavy quarks, bottom b and charm c, and was first observed in 1998 at Tevatron in Fermilab [115]. Because of two heavy quarks, the B_c mesons are rich in phenomenology compared to the other B mesons. At the Large Hadron Collider (LHC) the expected number of events for the production of the B_c meson are about $10^8 - 10^{10}$ per year [116, 117] which is a reasonable number to work on the phenomenology of the B_c meson. It also provides a frame work to study physics in and beyond the SM. In the literature, some of the possible radiative and semileptonic exclusive decays of B_c mesons like $B_c \to (\rho, K^*, D_s^*, B_u^*)\,\gamma, B_c \to \ell\nu\gamma$, $B_c \to B_u^*\ell^+\ell^-, B_c \to D_1^0\ell\nu, B_c \to D_{s0}^*\ell^+\ell^-$ and $B_c \to D_{s,d}^*\ell^+\ell^-$ have been studied using the frame work of relativistic constituent quark model [118], QCD Sum Rules and the Light Cone Sum Rules [10]. In this chapter we will focus on the $B_c \to D_s^*\ell^+\ell^-$ decay.

Theoretically, what makes the $B_c \to D_s^*\ell^+\ell^-$ more important compared to the other B meson decays such as $B^0 \to (K^*, K_1, \rho, \pi)l^+l^-$ is that this decay can occur in two different ways i.e. through FCNC transitions and due to Weak Annihilations (WA). In ordinary B meson decays the WA contributions are very small and can be ignored. However, for the B_c meson the WA contributions are proportional to the CKM matrix elements $V_{cb}V_{cs}^*$ and hence can not be ignored. While working on the exclusive B-meson decays, the main job is to calculate the form factors which are the non perturbative quantities and are scalar functions of the momentum transfer squared. In the literature the form factors for $B_c \to D_s^*\ell^+\ell^-$ decay were calculated using different approaches, such as light front constituent quark models, a relativistic quark model and the QCD sum rules [118, 119]. In this work we calculate the form factors for the above mentioned decay through Ward identities, which was earlier applied to $B \to \rho, \gamma$ [121, 120] and $B \to K_1$ decays [124]. This approach enables us to make a clear separation between the

pole and non pole type contributions, the former is known in terms of a universal function $\xi_\perp(q^2) \equiv g_+(q^2)$. The residue of the pole is then determined in a self consistent way in terms of $g_+(0)$ which will give information about the couplings of $B_s^*(1^-)$ and $B_{sA}^*(1^+)$ in $B_c D_s^*$ channel. The above mentioned coupling arises at lower pole masses because the higher pole masses of B_c meson do not contribute to the decay $B_c \to D_s^* \ell^+ \ell^-$. The form factors are then determined in terms of a known parameter $g_+(0)$ and the pole masses of the particles involved, which will then be used to calculate different physical observables like the branching ratios and the helicity fractions of final state meson (D_s^*) for these decays.

In this chapter we analyze the branching ratio and helicity fractions of D_s^* meson for $B_c \to D_s^* \ell^+ \ell^-$ decay both in the SM and ACD model. The chapter is organized as follows. In Sec. 6.2 we present the theoretical framework for the decay $B_c \to D_s^* \ell^+ \ell^-$ as well as the weak annihilation amplitude. Section 6.3 provides the definitions as well as the detailed calculation of the form factors using Ward Identities. Here we compare the dependence of our form factors on q^2 with the ones calculated using QCD sum rules [128]. In Sec. 6.4 we present the basic formulas for physical observables like decay rate and helicity fractions of D_s^* meson whereas the numerical analysis of these observables is given in Section 6.5. Section 6.6 gives the summary of the results.

6.2 Theoretical framework for $B_c \to D_s^* \ell^+ \ell^-$ decays

6.2.1 Weak Annihilation Amplitude

The weak annihilation amplitude (WA) for the decay $B_c \to D_s^* \ell^+ \ell^-$ can be written in analogy of $B_c \to D_s^* \gamma$ [129, 130].

$$\mathcal{M}^{\rm WA} = \frac{G_F \alpha}{2\sqrt{2}\pi} \frac{f_{D_s^*} f_{B_c}}{q^2} V_{cb} V_{cs}^* \left[-i\epsilon_{\mu\nu\alpha\beta} \varepsilon^{*\nu} p^\alpha q^\beta F_V^{D_s^*}(q^2) + \left(\varepsilon \cdot q p_\mu + p \cdot q \varepsilon_\mu \right) F_A^{D_s^*}(q^2) \right] \bar{l} \gamma^\mu l \tag{6.1}$$

where f_{B_c} and $f_{D_s^*}$ are the decay constants of B_c and D_s^* mesons, respectively. The functions $F_V^{D_s^*}(q^2)$ and $F_A^{D_s^*}(q^2)$ are the weak annihilation form factors which are calculated in QCD Sum Rules and can be parameterized as [128]:

$$F_{V,A}^{D_s^*}(q^2) = \frac{F_{V,A}^{D_s^*}(0)}{1 + \alpha \hat{q} + \beta \hat{q}^2} \tag{6.2}$$

where $\hat{q} = q^2/M_{B_c}^2$. In the present study we have parameterized the form factors in terms of double poles as follows

$$F_V^{D_s^*}(q^2) = \frac{(m_b + m_s)}{M_{B_c^-} + M_{D_s^{*-}}} \frac{F_V^{D_s^*}(0)}{(1 - q^2/M_{B_s^*}^2)(1 - q^2/M_{B_s^*}'^2)} \tag{6.3}$$

$$F_A^{D_s^*}(q^2) = \frac{m_b - m_s}{M_{B_c^-} - M_{D_s^{*-}}} \frac{F_A^{D_s^*}(0)}{(1 - q^2/M_{B_{sA}^*}^2)(1 - q^2/M_{B_{sA}^*}'^2)} \left(1 - \frac{q^2}{M_{B_c^-}^2 - M_{D_s^*}^2} \right) \tag{6.4}$$

The values of the form factors at $q^2 = 0$ are determined by using QCD sum rules [131]. The two set of form factors given in Eq. (6.2) and Eqs. (6.3-6.4) give respectively the branching ratios 2.20×10^{-6} and 2.82×10^{-6} for

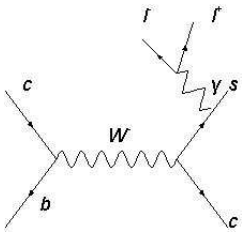

Figure 6.1: Weak annihilation diagram for the decay $B_c \to D_s^* \ell^+ \ell^-$

$B_c \to D_s^* \mu^+ \mu^-$. It follows that the branching ratios are independent on the choice of form factors. These values of the branching ratios are almost five times larger than the penguin one which is given in Table 6.2, and as such one cannot ignore the weak annihilation contribution for the process under consideration.

At quark level the semileptonic decay $B_c \to D_s^* \ell^+ \ell^-$ is governed by the FCNC transition $b \to s\ell^+\ell^-$ for which effective Hamiltonian is given in Eq. (2.8). The ACD model (see sec. 2.4) is the most economical one because it has only one additional parameter R i.e. the radius of the compactification, leaving the same operators basis as that of the SM. At the low values of $1/R$ the KK states couple with the low energy theory and modified the Wilson coefficients which now become the functions of the compactification radius R. The explicit form of these modified Wilson coefficients C_7^{eff} , C_9^{eff} and C_{10}^{eff} were given in Chapter 2. However, at large values of $1/R$ the new states become more and more massive, and will be decoupled from the low-energy theory,therefore one can recover the SM phenomenology.

6.3 Matrix Elements and Form Factors

The exclusive $B_c \to D_s^* \ell^+ \ell^-$ decay involves the hadronic matrix elements which can be obtained by sandwiching the quark level operators give in Eq. (2.9) between initial state B_c meson and final state D_s^* meson. These can be parameterized in terms of form factors which are the scalar functions of the square of the four momentum transfer($q^2 = (p-k)^2$). The non vanishing matrix elements for the process $B_c \to D_s^*$ can be parameterized exactly in the same fashion as that of $B \to K^*$ decay in chapter 3. The form factors for the decay $B_c \to D_s^*$ can be related through Ward identities [121] as

$$\left\langle D_s^*(k,\varepsilon) \left| \bar{s} i\sigma_{\mu\nu} q^\nu b \right| B_c(p) \right\rangle = -(m_b + m_s) \left\langle D_s^*(k,\varepsilon) \left| \bar{s}\gamma_\mu b \right| B_c(p) \right\rangle \tag{6.5}$$

$$\begin{aligned} \left\langle D_s^*(k,\varepsilon) \left| \bar{s} i\sigma_{\mu\nu} q^\nu \gamma^5 b \right| B_c(p) \right\rangle &= (m_b - m_s) \left\langle D_s^*(k,\varepsilon) \left| \bar{s}\gamma_\mu \gamma_5 b \right| B_c(p) \right\rangle \\ &\quad + (p+k)_\mu \left\langle D_s^*(k,\varepsilon) | \bar{s}\gamma_5 b | B_c(p) \right\rangle \end{aligned} \tag{6.6}$$

By using the parametrization of form factors in Eqs. (6.5) and (6.6) and comparing the coefficients of ε_μ^* and q_μ on both sides, one can get the following relations between the form factors:

$$F_1(q^2) = \frac{(m_b+m_s)}{M_{B_c^-}+M_{D_s^{*-}}}V(q^2) \tag{6.7}$$

$$F_2(q^2) = \frac{m_b-m_s}{M_{B_c^-}-M_{D_s^{*-}}}A_1(q^2) \tag{6.8}$$

$$F_3(q^2) = -(m_b-m_s)\frac{2M_{D_s^{*-}}}{q^2}\left[A_3(q^2)-A_0(q^2)\right] \tag{6.9}$$

The results given in Eqs. (6.7, 6.8, 6.9) are derived by using Ward identities and therefore are the model independent.

The universal normalization of the above form factors at $q^2 = 0$ is obtained by defining [121]

$$\begin{aligned}\left\langle D_s^*(k,\varepsilon)\left|\bar{s}i\sigma_{\alpha\beta}b\right|B_c(p)\right\rangle &= -i\epsilon_{\alpha\beta\rho\sigma}\varepsilon^{*\rho}\left[(p+k)^\sigma g_+ + q^\sigma g_-\right] - (\varepsilon^*\cdot q)\epsilon_{\alpha\beta\rho\sigma}(p+k)^\rho q^\sigma h \\ &\quad -i\Big[(p+k)_\alpha\varepsilon_{\beta\rho\sigma\tau}\varepsilon^{*\rho}(p+k)^\sigma q^\tau - \alpha\leftrightarrow\beta\Big]h_1\end{aligned} \tag{6.10}$$

Making use of the Dirac identity

$$\sigma^{\mu\nu}\gamma^5 = -\frac{i}{2}\epsilon^{\mu\nu\alpha\beta}\sigma_{\alpha\beta} \tag{6.11}$$

in Eq.(6.10), we get

$$\begin{aligned}\left\langle D_s^*(k,\varepsilon)\left|\bar{s}i\sigma_{\mu\nu}q^\nu\gamma^5 b\right|B_c(p)\right\rangle &= \varepsilon_\mu^*\left[(M_{B_c^-}^2-M_{D_s^{*-}}^2)g_+ + q^2 g_-\right] \\ &\quad -q\cdot\varepsilon^*\left[q^2(p+k)_\mu g_+ - q_\mu g_-\right] \\ &\quad +q\cdot\varepsilon^*\left[q^2(p+k)_\mu - (M_{B_c^-}^2-M_{D_s^{*-}}^2)q_\mu\right]h\end{aligned} \tag{6.12}$$

On comparing coefficients of q_μ, ε_μ^* and $\epsilon_{\mu\nu\alpha\beta}$ from the parametrization of the form factors, we have

$$F_1(q^2) = \left[g_+(q^2) - q^2 h_1(q^2)\right] \tag{6.13}$$

$$F_2(q^2) = g_+(q^2) + \frac{q^2}{M_{B_c^-}^2 - M_{D_s^{*-}}^2}g_-(q^2) \tag{6.14}$$

$$F_3(q^2) = -g_-(q^2) - (M_{B_c^-}^2 - M_{D_s^{*-}}^2)h(q^2) \tag{6.15}$$

One can see from Eqs. (6.13, 6.14) that at $q^2 = 0$, $F_1(0) = F_2(0)$. The form factors $V(q^2), A_1(q^2)$ and $A_2(q^2)$ can be written in terms of g_+, g_- and h as

$$V(q^2) = \frac{M_{B_c^-}+M_{D_s^{*-}}}{m_b+m_s}\left[g_+(q^2) - q^2 h_1(q^2)\right] \tag{6.16}$$

$$A_1(q^2) = \frac{M_{B_c^-}+M_{D_s^{*-}}}{m_b-m_s}\left[g_+(q^2) + \frac{q^2}{M_{B_c^-}^2 - M_{D_s^{*-}}^2}g_-(q^2)\right] \tag{6.17}$$

$$A_2(q^2) = \frac{M_{B_c^-} + M_{D_s^{*-}}}{m_b - m_s}\left[g_+(q^2) - q^2 h(q^2)\right] - \frac{2M_{D_s^{*-}}}{M_{B_c^-} - M_{D_s^{*-}}}A_0(q^2) \tag{6.18}$$

By looking at Eq. (6.16) and Eq. (6.17) it is clear that the normalization of the form factors V and A_1 at $q^2 = 0$ is determined by a single constant $g_+(0)$, where as from Eq. (6.18) the form factor A_2 at $q^2 = 0$ is determined by two constants i.e. $g_+(0)$ and $A_0(0)$.

6.3.1 Pole Contribution

In $B_c \to D_s^* \ell^+ \ell^-$ decay, there will be pole contributions to h_1, g_-, h and A_0 from $B_s^*(1^-)$, $B_{sA}^*(1^+)$ and $B_s(0^-)$ mesons which can be parameterized as

$$h_1|_{pole} = -\frac{1}{2}\frac{g_{B_s^* B_c D_s^*}}{M_{B_s^*}^2}\frac{f_T^{B^*}}{1 - q^2/M_{B^*}^2} = \frac{R_V}{M_{B_s^*}^2}\frac{1}{1 - q^2/M_{B_s^*}^2} \tag{6.19}$$

$$g_-|_{pole} = -\frac{g_{B_{sA}^* B_c D_s^*}}{M_{B_{sA}^*}^2}\frac{f_T^{B_{sA}^*}}{1 - q^2/M_{B_{sA}^*}^2} = \frac{R_A^S}{M_{B_{sA}^*}^2}\frac{1}{1 - q^2/M_{B_{sA}^*}^2} \tag{6.20}$$

$$h|_{pole} = \frac{1}{2}\frac{f_{B_{SA}^* B_c D_s^*}}{M_{B_{sA}^*}^2}\frac{f_T^{B_{SA}^*}}{1 - q^2/M_{B_{sA}^*}^2} = \frac{R_A^D}{M_{B_{sA}^*}^2}\frac{1}{1 - q^2/M_{B_{sA}^*}^2} \tag{6.21}$$

$$A_0(q^2)|_{pole} = \frac{g_{B_s^* B_c D_s^*}}{M_{B_s^*}^2} f_{B_s}\frac{q^2/M_B^2}{1 - q^2/M_B^2} = R_0\frac{q^2/M_{B_s}^2}{1 - q^2/M_{B_s}^2} \tag{6.22}$$

where the quantities R_V, R_A^S, R_A^D and R_0 are related to the coupling constants $g_{B_s^* B_c D_s^*}, g_{B_{sA}^* B_c D_s^*}$ and $g_{B_{sA}^* B_c D_s^*}$, respectively. Here we would like to mention that the above mentioned couplings arise at the lower pole mass, because the higher pole masses of B_c meson do not contribute for the $B_c \to D_s^* \ell^+ \ell^-$ decay. The form factors $A_1(q^2), A_2(q^2)$ and $V(q^2)$ can be written in terms of these quantities as

$$V(q^2) = \frac{M_{B_c^-} + M_{D_s^*}}{m_b + m_s}\left[g_+(q^2) - \frac{R_V}{M_{B_s^*}^2}\frac{q^2}{1 - q^2/M_{B_s^*}^2}\right] \tag{6.23}$$

$$A_1(q^2) = \frac{M_{B_c^-} - M_{D_s^{*-}}}{m_b - m_s}\left[g_+(q^2) + \frac{q^2}{M_{B_c^-}^2 - M_{D_s^{*-}}^2}\tilde{g}_-(q^2) + \frac{R_A^S}{M_{B_{sA}^*}^2}\frac{q^2}{1 - q^2/M_{B_{sA}^*}^2}\right] \tag{6.24}$$

$$A_2(q^2) = \frac{M_{B_c^-} + M_{D_s^{*-}}}{m_b - m_s}\left[g_+(q^2) - \frac{R_A^D}{M_{B_{As}^*}^2}\frac{q^2}{1 - q^2/M_{B_{sA}^*}^2}\right] - \frac{2M_{D_s^{*-}}}{M_{B_c} - M_{D_s^{*-}}}A_0(q^2) \tag{6.25}$$

Now, the behavior of $g_+(q^2), \tilde{g}_-(q^2)$ and $A_0(q^2)$ is known from LEET and their form is [121]

$$g_+(q^2) = \frac{\xi_\perp(0)}{(1 - q^2/M_B^2)^2} = -\tilde{g}_-(q^2) \tag{6.26}$$

$$A_0(q^2) = \left(1 - \frac{M_{D_s^{*-}}^2}{M_{B_c} E_{D_s^{*-}}}\right)\xi_\parallel(0) + \frac{M_{D_s^{*-}}}{M_{B_c}}\xi_\perp(0) \tag{6.27}$$

$$E_{D_s^*} = \frac{M_{B_c}}{2}\left(1 - \frac{q^2}{M_{B_c}^2} + \frac{M_{D_s^*}^2}{M_{B_c}^2}\right) \tag{6.28}$$

$$g_+(0) = \xi_\perp(0) \tag{6.29}$$

The pole terms given in Eqs.(6.23-6.25) dominate near $q^2 = M^2_{B^*_s}$ and $q^2 = M^2_{B^*_{sA}}$. Just to make a remark that relations obtained from the Ward identities can not be expected to hold for the whole q^2. Therefore, near $q^2 = 0$ and near the pole following parametrization is suggested [121]

$$F(q^2) = \frac{F(0)}{(1 - q^2/M^2)(1 - q^2/M'^2)} \tag{6.30}$$

where M^2 is $M^2_{B^*_s}$ or $M^2_{B^*_{sA}}$, and M' is the radial excitation of M. The parametrization given in Eq. (6.30) not only takes into account the corrections to single pole dominance suggested by the dispersion relation approach [122, 123] but also give the correction of off-mass shell-ness of the couplings of B^*_s and B^*_{sA} with the $B_c D^*_s$ channel.

Since $g_+(0)$ and $\tilde{g}_-(q^2)$ have no pole at $q^2 = M^2_{B^*_s}$, we get

$$V(q^2)(1 - \frac{q^2}{M^2_{B^*}})|_{q^2=M^2_{B^*}} = -R_V \left(\frac{M_{B_c} + M_{D^*_s}}{m_b - m_s} \right)$$

This becomes

$$R_V \equiv -\frac{1}{2} g_{B^*_s B_c D^*_s} f_{B^*_s} = -\frac{g_+(0)}{1 - M^2_{B^*}/M'^2_{B^*}} \tag{6.31}$$

and similarly

$$R^D_A \equiv \frac{1}{2} f_{B^*_{sA} B_c D^*_s} f_T^{B^*_{sA}} = -\frac{g_+(0)}{1 - M^2_{B^*_{sA}}/M'^2_{B^*_{sA}}} \tag{6.32}$$

We cannot use the parametrization given in Eq.(6.30) for the form factor $A_1(q^2)$, since near $q^2 = 0$, the behavior of $A_1(q^2)$ is $g_+(q^2)\left[1 - q^2/\left(M^2_{B_c^-} - M^2_{D_s^{*-}}\right)\right]$, therefore we can write $A_1(q^2)$ as follows

$$A_1(q^2) = \frac{g_+(0)}{\left(1 - q^2/M^2_{B^*_{sA}}\right)\left(1 - q^2/M'^2_{B^*_{sA}}\right)} \left(1 - \frac{q^2}{M^2_{B_c^-} - M^2_{D^*_s}} \right) \tag{6.33}$$

The only unknown parameter in the above form factors calculation is $g_+(0)$ and its value can be extracted by using the central value of branching ratio for the decay $B_c^- \to D_s^{*-}\gamma$ [131] for which the decay rate is

$$\Gamma\left(B_c \to D^*_s \gamma\right) = \frac{G_F^2 \alpha}{32\pi^4} \left|V_{tb} V^*_{ts}\right|^2 m_b^2 M^3_{B_c} \times \left(1 - \frac{M^2_{D^*_s}}{M_{B_c}}^2 \right)^3 \left| C_7^{eff} \right|^2 |g_+(0)|^2 \tag{6.34}$$

From Eq.(6.34), the value of unknown parameter $g_+(0)$ is found to be $g_+(0) = 0.42$. Using $f_{B_c} = 0.35$ GeV we have prediction from Eq.(6.31) that

$$g_{B^*_s B_c D^*_s} = 10.38 GeV^{-1}. \tag{6.35}$$

Similarly the ratio of S and D wave couplings as found to be

$$\frac{g_{B^*_{sA} B_c D^*_s}}{f_{B^*_{sA} B_c D^*_s}} = -0.42 GeV^2 \tag{6.36}$$

The different values of $F(0)$ are

$$V(0) = \frac{M_{B_c^-} + M_{D_s^{*-}}}{m_b + m_s} g_+(0) \tag{6.37}$$

$$A_1(0) = \frac{M_{B_c^-} - M_{D_s^{*-}}}{m_b - m_s} g_+(0) \tag{6.38}$$

$$A_2(0) = \frac{M_{B_c^-} + M_{D_s^{*-}}}{m_b - m_s} g_+(0) - \frac{2M_{D_s^{*-}}}{M_{B_c^-} - M_{D_s^{*-}}} A_0(0) \tag{6.39}$$

The calculation of the numerical values of $V(0)$ and $A_1(0)$ is quite trivial but for the value of $A_2(0)$, the value of $A_0(0)$ has to be known. Although LEET does not give any relationship between $\xi_\parallel(0)$ and $\xi_\perp(0)$, but in LCSR $\xi_\parallel(0)$ and $\xi_\perp(0)$ are related due to numerical coincidence [127]

$$\xi_\parallel(0) \simeq \xi_\perp(0) = g_+(0) \tag{6.40}$$

Thus from Eq. (6.27) we have

$$A_0(0) = 1.12 g_+(0)$$

For the other values of q^2 the form factors can be extrapolated as follows:

$$V(q^2) = \frac{V(0)}{(1 - q^2/M_{B_s^*}^2)(1 - q^2/M_{B_s^*}'^2)} \tag{6.41}$$

$$A_1(q^2) = \frac{A_1(0)}{(1 - q^2/M_{B_{sA}^*}^2)(1 - q^2/M_{B_{sA}^*}'^2)} \left(1 - \frac{q^2}{M_{B_c^-}^2 - M_{D_s^*}^2}\right) \tag{6.42}$$

$$A_2(q^2) = \frac{\tilde{A}_2(0)}{(1 - q^2/M_{B_{sA}^*}^2)(1 - q^2/M_{B_{sA}^*}'^2)} - \frac{2M_{D_s^{*-}}}{M_{B_c^-} - M_{D_s^{*-}}} \frac{A_0(0)}{(1 - q^2/M_{B_s}^2)(1 - q^2/M_{B_s}'^2)} \tag{6.43}$$

The behavior of the form factors $V(q^2)$, $A_1(q^2)$ and $A_2(q^2)$ which are given in Eqs.(6.41-6.43) are plotted as a function of q^2 shown in Fig. 6.1. One can see that the value of the form factors increases with increasing q^2 except for $A_2(q^2)$ where the second term starts dominating at large q^2. This behavior of form factors also differs from the one calculated using three point QCD sum rules shown in Fig. 6.2. The form factors obtained by QCD sum rules for the decay $B_c \to D_s^* \ell^+ \ell^-$[128] are given in Table 6.1

(a) (b) (c)

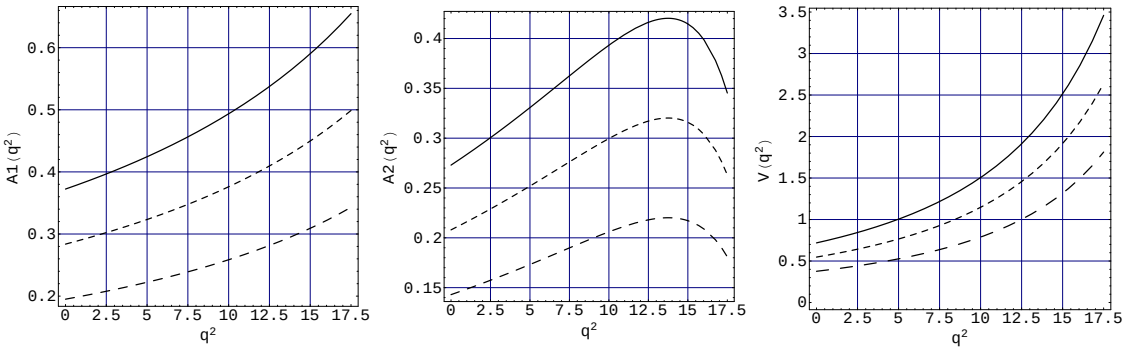

Figure 6.2: Form factors are plotted as a function of q^2. Solid line, dashed line and long-dashed line correspond to $g_+(0)$ equal to 0.42, 0.32 and 0.22 respectively.

(a) (b) (c)

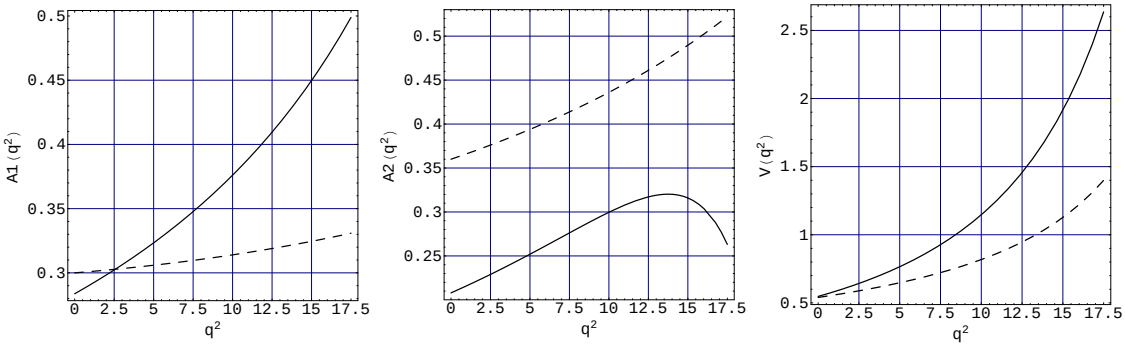

Figure 6.3: Form factors are plotted as a function of q^2. Solid line is drawn by using Ward Identities (our case) and dashed line is drawn by using 3 point QCD sum rules. In both cases we took the central value of the form factors.

Table 6.1: The values of form factors at $q^2 = 0$ obtained by three point QCD sum rules [128]

	$B_c \to D_s^* l^+ l^-$
$A_V(0)$	0.54 ± 0.018
$A_0(0)$	0.30 ± 0.017
$A_+(0)$	0.36 ± 0.013
$A_-(0)$	-0.57 ± 0.04
$F_1(0)$	0.31 ± 0.017
$F_2(0)$	0.33 ± 0.016
$F_3(0)$	0.29 ± 0.034

6.4 Physical Observables for $B_c \to D_s^* \ell^+ \ell^-$

In this section we will present the calculations of the physical observables like the decay rates and the helicity fractions of D_s^* meson using the weak annihilation (WA) and the penguin amplitude that corresponds to the FCNC. From Eq. (2.9) it is straightforward to write the penguin amplitude

$$\mathcal{M}^{\rm PENG} = -\frac{G_F \alpha}{2\sqrt{2}\pi} V_{tb} V_{ts}^* \left[T_\mu^1 (\bar{l}\gamma^\mu l) + T_\mu^2 \left(\bar{l}\gamma^\mu \gamma^5 l\right)\right]$$

where

$$T_\mu^1 = f_1(q^2)\epsilon_{\mu\nu\alpha\beta}\varepsilon^{*\nu} p^\alpha k^\beta - i f_2(q^2)\varepsilon_\mu^* + i f_3(q^2)(\varepsilon^* \cdot q) P_\mu \tag{6.44}$$

$$T_\mu^2 = f_4(q^2)\epsilon_{\mu\nu\alpha\beta}\varepsilon^{*\nu} p^\alpha k^\beta - i f_5(q^2)\varepsilon_\mu^* + i f_6(q^2)(\varepsilon^* \cdot q) P_\mu \tag{6.45}$$

The functions f_1 to f_6 in Eq.(6.44) and Eq. (6.45) are known as auxiliary functions, which contain both long distance (form factors) and short distance (Wilson coefficients) effects and these can be written as

$$\begin{aligned}
f_1(q^2) &= 4(m_b + m_s)\frac{C_7^{eff}}{q^2} F_1(q^2) + 2C_9^{eff}\frac{V(q^2)}{M_{B_c} + M_{D_s^*}} \\
f_2(q^2) &= \frac{C_7^{eff}}{q^2} 2(m_b - m_s) F_2(q^2)\left(M_{B_c}^2 - M_{D_s^*}^2\right) + C_9^{eff} A_1(q^2)\left(M_{B_c} + M_{D^*}\right) \\
f_3(q^2) &= \left[4\frac{C_7^{eff}}{q^2}(m_b - m_s)\left(F_2(q^2) + q^2\frac{F_3(q^2)}{\left(M_{B_c}^2 - M_{D_s^*}^2\right)}\right) + C_9^{eff}\frac{A_2(q^2)}{M_{B_c} + M_{D_s^*}}\right] \\
f_4(q^2) &= C_{10}\frac{2V(q^2)}{M_{B_c} + M_{D_s^*}} \\
f_5(q^2) &= C_{10} A_1(q^2)\left(M_{B_c} + M_{D_s^*}\right) \\
f_6(q^2) &= C_{10}\frac{A_2(q^2)}{M_{B_c} + M_{D_s^*}} \\
f_0(q^2) &= C_{10} A_0(q^2)
\end{aligned} \tag{6.46}$$

The next task is to calculate the decay rate and the helicity fractions of the D_s^* meson in terms of these auxiliary functions.

6.4.1 The Differential Decay Rate of $B_c \to D_s^* \ell^+ \ell^-$

In the rest frame of B_c meson the differential decay width of $B_c \to D_s^* \ell^+ \ell^-$ can be written as

$$\frac{d\Gamma(B_c \to D_s^* \mu^+ \mu^-)}{dq^2} = \frac{1}{(2\pi)^3} \frac{1}{32 M_{B_c}^3} \int_{-u(q^2)}^{+u(q^2)} du\, |\mathcal{A}|^2 \tag{6.47}$$

where

$$\mathcal{A} = \mathcal{M}^{\rm WA} + \mathcal{M}^{\rm PENG} \tag{6.48}$$

$$q^2 = (p_{l^+} + p_{l^-})^2 \tag{6.49}$$

$$u = (p - p_{l^-})^2 - (p - p_{l^+})^2 \tag{6.50}$$

Now the limits on q^2 and u are

$$4m_l^2 \leq q^2 \leq (M_{B_c} - M_{D_s^*})^2 \tag{6.51}$$

$$-u(q^2) \leq u \leq u(q^2) \tag{6.52}$$

with

$$u(q^2) = \sqrt{\lambda\left(1 - \frac{4m_l^2}{q^2}\right)} \tag{6.53}$$

and

$$\lambda \equiv \lambda(M_{B_c}^2, M_{D_s^*}^2, q^2) = M_{B_c}^4 + M_{D_s^*}^4 + q^4 - 2M_{B_c}^2 M_{D_s^*}^2 - 2M_{D_s^*}^2 q^2 - 2q^2 M_{B_c}^2$$

Here m_l corresponds to the mass of the lepton which for our case is the μ or τ. The total decay rate for the decay $B_c \to D_s^* \ell^+ \ell^-$ can be expressed in terms of WA, penguin amplitude and interference of these two which takes the form

$$\frac{d\Gamma}{dq^2} = \frac{d\Gamma^{\rm WA}}{dq^2} + \frac{d\Gamma^{\rm PENG}}{dq^2} + \frac{d\Gamma^{\rm WA\text{-}PENG}}{dq^2} \tag{6.54}$$

with

$$\frac{d\Gamma^{\rm WA}}{dq^2} = \frac{G_F^2 \left|V_{cb} V_{cs}^*\right|^2 \alpha^2}{2^{11}\pi^5 3 M_{B_c}^3 M_{D_s^*}^2 q^2} u(q^2) \times g\left(q^2\right) \tag{6.55}$$

$$\frac{d\Gamma^{\rm PENG}}{dq^2} = \frac{G_F^2 \left|V_{tb} V_{ts}^*\right|^2 \alpha^2}{2^{11}\pi^5 3 M_{B_c}^3 M_{D_s^*}^2 q^2} u(q^2) \times h\left(q^2\right) \tag{6.56}$$

$$\frac{d\Gamma^{\rm WA\text{-}PENG}}{dq^2} = \frac{G_F^2 \left|V_{cb} V_{cs}^*\right| \left|V_{tb} V_{ts}^*\right| \alpha^2}{2^{11}\pi^5 3 M_{B_c}^3 M_{D_s^*}^2 q^2} u(q^2) \times I\left(q^2\right). \tag{6.57}$$

The function $u(q^2)$ is defined in Eq. (6.53) and $g(q^2)$, $h(q^2)$ and $I(q^2)$ are

$$g\left(q^2\right) = \frac{1}{2}\left(2m_l^2 + q^2\right)\kappa^2 \Big[8\lambda M_{D_s^*}^2 q^2 \left(F_V^{D_s^*}(q^2)\right)^2 + \left(F_A^{D_s^*}(q^2)\right)^2 [12 M_{D_s^*}^2 q^2 (\lambda$$

$$
\begin{aligned}
& +4M_{B_c}^2 q^2) + \lambda^2 + \lambda(\lambda + 4q^2 M_{D_s^*}^2 + 4q^4)]\Big] \\
h(q^2) &= 24\left|f_0(q^2)\right|^2 m_l^2 M_{D_s^*}^2 \lambda + 8M_{D_s^*}^2 q^2 \lambda(2m_l^2 + q^2)\left|f_1(q^2)\right|^2 - (4m_l^2 - q^2)\left|f_4(q^2)\right|^2] \\
& +\lambda(2m_l^2 + q^2)\left|f_2(q^2) + (M_{B_c}^2 - M_{D_s^*}^2 - q^2) f_3(q^2)\right|^2 - (4m_l^2 - q^2)|f_5(q^2) \\
& +(M_{B_c}^2 - M_{D_s^*}^2 - q^2) f_6(q^2)|^2] + 4M_{D_s^*}^2 q^2[(2m_l^2 + q^2)(3\left|f_2(q^2)\right|^2 - \lambda\left|f_3(q^2)\right|^2) \\
& -(4m_l^2 - q^2)(3\left|f_5(q^2)\right|^2 - \lambda\left|f_6(q^2)\right|^2)] \qquad (6.58) \\
I(q^2) &= 2\kappa[f_2(q^2) F_A^{D_s^*}(q^2) q^2 (2m_l^2 + q^2)(\lambda + 6M_{D_s^*}^2 (M_{B_c}^2 - M_{D_s^*}^2 + q^2)) \\
& -(\lambda(2f_1(q^2) F_V^{D_s^*}(q^2) M_{D_s^*}^2 q^4 + f_3(q^2) F_A^{D_s^*}(q^2)(2m_l^2 + q^2)(\lambda + q^4 + 4M_{B_c} M_{D_s^*}))].
\end{aligned}
$$

where

$$
\kappa = \frac{8\pi^2 M_{D_s^*} f_{B_c} f_{D_s^*}}{(m_c^2 - m_s^2)\, q^2} \qquad (6.59)
$$

6.4.2 Helicity Fractions Of D_s^* In $B_c \to D_s^* \ell^+ \ell^-$

We now discuss the helicity fractions of D_s^* in $B_c \to D_s^* \ell^+ \ell^-$ which are interesting variables and as such are independent of the uncertainties arising due to form factors and other input parameters. The final state meson helicity fractions were already discussed in literature for $B \to K^*(K_1)\,\ell^+\ell^-$ decays [125, 124]. For the K^* vector meson, the longitudinal helicity fraction f_L has been measured by Babar collaboration for the decay $B \to K^* l^+ l^- (l = e, \mu)$ in two bins of momentum transfer and the results are [126]

$$
\begin{aligned}
f_L &= 0.77^{+0.63}_{-0.30} \pm 0.07, \quad 0.1 \le q^2 \le 8.41 GeV^2 \\
f_L &= 0.51^{+0.22}_{-0.25} \pm 0.08, \quad q^2 \ge 10.24 GeV^2
\end{aligned} \qquad (6.60)
$$

while the average value of f_L in full q^2 range is

$$
f_L = 0.63^{+0.18}_{-0.19} \pm 0.05, \;\; q^2 \ge 0.1 GeV^2 \qquad (6.61)
$$

The explicit expression for the decay rate for $B_c^- \to D_s^{*-} l^+ l^-$ decay can be written in terms of longitudinal Γ_L and transverse components Γ_T as

$$
\frac{d\Gamma_L(q^2)}{dq^2} = \frac{d\Gamma_L^{\rm WA}(q^2)}{dq^2} + \frac{d\Gamma_L^{\rm PENG}(q^2)}{dq^2} + \frac{d\Gamma_L^{\text{WA-PENG}}(q^2)}{dq^2} \qquad (6.62)
$$

$$
\frac{d\Gamma_\pm(q^2)}{dq^2} = \frac{d\Gamma_\pm^{\rm WA}(q^2)}{dq^2} + \frac{d\Gamma_\pm^{\rm PENG}(q^2)}{dq^2} + \frac{d\Gamma_\pm^{\text{WA-PENG}}(q^2)}{dq^2} \qquad (6.63)
$$

$$
\frac{d\Gamma_T(q^2)}{dq^2} = \frac{d\Gamma_+(q^2)}{dq^2} + \frac{d\Gamma_-(q^2)}{dq^2}. \qquad (6.64)
$$

where

$$\frac{d\Gamma_L^{\rm WA}(q^2)}{dq^2} = \frac{G_F^2\left|V_{cb}V_{cs}^*\right|^2\alpha^2}{2^{11}\pi^5}\frac{u(q^2)}{M_{B_c}^3}\times\frac{1}{3}A_L^{\rm WA} \tag{6.65}$$

$$\frac{d\Gamma_L^{\rm PENG}(q^2)}{dq^2} = \frac{G_F^2\left|V_{tb}V_{ts}^*\right|^2\alpha^2}{2^{11}\pi^5}\frac{u(q^2)}{M_{B_c}^3}\times\frac{1}{3}A_L^{\rm PENG} \tag{6.66}$$

$$\frac{d\Gamma_L^{\rm WA\text{-}PENG}(q^2)}{dq^2} = \frac{G_F^2\left|V_{cb}V_{cs}^*\right|\left|V_{tb}V_{ts}^*\right|\alpha^2}{2^{11}\pi^5}\frac{u(q^2)}{M_{B_c}^3}\times\frac{1}{3}A_L^{\rm WA\text{-}PENG} \tag{6.67}$$

$$\frac{d\Gamma_\pm^{\rm WA}(q^2)}{dq^2} = \frac{G_F^2\left|V_{cb}V_{cs}^*\right|^2\alpha^2}{2^{11}\pi^5}\frac{u(q^2)}{M_{B_c}^3}\times\frac{2}{3}A_\pm^{\rm WA} \tag{6.68}$$

$$\tag{6.69}$$

$$\frac{d\Gamma_\pm^{\rm PENG}(q^2)}{dq^2} = \frac{G_F^2\left|V_{tb}V_{ts}^*\right|^2\alpha^2}{2^{11}\pi^5}\frac{u(q^2)}{M_{B_c}^3}\times\frac{4}{3}A_\pm^{\rm PENG} \tag{6.70}$$

$$\frac{d\Gamma_\pm^{\rm WA\text{-}PENG}(q^2)}{dq^2} = \frac{G_F^2\left|V_{cb}V_{cs}^*\right|\left|V_{tb}V_{ts}^*\right|\alpha^2}{2^{11}\pi^5}\frac{u(q^2)}{M_{B_c}^3}\times\frac{2}{3}A_\pm^{\rm WA\text{-}EP}. \tag{6.71}$$

The different functions appearing in above equation can be expressed in terms of auxiliary functions (c.f. Eq. (6.46)) as

$$\begin{aligned}
A_L^{\rm WA} &= \frac{\kappa^2}{4q^2M_{D_s^*}^2}\Big[\left(F_V^{D_s^*}(q^2)\right)^2\Big\{q^2\lambda(\lambda+4q^2M_{D_s^*}^2)-4M^2\lambda(2\lambda+8q^2M_{D_s^*}^2)\\
&\quad-q^2\left(M_{B_c}^2-M_{D_s^*}^2-q^2\right)^2\left(\lambda-2u^2(q^2)\right)\Big\}+\left(F_A^{D_s^*}(q^2)\right)^2\Big\{12\lambda q^2((M_{B_c}^2-M_{D_s^*}^2)^2-M_{D_s^*}^2)\\
&\quad-\lambda^2(q^2-4m_l^2)+q^2(8q^2M_{D_s^*}^2-\lambda)(M_{B_c}^2-M_{D_s^*}^2+q^2)^2\\
&\quad-2u^2(q^2)q^2((M_{B_c}^2-M_{D_s^*}^2)^2+q^4)+4m_l^2((M_{B_c}^2-M_{D_s^*}^2)^2-q^4)^2\Big\}\Big]\\
A_L^{\rm PENG} &= \frac{1}{2M_{D_s^*}^2q^2}[24\left|f_0(q^2)\right|^2m_l^2M_{D_s^*}^2\lambda+(2m_l^2+q^2)\left|(M_{B_c}^2-M_{D_s^*}^2-q^2)f_2(q^2)+\lambda f_3(q^2)\right|^2\\
&\quad+(q^2-4m_l^2)\left|(M_{B_c}^2-M_{D_s^*}^2-q^2)f_5(q^2)+\lambda f_6(q^2)\right|^2]\\
A_L^{\rm WA\text{-}PENG} &= \frac{\kappa}{q^2M_{D_s^*}^2}\Big[\Re(f_1\left(q^2\right)F_V^{D_s^*}(q^2))\left\{(\lambda+4M_{D_s^*}^2q^2)\left(8m_l^2\sqrt{\lambda}+q^2(2u(q^2)-\sqrt{\lambda})\right)-4M_{D_s^*}^2q^2\lambda\right\}\\
&\quad+\Re(f_2\left(q^2\right)F_A^{D_s^*}(q^2))\Big\{q^2u^2(q^2)(M_{B_c}^2-M_{D_s^*}^2-q^2)+6q^2\lambda(M_{D_s^*}^2-M_{B_c}^2)\\
&\quad+q^2(\lambda-8q^2M_{D_s^*}^2)(M_{B_c}^2-M_{D_s^*}^2+q^2)-4m_l^2q^2(4q^2M_{D_s^*}^2+\lambda)\Big\}\\
&\quad+\Re(f_3\left(q^2\right)F_A^{D_s^*}(q^2))\Big\{\lambda^2(4m_l^2-q^2)+q^4(q^2u(q^2)\sqrt{\lambda}\\
&\quad-6\lambda(M_{B_c}^2+M_{D_s^*}^2))+q^2(M_{B_c}^2-M_{D_s^*}^2)(6\lambda-u^2(q^2))\Big\}\Big]\\
A_\pm^{\rm WA} &= \kappa^2\Big[\left(2m_l^2+q^2\right)\Big[\lambda\left(F_V^{D_s^*}(q^2)\right)^2+\left(F_A^{D_s^*}(q^2)\right)^2\left(\lambda+4M_{D_s^*}^2q^2\right)\Big]\Big]\\
A_\pm^{\rm PENG} &= (q^2-4m_l^2)\left|f_5(q^2)\mp\sqrt{\lambda}f_4(q^2)\right|^2+\left(q^2+2m_l^2\right)\left|f_2(q^2)\pm\sqrt{\lambda}f_1(q^2)\right|^2\\
A_\pm^{\rm WA\text{-}PENG} &= -\kappa\Big\{2\sqrt{\lambda}(q^2-4m_l^2)\Re(f_2\left(q^2\right)F_V^{D_s^*}(q^2))+4\lambda(q^2+2m_l^2)\Re(f_1\left(q^2\right)F_V^{D_s^*}(q^2))
\end{aligned}$$

$$\pm 2(q^2+2m_l^2)(M_{B_c}^2-M_{D_s^*}^2+q^2)[2\Re[(f_1\left(q^2\right)F_A^{D_s^*}(q^2))]\sqrt{\lambda}\mp 2\Re(f_2\left(q^2\right)F_V^{D_s^*}(q^2))]\Big\} \tag{6.72}$$

Finally, the longitudinal and transverse helicity fractions can be evaluated by the formula given in Eq. (5.33)

6.5 Numerical Analysis.

In this section we present the numerical analysis of the branching ratio and helicity fractions of D_s^* meson both in the SM and in ACD model. Among the different input parameters the important one are the form factors which are the major source of uncertainties. To study the above mentioned physical observables we use two different form factors, in one where we parameterized the form factors in terms of double pole and then relate them through the Ward identities which are given in section 6.3, the other one obtained by three point QCD sum rules given in Table 6.1 . The differences in the results obtained in physical observables using two different approaches of form factors represents an indication of the error related to the hadronic uncertainty. We have used next-to-leading order approximation for the Wilson Coefficients at the renormalization scale $\mu = m_b$. It has already been mentioned that besides the contribution in the C_9^{eff}, there are long distance contributions resulting from the $c\bar{c}$ resonances like J/ψ and its excited states. For the present analysis we do not take into account these long distance effects. The numerical results for the branching ratio and helicity fractions of D_s^* for the decay mode $B_c \to D_s^*\ell^+\ell^-$ using the form factors given in section 6.3 and QCD sum rules are depicted in Figs. 6.3-6.8, both in the SM and the ACD model. Figs. (6.3-6.4) represents the branching ratio of $B_c \to D_s^*\ell^+\ell^-$ decay. One can clearly see from the Figs.(6.3) and (6.4) that the branching ratio is increased due to the increment in the inverse of the compactification radius R of the KK-contribution, while at the larger values of the inverse of the compactification radius R the branching ratio is shifted towards the SM. We have also displayed the numerical results of the branching ratio for the decay $B_c \to D_s^*\ell^+\ell^-$ separately for penguin, WA and combination of both are given in Table 6.2.

Table 6.2: Branching ratio for $B_c \to D_s^*\mu^+\mu^-(\tau^+\tau^-)$ decay in the SM.

	Form factors defined in section 5.3	QCD Sum Rule
$BR^{(\mathrm{PENG})}(B_c \to D_s^*\mu^+\mu^-(\tau^+\tau^-))$	$4.17\times10^{-7}(2.22\times10^{-8})$	$2.57\times10^{-7}\left(1.13\times10^{-8}\right)$
$BR^{(\mathrm{WA})}(B_c \to D_s^*\mu^+\mu^-(\tau^+\tau^-))$	$2.82\times10^{-6}\left(0.92\times10^{-9}\right)$	$2.20\times10^{-6}\left(0.35\times10^{-9}\right)$
$BR^{(\mathrm{Total})}(B_c \to D_s^*\mu^+\mu^-(\tau^+\tau^-))$	$3.24\times10^{-6}\left(3.03\times10^{-8}\right)$	$2.46\times10^{-6}\left(1.49\times10^{-8}\right)$

From Table 6.2 one can also see that the branching ratio for the decay $B_c \to D_s^*\mu^+\mu^-$ obtained from the WA is about 5 times larger than the corresponding penguin one. It is therefore expected that these WA contributions will reduce the new physics effects in helicity fractions of the final state meson.

In general the sensitivity of NP on the branching ratio is affected by the uncertainties which arises due to the number of different input parameters. Among them the major one lies in the numerical analysis of $B_c \to D_s^*\ell^+\ell^-$ decay originated from the $B_c \to D_s^*$ transition form factors. The large uncertainties involved in the form factors are mainly from the variations of the decay constant of B_c meson and also there are some uncertainties from the

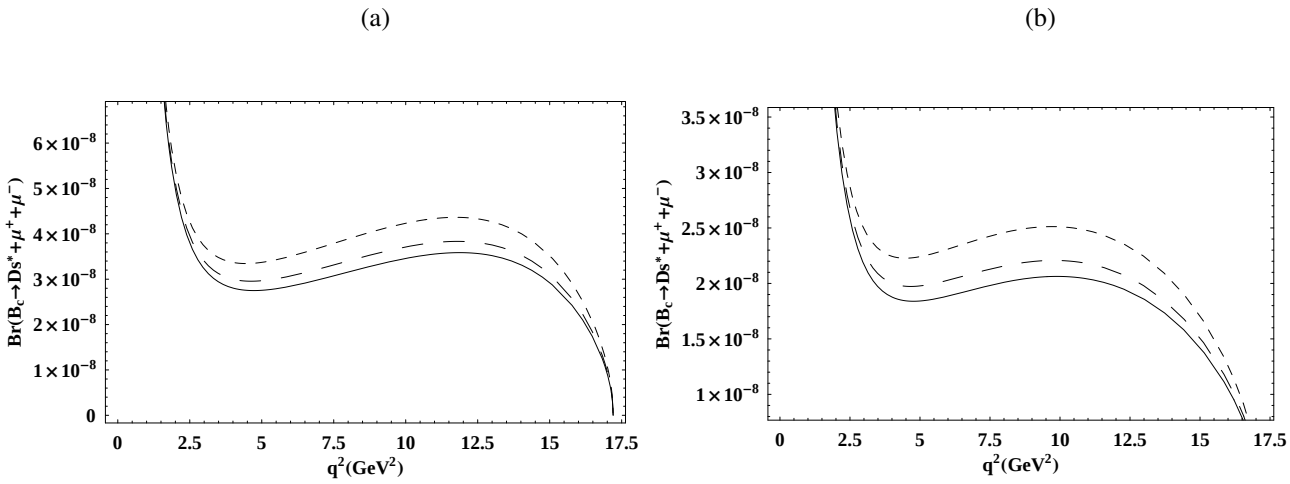

Figure 6.4: (a)Branching ratio using double pole parametrization and (b) using three point QCD sum rules for the $B \to D_s^* \mu^+ \mu^-$ decay as functions of q^2 for different values of $1/R$. Solid line correspond to SM value,dashed line is for $1/R = 300$, long dashed is for $1/R = 500$.

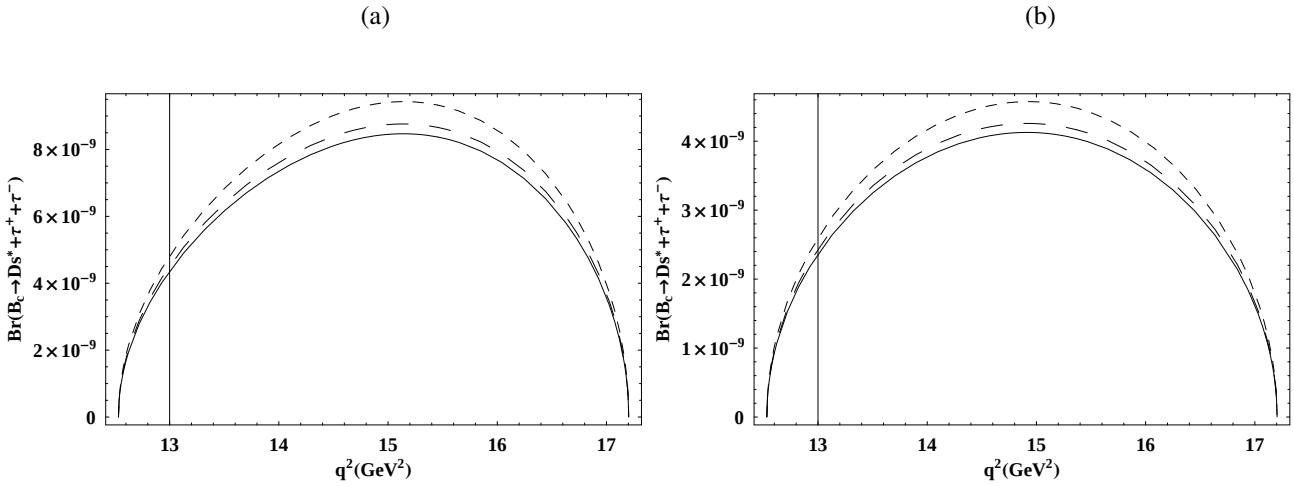

Figure 6.5: Branching ratio for the decay $B_c \to D_s^* \tau^+ \tau^-$. The legends are same as that of Fig. 6.4

strange quark mass m_s. The latter are expected to be tiny on account of the negligible role of m_s suppressed by the much larger energy scale of m_b. Moreover, the uncertainties of the charm quark and bottom quark mass are at the 1% level, which will not play significant role in the numerical analysis and can be dropped out safely. It also needs to be stressed that these hadronic uncertainties almost have no influence on the various asymmetries including the polarization asymmetries of final state meson on account of their cancelation among different polarization states and this makes them as one of the best tools to look for physics beyond the SM.

Figs. 6.5(a, b, c, d) and 6.6(a, b, c, d) show the longitudinal and transverse helicity fractions of D_s^* for the decay $B_c \to D_s^* \mu^+ \mu^-$ as a function of q^2, where we have used the form factors calculated in section 6.3. Choosing the different values of the compactification radius $1/R$, one can see from these figures that the effect of extra dimensions are visible at low q^2 region. In this case these effects interfere constructively to the SM value for the

case of transverse helicity fraction and destructive for the case of longitudinal helicity fraction. Just to see their dependence on the choice of the form factors we have plotted these longitudinal and transverse helicity fractions of D_s^* in Figs. 6.6(a, b) using three point QCD sum rules form factors (c.f. Table 6.1). Here we want to emphasize that the behavior of longitudinal and transverse helicity fraction changes when we consider WA (c.f. Figs. 6.5(b,d) and 6.6(b,d)) contribution in addition to the penguin one (c.f. Figs. 6.5(a,c) and 6.6(a,c)). This is due to the large contribution of WA amplitude in the decay rate of $B_c \to D_s^* \mu^+ \mu^-$.

Figs. 6.7(a, b, c, d) and 6.8(a, b, c, d) show the longitudinal and transverse helicity fractions of D_s^* for the decay $B_c \to D_s^* \tau^+ \tau^-$ decay as a function of q^2 for the form factors given in section 6.3 and three point QCD sum rules. Here one can see that the shift from the SM value is very mild for both choices of form factors as well as due to the WA contribution.

Hence one can see that the helicity fractions of the final state meson have mild dependence on the choice of form factors and NP effects are quite significant in the lower q^2 region. Moreover from Figs. 6.5-6.8 it is clear that for each value of the momentum transfer q^2 the sum of the longitudinal and transverse helicity fractions are equal to one, i.e. $f_L(q^2) + f_T(q^2) = 1$ as we have mentioned in the previous chapter.

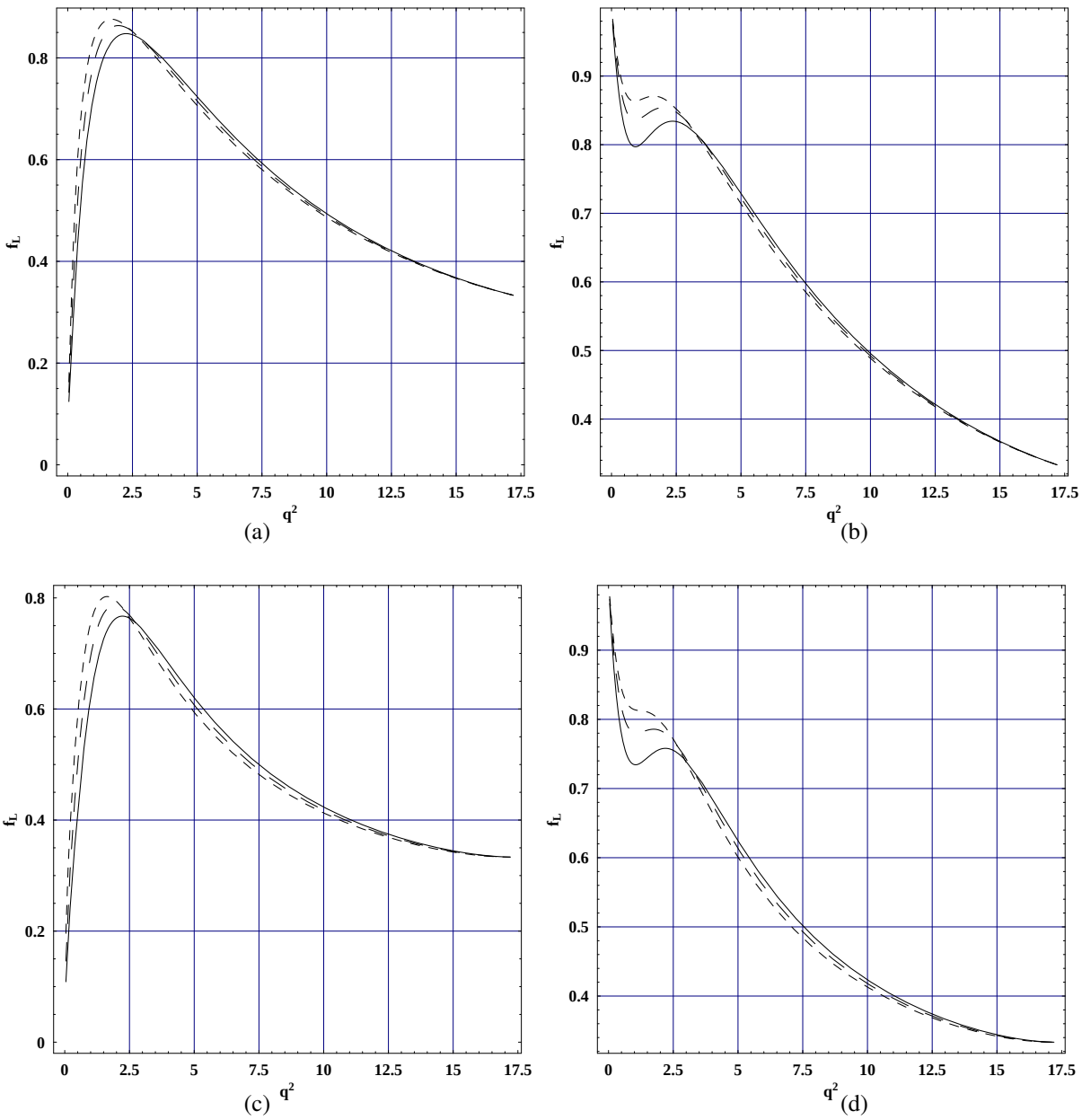

Figure 6.6: Longitudinal helicity fraction for the $B \to D_s^* \mu^+ \mu^-$ as a function of q^2 for different values of $1/R$.The legends are same as that of Fig 6.4.

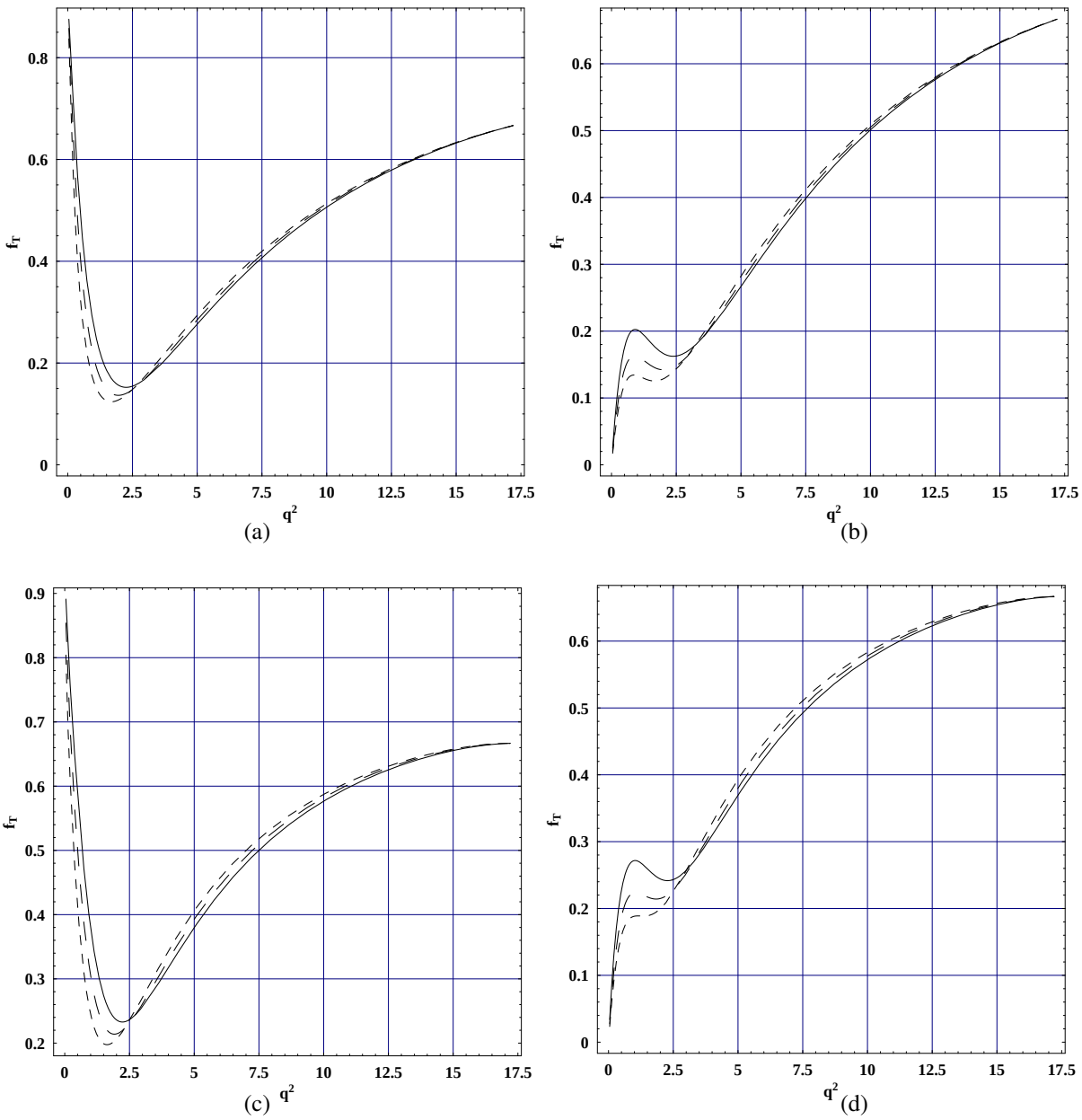

Figure 6.7: Transverse helicity fraction for the $B \to D_s^* \mu^+ \mu^-$ as a function of q^2 for different values of $1/R$.The legends are same as that of Fig 6.4.

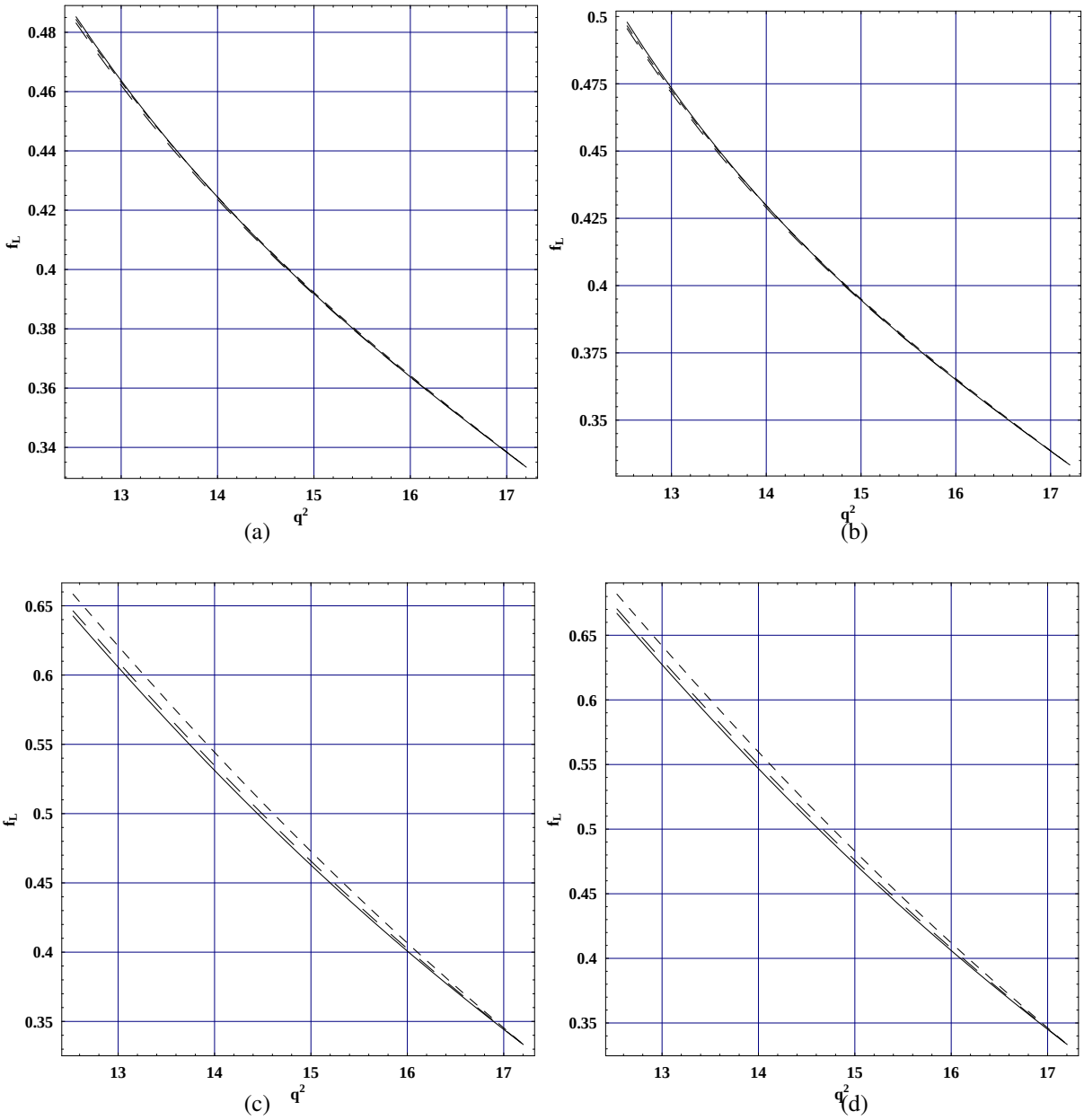

Figure 6.8: Longitudinal helicity fraction for the $B \to D_s^* \tau^+ \tau^-$ as a function of q^2 for different values of $1/R$.The legends are same as that of Fig 6.4.

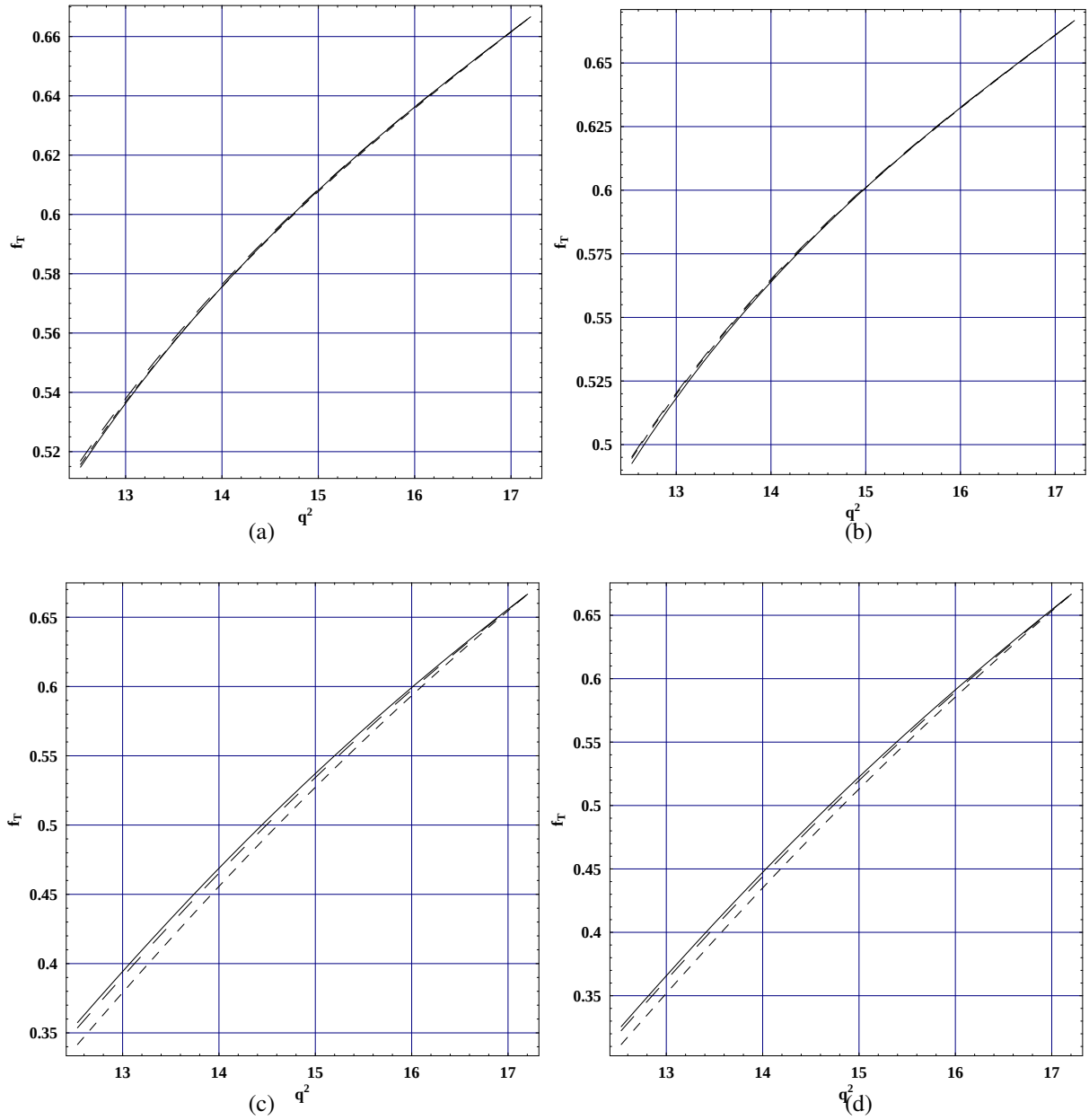

Figure 6.9: Transverse helicity fraction for the $B \to D_s^* \tau^+ \tau^-$ as a function of q^2 for different values of $1/R$. The legends are same as that of Fig 6.4.

6.6 Conclusion:

We have investigated the semileptonic decay $B_c \to D_s^* \ell^+ \ell^-$ by including both the penguin and WA contributions. In particular we found that branching ratio obtained from WA amplitude is 6.7 times large as compared to penguin amplitude for $B_c \to D_s^* \ell^+ \ell^-$ decay. In order to calculate the WA form factors $F_V^{D_s^*}(q^2)$ and $F_A^{D_s^*}(q^2)$, we use Eqs. (6.2, 6.3, 6.4), where the value of the form factors at $q^2 = 0$ can be obtained from QCD sum rules [131]. However for the penguin amplitude the form factors for the above mentioned decay are calculated using the framework of Ward identities which is discussed in section 6.3. Here we have also compared the values of our form factors with the ones calculated using three point QCD sum rules [128].

The form factors contributing to the penguin amplitudes were calculated in the framework of Ward identities which can be expressed in terms of a single universal constant $g_+(0)$. The value of $g_+(0) = (0.42)$ is obtained from the decay $B_c \to D_s^* \gamma$ [131]. Considering the radial excitation at lower pole masses M (where $M = M_{B_s^*}$ and $M_{B_{sA}^*}$) one can predict the coupling of B_s^* with $B_c D_s^*$ channel as indicated in Eq.(6.35) which is $g_{B_s^* B_c D_s^*} = 10.38$ GeV^{-1}. Also we predicted the ratio of S and D wave couplings $\frac{g_{B_{sA}^* B_c D_s^*}}{f_{B_{sA}^* B_c D_s^*}} = -0.42\, GeV^2$ given in Eq.(6.36). We have studied the physical observables such as the branching ratio and the helicity fraction of D_s^* in the decay $B_c \to D_s^* \ell^+ \ell^-$ both in SM and in the ACD model. We have seen that the effects of ACD model in the helicity fractions of D_s^* meson for the decay $B_c \to D_s^* \mu^+ \mu^-$ are quite significant at low q^2 region. Furthermore to see the sensitivity of the said physical observables on the choice of form factors against q^2 using the three point QCD sum rules form factors. We have shown that the helicity fractions of the final state meson have weak dependence on the choice of form factors which make them good tool to look for NP which we hope to be seen at LHC.

In short, the experimental measurements of the extra dimensions effects in the above mentioned observables at LHC will be a useful tool to describe the status of physics beyond the SM. Further we are hopeful that when more data will be collected at LHC, it will not only test the SM but also puts some stringent constraints on the compactification radius $1/R$.

Bibliography

[1] T. Asltonen et al. (CDF Collaboration), V. M. Abazov et al. (DØ Collaboration), CDF Note No. CDF/PHYS/BOTTOM/CDFR/9878, 2009;DØ Note No. 5928-CONF, 2009

[2] B. Aubert et al. [BABAR Collaboration] Phys. Rev. Lett. **91** (2003) 171802 [arXiv:hep-ex/0307026].

[3] K. F. Chen et al. [Belle Collaboration], Phys. Rev. Lett. **91** (2003) 201801 [arXiv:hep-ex/0307014].

[4] B. Aubert et al. [BABAR Collaboration], Phys. Rev. **D 79** (2009) 031102 [arXiv:hep-ex/0804.4412].

[5] V. M. Abazov et al. [The DØ Collaboration], arXiv:1005.2757 [hep-ex].

[6] A. H. Gilani et al. JHEP0309:065, 2003. hep-ph/0304183.

[7] M. S. Alam et al. Phys. Rev. Lett. **74**, 2885 (1995).

[8] R. Ammar et al., Phys. Rev. Lett. **71**, 674 (1993); CLEO CONF 96-05 (1996).

[9] A. Ali, P. Ball, L.T. Handoko, G. Hiller, Phys. Rev. D 61, 074 024 (2000) [arXiv:hep-ph/9910221]; A. Ali, E. Lunghi, C. Greub, G. Hiller, Phys. Rev. D 66, 034 002 (2002) [arXiv:hep-ph/0112300].

[10] T.M. Aliev, M.K. Cakmak, M. Savci, Nucl. Phys. B 607, 305 (2001) [arXiv:hep-ph/0009133]; T.M. Aliev, A. Ozpineci, M. Savci, C. Yuce, Phys. Rev. D 66, 115 006 (2002) [arXiv:hep-ph/0208128]; T.M. Aliev, A. Ozpineci, M. Savci, Phys. Lett. B 511, 49 (2001) [arXiv:hep-ph/0103261]; T.M. Aliev, M. Savci, Phys. Lett. B 481, 275 (2000) [arXiv:hep-ph/0003188];T.M. Aliev, D.A. Demir, M. Savci, Phys. Rev. D 62, 074 016 (2000) [arXiv:hep-ph/9912525]; T.M. Aliev, C.S. Kim, Y.G. Kim, Phys. Rev. D 62, 014 026 (2000) [arXiv:hep-ph/9910501]; T.M. Aliev, E.O. Iltan, Phys. Lett. B 451, 175 (1999) [arXiv:hep-ph/9804458]; T.M. Aliev, V. Bashiry, M. Savci, JHEP 0405, 037 (2004) [arXiv:hep-ph/0403282].

[11] C.H. Chen, C.Q. Geng, Phys. Rev. D 66, 034 006 (2002) [arXiv:hep-ph/0207038]; C.H. Chen, C.Q. Geng, Phys. Rev. D 66, 014 007 (2002) [arXiv:hep-ph/0205306].

[12] G. Erkol, G. Turan, Nucl. Phys. B 635, 286 (2002) [arXiv:hep-ph/0204219]; E.O. Iltan, G. Turan, I. Turan, J. Phys. G 28, 307 (2002) [arXiv:hep-ph/0106136].

[13] W.J. Li, Y.B. Dai, C.S. Huang, arXiv:hep-ph/0410317.

[14] Q.S. Yan, C.S. Huang, W. Liao, S.H. Zhu, Phys. Rev. D 62, 094 023 (2000) [arXiv:hep-ph/0004262].

[15] S.R. Choudhury, N. Gaur, A.S. Cornell, G.C. Joshi, Phys. Rev. D 68, 054 016 (2003) [arXiv:hep-ph/0304084]; S.R. Choudhury, A.S. Cornell, N. Gaur, G.C. Joshi, Phys. Rev. D 69, 054 018 (2004) [arXiv:hep-ph/0307276].

[16] F. Kruger, E. Lunghi, Phys. Rev. D 63, 014 013 (2001) [arXiv:hep-ph/0008210].

[17] R. Mohanta, A.K. Giri, arXiv:hep-ph/0611068.

[18] S.R. Choudhury, N. Gaur, N. Mahajan, Phys. Rev. D 66, 054 003 (2002) [arXiv:hep-ph/0203041]; S.R. Choudhury, N. Gaur, arXiv:hep-ph/0205076; S.R. Choudhury, N. Gaur, arXiv:hep-ph/0207353.

[19] T.M. Aliev, V. Bashiry, M. Savci, Phys. Rev. D 71, 035 013 (2005) [arXiv:hep-ph/0411327].

[20] U.O. Yilmaz, B.B. Sirvanli, G. Turan, Nucl. Phys. 692, 249 (2004) [arXiv:hep-ph/0407006]; U.O. Yilmaz, B.B. Sirvanli, G. Turan, Eur. Phys. J. C 30, 197 (2003) [arXiv:hep-ph/0304100].

[21] S. R. Choudhury and N. Gaur, Phys. Lett. B451, 86 (1999) [arXiv:hep-ph/9810307]; J. K. Mizukoshi, X. Tata and Y. Wang, Phys. Rev. D66, 115003 (2002) [arXiv:hep-ph/0208078] ; T. Ibrahim and P. Nath, Phys. Rev. D67, 016005 (2003) [arXiv:hep-ph/0208142] ; G. L. Kane, C. Kolda and J. E. Lennon, arXiv:hep-ph/0310042 ; A. J. Buras, P. H. Chankowski, J. Rosiek and L. Slawianowska, Nucl. Phys. B659, 3 (2003) [arXiv:hep-ph/0210145] ; A. J. Buras, P. H. Chankowski, J. Rosiek and L. Slawianowska, Phys. Lett. B546, 96 (2002) [arXiv:hep-ph/0207241] ; A. Dedes, H. K. Dreiner and U. Nierste, Phys. Rev. Lett. 87, 251804 (2001) [arXiv:hepph/0108037].

[22] C.S. Kim et al., Phys. Lett. B 218 (1989) 343; X. G. He et al., Phys. Rev. D 38 (1988) 814; B. Grinstein et al., Nucl. Phys. B 319 (1989) 271; N. G. Deshpande et al., Phys. Rev. D 39 (1989) 1461; P. J. ODonnell and H. K. K. Tung, Phys. Rev. D 43 (1991) 2067; N. Paver and Riazuddin, Phys. Rev. D 45 (1992) 978; J. L. Hewett, Phys. Rev. D 53, 4964 (1996); T. M. Aliev, V. Bashiry, and M. Savci, Eur. Phys. J. C 35, 197 (2004); T. M. Aliev, V. Bashiry, and M. Savci, Phys. Rev. D 72, 034031 (2005); T. M. Aliev, V. Bashiry, and M. Savci, J. High Energy Phys. 05 (2004) 037; T. M. Aliev, V. Bashiry, and M. Savci, Phys. Rev. D 73, 034013 (2006); T. M. Aliev, V. Bashiry, and M. Savci, Eur. Phys. J. C 40, 505 (2005); F. Kruger and L. M. Sehgal Phys. Lett. B 380, 199 (1996); Y. G. Kim, P. Ko, and J. S. Lee,Nucl. Phys. B544, 64 (1999); Chuan-Hung Chen and C. Q. Geng, Phys. Lett. B 516, 327 (2001); V. Bashiry, Chin. Phys. Lett. 22, 2201 (2005); W.S. Hou, A. Soni and H. Steger, Phys. Lett. B 192, 441 (1987); W.S. Hou, R.S. Willey and A. Soni, Phys. Rev. Lett. 58, 1608 (1987) [Erratum-ibid. 60, 2337 (1987)]; T. Hattori, T. Hasuike and S. Wakaizumi, Phys. Rev. D 60, 113008 (1999); T.M. Aliev, D.A. Demir and N.K. Pak, Phys. Lett. B 389, 83 (1996); Y. Dincer, Phys. Lett. B 505, 89 (2001) and references therin; C.S. Huang, W.J. Huo and Y.L. Wu, Mod. Phys. Lett. A 14, 2453 (1999); C.S. Huang, W.J. Huo and Y.L. Wu, Phys. Rev. D 64, 016009 (2001).

[23] A. Ali, T. Mannel and T. Morosumi, Phys. Lett. B 273, 505 (1991).

[24] G. Buchalla, A. J. Buras and M. E. Lautenbacher, Rev. Mod. Phys. **68** (1996) 1125.

[25] A. J. Buras and M. Munz, Phys. Rev. D **52**, 186 (1995) [arXiv:hep-ph/9501281].

[26] A. J. Buras, M. Misiak, M. Munz and S. Pokorski, Nucl. Phys. **B424** (1994) 374.

[27] F. Kruger and L. M. Sehgal, Phys. Lett. **380** (1996) 199 [arXiv:hep-ph/9603237].

[28] B. Grinstein, M. J. Savag and M. B. Wise, Nucl. Phys. **B319** (1989) 271.

[29] G. Cella, G. Ricciardi adn A. Vicere, Phys. Lett. **B258** (1991) 212.

[30] C. Bobeth, M. Misiak and J. Urban, Nucl. Phys. **B574** (2000) 291.

[31] H. H. Asatrian, H. M. Asatrian, C. Grueb and M. Walker, Phys. Lett. B507 (2001) 162.

[32] M. Misiak, Nucl. Phys. **B393** (1993) 23, Erratum, ibid. **B439** (1995) 461.

[33] T. Huber, T. Hurth, E. Lunghi, arXiv: 0807.1940.

[34] Andrzej J. Buras and Robert Fleischer, Adv.Ser.Direct.HighEnergyPhys.15:65-238,1998.

[35] W. Altmannshofer, P. Ball,. A. Bharucha, A. J. Buras, D. M. Straub and M. Wick, JHEP **0901** (2009) 019 [arXiv:0811.1214 [hep-ph]]

[36] W. Altmannshofer, P. Ball, A. Bharucha, A. J. Buras, D. M. Straub and M. Wick, JHEP **0901**, 019 (2009) [arXiv:0811.1214 [hep-ph]].

[37] A. K. Kumar, A. Dighe, D. Ghosh, D. London, J. Matias, M. Nagashima and A. Sznkman, JHEP **02** (2010) 053, [arXiv: 0912.1382 [hep-ph]].

[38] P. Langacker and M. Plumacher, Phys. Rev. D **62** (2000) 013006 [hep-ph/0001204]; P. Langacker, arXiv:0801.1345 [hep-ph].

[39] Q. Chang, Yin-Hao Gao arXiv:1101.1272v1 [hep-ph] 6 Jan 2011; Y. Li, J. Hua arXiv:1107.0630v2 [hep-ph] 6 Nov 2011.

[40] K. Cheung, et. al, Phys. Lett. B **652**, 285 (2007); C. H. Chen and H. Hatanaka, Phys. Rev. D **73**, 075003 (2006); C. W. Chiang, et. al, JHEP **0608**, 075 (2006).

[41] V. Berger, et. al, Phys. Lett. B **580**, 186 (2004); V. Berger, et. al, Phys. Rev. D **80**, 055008 (2009); R. Mohanta and A. K. Giri, Phys. Rev. D **79**, 057902 (2009); J. Hua, C. S. Kim and Y, Li, Eur. Phys. J. C **69**, 139 (2010)

[42] Q.Chang, X. Q. Li and Y. D. Yang, JHEP **0905**, 056 (2009); Q.Chang, X. Q. Li and Y. D. Yang, JHEP **1004**, 052 (2010).

[43] T. Appelquist, H. C. Cheng and B. A. Dobrescu, Phys. Rev. **D64**, 035002 (2001).

[44] P. Colangelo, F. De Fazio, R. Ferrandes, T.N. Pham, Phys.Rev. **D73**, 115006 (2006); P. Colangelo, F. De Fazio, P. Santorelli, E. Scrimieri, Phys. Rev. D 53, 3672 (1996);P. Colangelo, Phys. Rev. D 57, 3186 (1998), Erratum; A. Saddique *et al.*, Eur. Phys. J. **C 56** (2008) 267.

[45] A.J. Buras, M. Spranger, A.Weiler, Nucl. Phys. B 660, 225 (2003).

[46] A.J. Buras, A. Poschenrieder, M. Spranger, A. Weiler, Nucl. Phys. B 678, 455 (2004).

[47] B. Aubert et al. [BABAR Collaboration] *Direct CP, Lepton Flavor and Isospin Asymmetries in the Decays* $B \to K^{(*)}\ell^+\ell^-$, Phys. Rev. Lett. **102** (2009) 091803 [arXiv:0807.4119 [hep-ex]].

[48] A.J. Buras et al., Nucl. Phys. B 424, 374 (1994).

[49] N. Arkani-Hamed, A. G. Cohen, E. Katz and A. E. Nelson, J. High Energy Phys. 07 (2002) 034.

[50] S. Chang and H. J. He, Phys. Lett. B **586**, 95 (2004).

[51] T. Appelquist, H. C. Cheng, and B. A. Doberscu, Phys. Rev. D **64**, 035002 (2001).

[52] C. Csaki, Mod. Phys. Lett. A **11**, 599 (1996).

[53] P. Frampton, P. Hung and M. Sher, Phys. Rept. 330 (2000) 263.

[54] V. Barger, L. Everett, J. Jiang, P. Langacker, T. Liu and C. Wagner, Phys. Rev. D 80 (2009) 055008 arXiv:0902.4507 [hep-ph]; JHEP 0912 (2009) 048 arXiv:0906.3745 [hep-ph].

[55] Q. Chang, X. Q. Li and Y. D. Yang, JHEP **1002** (2010) 082, arXiv:0907.4408 [hep-ph]

[56] V. Barger, C. W. Chiang, P. Langacker and H. S. Lee, Phys. Lett. B **598** (2004) 218; first ref in 48.

[57] C. W. Chiang, R. H. Li and C. D. Lu, Chin.Phys. C36 (2012) 14-24 arXiv:0911.2399.

[58] Cheng-Wei. Chiang, Run-Hui Li, Cai-Dian Lu, arXiv:0911.2399v1 [hep-ph] 12 Nov 2009.

[59] A. K. Alok, A. Datta, A. Dighe, M. Duraisamy, D. Ghosh and D. London, JHEP **1111** (2011) 121 [arXiv:1008.2367 [hep-ph]].

[60] F. Kruger and E. Lunghi, Phys. Rev. D **63**, 014013 (2001) [arXiv:hep-ph/0008210].

[61] A. Ali, E. Lunghi, C. Greub and G. Hiller, Phys. Rev. D **66**, 034002 (2002) [arXiv:hep-ph/0112300].

[62] A. Ghinculov, T. Hurth, G. Isidori and Y. P. Yao, Eur. Phys. J. C **33**, S288 (2004) [arXiv:hep-ph/0310187].

[63] D. Melikhov and B. Stech, Phys. Rev. D **62**, 014006 (2000).

[64] A. Ali, P. Ball, L. T. Handoko and G. Hiller, Phys. Rev. D **61**, 074024 (2000) [arXiv:hep-ph/9910221].

[65] C. Chen and C. Q. Geng, Nucl.Phys. B636 (2002) 338-364, hep-ph/0203003 [hep-ph].

[66] A. K. Alok, A. Dighe, D. Ghosh, D. London, J. Matias, M. Nagashima and A. Szynkman, JHEP **1002**, 053 (2010) [arXiv:0912.1382 [hep-ph]].

[67] S. Fukae, C. S. Kim and T. Yoshikawa, Phys. Rev. D **61**, 074015 (2000) [arXiv:hep-ph/9908229].

[68] W. Bensalem, D. London, N. Sinha and R. Sinha, Phys. Rev. D **67**, 034007 (2003) [arXiv:hep-ph/0209228].

[69] K. S. Babu, K. R. S. Balaji, and I. Schienbein, Phys. Rev. D **68**, 014021 (2003)

[70] T. M. Aliev, V. Bashiry, and M. Savci, Eur. Phys. J. C **31**, 511 (2003); V. Bahiry, Phys. Rev. D **77**, 096005 (2008); V. Bashiry, N. Shrikhanghah, and K. Zeynali, Phys. Rev. D **80**, 015016 (2009).

[71] M. Bona et al., (UTfit collaboration), PMC Phys. a **3**, 6 (2009)[arXiv:0803.0659 [hep-ph]]; M. Bona et al., arXiv: 0906.0953 [hep-ph].

[72] K. Nakamura et al. (Particle Data Group), *Review of particle Physics, J. Phys.* **G 37** (2010) 075021.

[73] P. Ball , R. Zwicky, Phys. Rev. D **71** (2005) 014029 [hep-ph/0412079].

[74] T. Goto et al., Phys. Rev. D **55** (1997) 4273; T. Goto, Y. Okada and Y. Shimizu, Phys. Rev. D **58** (1998) 094006; S. Bertolini, F. Borzynatu, A. Masiero and G. Ridolfi, Nucl. Phys. B **353** (1991) 591.

[75] S. Fukae, C. S. Kim, T. Morozumi, and T. Yoshikawa, Phys. Rev. **D62** (1999) 074013.

[76] T. M. Aliev, C. S. Kim and Y. G. Kim, Phys. Rev. **D62** (2000) 014026.

[77] S. Fuake, C. S. Kim and T. Yoshikawa, Phys. Rev. **D61** (2000) 074015, T. M. Aliev, A. Ozpineci and M. Savci, Phys. Lett. **B511** (2001) 49.

[78] H. Hatanaka, K.-C. Yang, Phys. Rev. **D77** (2008) 094023.

[79] K.-C. Yang, Phys. Rev. **D78** (2008) 034018; S. R. Choudhary, A. S. Cornell, N. Gaur, Eur. Phys. J. **C58** (2008) 251; V. Bashiry, JHEP 0906 (2009) 062; V. Bashiry, K.Azizi, arXiv: hep-ph/0903.1505; M. Ali Paracha, Ishtiaq Ahmed and M. Jamil Aslam, Eur. Phys. J.**C52** (2007) 967; Ishtiaq Ahmed, M. Ali Paracha and M.Jamil Aslam, Eur. Phys. J. **C54**(2008) 591; A. Saddique, M. J. Aslam and C. D. Lu, Eur.Phys.J. **C56** (2008) 267; J. P. Lee, Phys. Rev. **D74** (2006) 074001; M. J. Aslam and Riazuddin, Phys.Rev. **D72** (2005) 094019; M. J. Aslam, Eur.Phys.J. **C49** (2007) 651; K.-C. Yang, Nucl. Phys. **B776** (2007) 187; H. Dag, A. Ozpineci, M. T. Zeyrek, arXiv:1001.0939.

[80] H. Hatanaka and K. -C. Yang, "K(1)(1270)-K(1)(1400) Mixing Angle and New-Physics Effects in B —¿ K(1) l+ l- Decays," Phys. Rev. D **78**, 074007 (2008) [arXiv:0808.3731 [hep-ph]].

[81] J.Dickens, V.Gibon, C.Lazzeroni and M.Patel, CERN-LHCB-2007-038, J.Dickens, V.Gibon, C.Lazzeroni and M.Patel, CERN-LHCB-2007-039.

[82] B.Aubert *etal* [BABAR Collaboration], Phys.Rev.Lett 91 (2003) 221802 [hep-ex/0308042] ; A.Ishikawha *etal*, Phys.Rev.Lett. 96(2006) 092001 [hep-ex/0604007]; B.Aubert *etal*, arXiv:0804.4412 ; I.Adachi *etal*, arXiv: 0810.0335.

[83] M. Ali Paracha, Ishtiaq Ahmed and M. Jamil Aslam, Eur. Phys. J.**C52**, 967-973 (2007)

[84] Altug Arda and Muge Boz, Physical Review D **66**, 075012 (2002).

[85] M-O Bettler *et al.*, for LHCb Collaboration, CERN-LHCB-CONF-2009-038, LPHE-2009-05, arXiv: 0910.0942.

[86] A. Ishikawa *et al*., Phys. Rev. Lett. **96** (2006) 251801; J. T. Wei *et al*. [BELLE Collaboration], Phys. Rev. Lett. **103** (2009) 171801.

[87] B. Aubert *et al*. [BABAR Collaboration], Phys. Rev. **D 73** (2006) 092001, Phys. Rev. **D 79** (2009) 031102.

[88] A. K. Alok *et al*., JHEP **1002**, (2010)053.

[89] Ashutosh Kumar Alok *et al*., JHEP 1111, 121 (2011).

[90] A. S. Cornell, Naveen Gaur, Sushil K. Singh, hep-ph/0505136.

[91] LHCb Collaboration: LHCb-CONF-2011-038.

[92] W. Wang, Phys. Rev. **D83** (2011) 014008, [arXiv:1008.5326 [hep-ph]].

[93] K. C. Yang, Phys. Lett. **B695** (2011) 444-448, [arXiv: 1010.2944 [hep-ph]].

[94] Run-Hui Li, Cai-Dian Lu, Wei Wang, Phys.Rev.D83:034034,2011,[arXiv:1012.2129 [hep-ph]].

[95] N. Katirci, K. Azizi, JHEP 1107:043,2011,[arXiv:1105.3636 [hep-ph]].

[96] H. Hatanaka and K. C. Yang, **D79**,114008,2009, [arXiv:0903.1917 [hep-ph]].

[97] S. R. Choudhury, A. S. Cornell and N. Gaur, *Analysis of* $\bar{B} \to \bar{K}_2(1430) l^+ l^-$ *decay, Phys. Rev.* **D81** (2010) 094018.

[98] S. R. Choudhury, A. S. Cornell and J. D. Roussos, Eur.Phys.J.C71:1751,2011, [arXiv:1105.5901 [hep-ph]].

[99] M. Junaid and M. Jamil Aslam , et. al, arXiv: 1103.3934 [hep-ph].

[100] T. M. Aliev, M. Savci, arXiv: 1109.2738 [hep-ph].

[101] M. Beneke, Th. Feldmann and D. Seidel, **B612** (2001) 25; [arXiv: 0106067 [hep-ph]].

[102] G . Burdman, Phys. Rev. **D57** (1998) 4254 [hep-ph/9710550]

[103] A. Ali, P. Ball, L. T. Handoko and G. Hiller, Phys. Rev. **D61** (2000) 074024 [hep-ph/9910221].

[104] M. Beneke, T. Feldmann and D. Seidel, Nucl. Phys. **B612** (2001) 25 [hep-ph/0106067].

[105] A. Ali, P. Ball, L. T. Handoko and G. Hiller, Ref. [[103]]

[106] J. P. Lee, **D69** (2004) 114007.

[107] M. Beneke, **A21** (2006) 642-649, [arXiv: 0509297 [hep-ph]].

[108] T. Aaltonen *et al.* [CDF Collaboration], Phys. Rev. Lett. **100** (2008) 101802 [arXiv:0712.1708 [hep-ex]].

[109] C. Amsler *et al.* [Particle Data Group], Phys. Lett. **B667** (2008) 1.

[110] E. Barberio *et al.* [Heavy Flavor Averaging Group], arXiv: 0808.1297 [hep-ex], and outline update at http://www.slac.stanford.edu/xorg/hfag

[111] B. Aubert *et al.* [BaBar Collaboration], Phys. Rev. Lett. **93** (2004) 081802 [arXiv: hep-ex/0404006].

[112] M. Iwasaki *et al.* [Belle Collaboration], Phys. Rev. **D72** (2005) 092005 [arXiv:hep-ex/0503044].

[113] A. K. Aloke, A. Datta, A. Dighe, D. Ghosh, D. London and S. U. Sankar, [arXiv: 1008.2367 [hep-ph]].

[114] A. K. Aloke, A. Datta, A. Dighe, M. Suraisamy, D. Ghosh and D. London, [arXiv: 1103.5344 [hep-ph]]

[115] F. Abe et al. (CDF Collaboration) Phys. Rev. D 58, 112004 (1998).

[116] D. S. Du and Z.Wang, Phys. Rev. D 39, 1342 (1989); C.H. Chang and Y. Q. Chen, ibid. 48, 4086 (1993); K. Cheung, Phys. Rev. Lett. 71, 3413 (1993); E. Braaten, K. Cheung, and T. Yuan, Phys. Rev. D 48, R5049 (1993).

[117] Sheldon Stone, arXiv:hep-ph/9709500.

[118] A. Faessler, Th. Gutsche, M. A. Ivanov, J.G. Korner, and V. E. Lyubovitskij, Eur. Phys. J. direct C 4, 1 (2002).

[119] C. Q. Geng, C.W. Hwang, and C. C. Liu, Phys. Rev. D 65, 094037 (2002).

[120] M. S. Khan, M. J. Aslam, A. H. S. Gilani, and Riazuddin, Eur. Phys. J. C 49, 665 (2006).

[121] A.H.S. Gilani, Riazuddin, T.A. Al-Aithan, JHEP 09, 065 (2003).

[122] C. A. Dominguez, N. Paver, Riazuddin, Z. Phys. **C48** (1990) 55; C. A. Dominguez, N. Paver, Riazuddin, Phys. Lett. **B214** (1988) 459.

[123] C. A. Dominguez, N. Paver, Z. Phys. **C41** (1988) 217.

[124] M. A. Paracha *et al.*, Eur. Phys. J. **C 52** (2007) 967 [arXiv:0707.0733]; I. Ahmed *et al.*, Eur. Phys. J. **C 54** (2008) 591 [arXiv:0802.0740]; I. Ahmed *et al.*, Eur. Phys. J. **C 71** (2011) 1521 [arXiv:1002.3860]; A. Saddique *et al.*, Eur. Phys. J. **C 56** (2008) 267 [arXiv:0803.0192]; M.Jamil Aslam and Riazuddin, Phys. Rev. **D 66** (2002) 096005 [hep-ph/0209106]; V. Bashiry, K. Azizi, JHEP 1001:033, (2010) [arXiv:0903.1505].

[125] P. Colangelo, F. De Fazio, R. Ferrandes, T.N. Pham, Phys.Rev. **D73**, 115006 (2006); P. Colangelo, F. De Fazio, P. Santorelli, E. Scrimieri, Phys. Rev. D 53, 3672 (1996);P. Colangelo, Phys. Rev. D 57, 3186 (1998), Erratum; A. Saddique *et al.*, Eur. Phys. J. **C 56** (2008) 267.

[126] B. Aubert *et al.* [BABAR Collaboration], Phys. Rev. **D 73**, 092001 (2006) [arXiv:hep-ex/0604007].

[127] J. Charles, A. Le Yaouanc, L. Oliver, O. Pene, and J. C. Raynal, Phys. Rev. D 60, 014001 (1999); M. Jamil Aslam and Riazuddin, Phys. Rev. D 72, 094019 (2005); M. Jamil Aslam, Eur. Phys. J. C 49, 651 (2006).

[128] K. Azizi, F. Falahati,V. Bashiry, and S. M.Zebarjad, Phys. Rev. D 77, 114024 (2008).

[129] H.Y. Cheng et al., Phys. Rev. D 51, 1199 (1995).

[130] D. Du, X. Li, and Y. Yang, Phys. Lett. B 380, 193 (1996).

[131] K. Azizi and V. Bashiry, Phys. Rev. D 76, 114007 (2007).